공학박사학위논문

A Study on Design Parameters and Aerodynamic Stability during Construction Stages for a Cable-stayed Suspension Bridge

사장-현수교의 설계변수 및 가설 중 내풍 안정성 연구

2016년 8월

서울대학교 대학원
건설환경공학부
이 호

ABSTRACT

A cable-stayed suspension bridge, which can be applicable to road and railway bridge, is investigated both parameter study on structural characteristic and study on construction sequence to secure aerodynamic stability. The cable-stayed suspension bridge with the main span length of 1408m is considered as an example bridge and this bridge accommodates eight road lane and two railway track.

Parametric study is carried out. Two design parameters: suspension-to-span ratio and length of transition part are considered and studied for their effects on the structural behavior under live loads which consist of trains and road vehicles. As a result, a suspension-to-span ratio of 0.22to 0.56 is effective to increase the overall rigidity of structure as compared to responses of cable-stayed bridge and suspension bridge. As the length of suspended portion in main span increases, the vertical displacement of the deck gradually increases and the negative vertical bending moment of deck at the junction between cable-stayed parts and suspended part in main span sharply increases. Also, the cable tension in the longest hanger rapidly increases due to different stiffness in two structure systems namely the cable-stayed part and the suspension part. This can lead to fatigue problems which can be solved by installing the transition part. To investigate the effect of the transition parts, the ratio of transition part to cable-stayed part is changed from 0 to 0.45, by adding additional hangers in the cable-stayed part. As a result, the increase

of the transition part is effective to reduce the cable tension in the longest hanger. The transition part to cable-stayed part ratio ranging from 0.1 to 0.32 is favorable for this case study bridge.

In the long-span cable-supported bridges, construction stage has lower stiffness relative to completed stage and is vulnerable to vibration by wind. Therefore, aerodynamic stability in construction is a major design issue. Based on the deck erection, two different construction schemes are considered to investigate aerodynamic stability of construction scheme by buffeting analysis for the cable-stayed suspension bridge. The first construction scheme is the construction Plan 0 (series sequence) and the second scheme is the construction Plan 1(simultaneously construction sequence). As a result, applying construction Plan 0 scheme, aerodynamic stability of the suspended deck in construction phase is assured. However, one of the hangers is required to increase the cross-sectional area or adjusts its length after installation in order to secure aerodynamic stability. In case of applying construction Plan 1, the excessive rigid body torsional deformation in the suspended deck is found in the initial construction stage due to the rigid body motion of the suspended deck by the vertical mode of main cable. In order to control the rigid body torsional displacement of deck, X-Type bracing, Rigid beam and Strut system are considered as structural stabilization measures. The most effective structural stabilization measure is the strut system by installing on the main cables. When construction Plan 1 scheme with Strut system, aerodynamic stability is possible and construction period can be reduced by 48 days compared to

construction Plan 0 as series construction scheme. However, it is required to have proper construction management of two type of bridge structure according to simultaneous construction in both deck of cable-stayed parts and suspended part. The lifting gantry can be applicable for an aerodynamic stabilization measure to control the rigid body torsional deformation during erection of suspended decks.

Keywords: Cable-stayed suspension bridge, Suspension-to-span ratio, Transition part, aerodynamic stability, Construction phase, Deck erection sequence, Parameter study

Student Number: 2012-30248

TABLE OF CONTENTS

LIST OF FIGURES

LIST OF TABLES

Chapter 1

Introduction

The cable-stayed suspension bridge (CSSB) is a combined structure of the cable-stayed bridge (CSB) and the suspension bridge (SB). The American famous bridge designer J.A. Roebling applied the idea of reinforcing vertical stiffness of suspension bridge by additional stay cable in Brooklyn Bridge. And then the Germanic famous bridge designer Dichinger improved the concept by eliminating the vertical hangers in the cable stayed parts (Gimsing and Georgakis, 2012), as shown in Fig. 1.1.

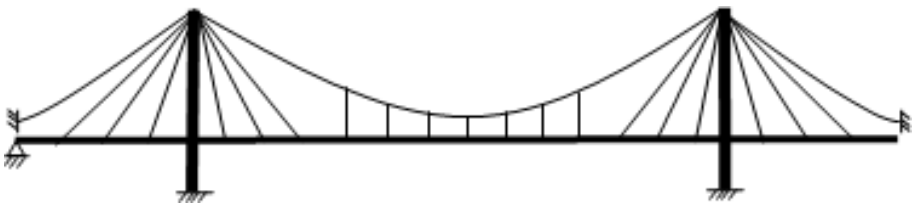

Fig. 1. 1 Dichinger's structural system

In 1997, Wujiang bridge, which is the first modern cable-stayed suspension bridge, was built in China with spans of 66 + 288 + 66 m, as shown Fig. 1.2.

The CSSB has the efficiency in the structural behavior, construction, economy and the wind stability compared with the conventional SB and CSB, and becomes

an attractive alternative in the design of long span bridges (Zhang, 2006; Gimsing and Georgakis, 2012). Based on advantages mentioned above, long-span road-railway cable-stayed suspension bridge was designed and is now on construction.

Fig. 1. 2 Wujiang bridge (China, 1997). Reprinted from highestbridges.com, by Eric Sakowski, 2015

From the comparison with cable-stayed bridges and suspension bridges, the cable-stayed suspension bridges have some different structural characteristics due to the interaction between the cable-stayed portions and suspended portion in mid-span. For the design of CSSB, the mechanics performance including the static and dynamic characteristics, construction, and wind stability need to be fully investigated for understanding and a realistically predict the structural behavior. However, few publications about structural behavior and wind stability are

available in the literature.

From recent publications, the initial equilibrium state of CSSB which is the starting point of static and dynamic load analysis. Kim (2011) studied initial equilibrium state by Target configuration under dead load (Kim and Lee, 2001) method considering two different analysis approach such as combining and separating the two structural parts. Sun et al. (2013) proposed a four-step approach for determining the reasonable initial equilibrium state using commercial finite element (FE) programs, focusing on the optimization of the cable tension and shapes of all cables. Lonetti and Pascuzzo (2014) proposed a design methodology to predict optimum cable tension and dimensioning of the cable system based on the combination of a finite element approach and an iterative optimization procedure.

For the structural behavior, Zhang (2007) studied the mechanics performance of CSSB including the static and aerodynamic stability, and compared to the suspension bridge and cable-stayed bridge with the same main span of 1400 m. Sun et al. (2013) proposed a systematic nonlinear analysis strategy for CSSB, and studied parameters related to the structural behavior with an example of a 1400 m span considering road load and static wind load.

However, most research on structural performance analysis of CSSB is focused on road vehicle. The suspension bridge system has huge vertical deflection by the train load and does not satisfy the serviceability criteria (Bruno et al, 2009). The CSSB is an alternative structural system which can meet severe deflection

restriction of railway bridges by supplementing stay cables, as shown in Fig. 1.3.

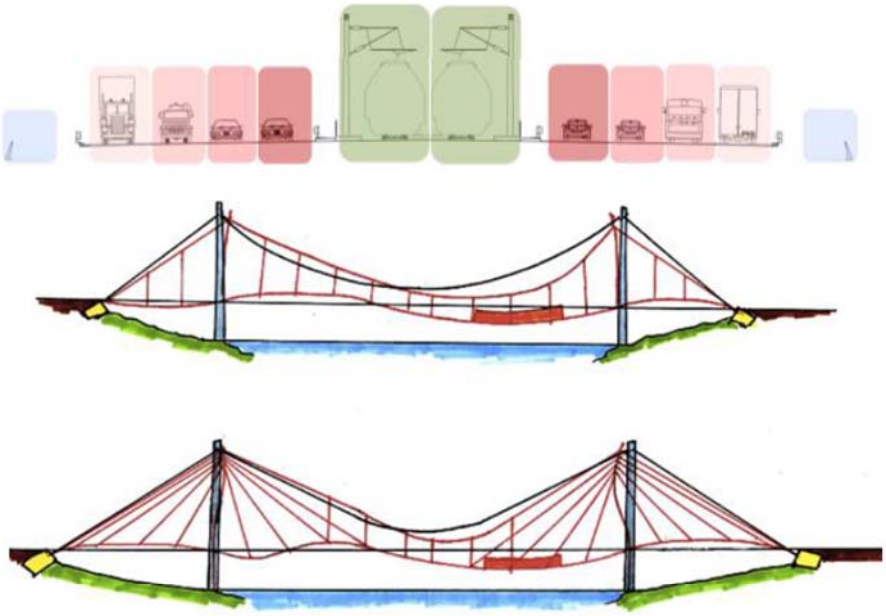

Fig. 1. 3 The bridge behavior under train load in a suspension bridge and a cable-stayed suspension bridge (Source : Michel Virlogeux)

Therefore, study on the structural parameters of CSSB including train load is required in consideration of the applicability of the railway bridge. Especially, the effect of structural parameter with the suspension-to-span ratio, which affects the overall vertical stiffness, needs to be reviewed in the perspective of improving the excessive vertical deflection occurred due to the train load.

With an increasing span length of cable-stayed suspension bridges become a flexible structure and very susceptible to wind action. From recent publications, Zhang (2006) studied effects of some design parameters on the flutter stability of a

CSSB with main span of 1400 m. The study found that some design parameters are helpful for improving the flutter stability. Nakamura (2006) examined the effects of some countermeasure on the flutter stability of a CSSB. The study found that rigid beam is effective for improving the flutter stability in the completed state. Zhang et al. (2008) examined parameters related to nonlinear aerostatic and aerodynamic, and determined the optimal values of these design parameters such as the cable sag to span ratio, the suspension to span ratio, the side span length, and the layout of stay cable planes, and the subsidiary piers in side spans. For the aerodynamic stability for cable-stayed suspension bridges during construction, Lee et al. (2015) studied for enhancement of wind stability of a cable-stayed suspension bridge in construction with several structural stabilization measures and recommended strut system in order to control the torsional deformation of suspended deck.

Most of the references were reviewed in terms of aerodynamic stability of the completed state. However, the construction stage of bridge is vulnerable to vibration by wind due to less structural rigidity than completed state. As a result, the review on wind stability during the construction state needs to be studied.

Cable-stayed suspension bridges can be constructed by series construction sequence which erects the deck of cable-stayed parts and afterwards suspension part. When the erection of main cable is completed, above construction scheme can be erected without aerodynamic stability improvement measures since deck of suspended part is attached to the deck of cable-stayed part. However, reducing the construction time can be necessary due to demand of owner and environmental

restrictions. From a structural point of view, cable-stayed suspension bridges can be reduced the construction period by erecting in the main span deck simultaneously from suspended part and cable-stayed parts after completed erection of main cables. However, it is required both to verify the aerodynamic stability on the construction phase of suspended deck and to find the potential improvement measures in the aerodynamic stability for the erection of the deck in suspended part. Therefore, it is necessary to investigate applicable aerodynamic stability enhancement measures.

In this thesis, analysis of CSSB was done in the two perspectives of views. Firstly, parametric study is carried out. Two design parameters such as suspension-to-span ratio and length of transition part are considered and studied for their effects on the structural behavior under live loads which consist of trains and road vehicles. Secondly, applicable construction sequences for cable-stayed suspension bridges were defined based on the established construction method, and studied on the aerodynamic stability of its construction sequences focus on the erection of suspended deck. Especially, owner's requests and environmental restriction and the case when rapid construction is required due to the short construction period were also included.

With the above objectives, this thesis is organized in 6 chapters. The main text of each chapter is intentionally kept as short as possible in favor of easy reading.

In this Chapter has been described for background, objective and a literature review for the structural characteristic of cable-stayed suspension bridge and its

aerodynamic stability in construction.

In Chapter 2, the theories and analytical method that are used in present studies are presented. It briefly introduced that considered cable element and TCUD method for initial shape analysis of cable-stayed suspension bridges. On the basis of these methods, a configuration analysis procedure is proposed based on practical approach. Also, the theory of buffeting analysis for the evaluation of aerodynamic stability in construction is presented.

In Chapter 3, an example bridge considered in this study is described and found their initial equilibrium state under dead load by proposed practical approach. Also, validity of practical method above mentioned is identified through the comparison between initial equilibrium state of the example bridge obtained by practical method and design values. Initial shape analysis is also performed on seven bridge analysis models for design parameter study of cable-stayed suspension bridges.

In Chapter 4, in order to identify the effect of suspension-to-span ratio as one of design parameters, nonlinear static analysis is performed to seven bridge analysis models considering wind and live load consisting train load and road vehicle load and its effect is identified. In order to identify the effect of transition part which is reducing the tension amplitude of the longest hanger, moving load analysis under fatigue train load is performed to five bridge analysis models with Midas civil program.

In Chapter 5, aerodynamic stability of suspended deck in construction is

investigated with erection scheme of series construction (Construction Plan 0) and simultaneously construction (Construction Plan 1) as considering fast-track construction. Three structural stabilization measures are considered to control the torsional deformation of suspended deck in the initial erection stage of construction plan 1. The most effective measure is applied on construction plan 1 and has identified their applicability. The lifting gantry, which is the construction equipment for the suspended deck, can be applicable for an aerodynamic stabilization measure to control the rigid body torsional deformation during erection of suspended decks.

Finally in Chapter 6, the main conclusions and major contributions of the thesis are first summarized, then, a set of future researches are proposed.

Chapter 2

Analysis theory

2.1 Cable elements

The formulation of cable element considering the unstrained length as the unknown is described in the following section.

(1) Elastic catenary cable element

The elastic catenary cable element, which is derived from the exact solution of the elastic catenary cable theory in two-dimensional (Irvine, 1981), is proposed by O'Brien and Francis (1964) and later developed by Jayaraman and Knudson (1981), Ahn (1991), and Andreu et al. (2006). The cable element suspended between point i(0,0,0) and j(Lx,Ly,Lz), and the Lagrangian coordinates of undeformed and deformed configurations are *s* and *p*, as shown in Fig. 2.1.

The geometric constraint is given by

$$\left(\frac{dx}{dp}\right)^2 + \left(\frac{dy}{dp}\right)^2 + \left(\frac{dz}{dp}\right)^2 = 1 \tag{2.1}$$

The force equilibrium equation for the cable can be expressed as

$$T\frac{dx}{dp}+F_1=0,\ \ T\frac{dy}{dp}+F_2=0,\ \ T\frac{dz}{dp}+F_3-ws=0 \tag{2.2}$$

where T = cable tension.

The cable tension can be expressed with the Lagrangian coordinate *s*, and the force components eq. (2.2).

$$T=\sqrt{F_1^2+F_2^2+(F_3-ws)^2} \tag{2.3}$$

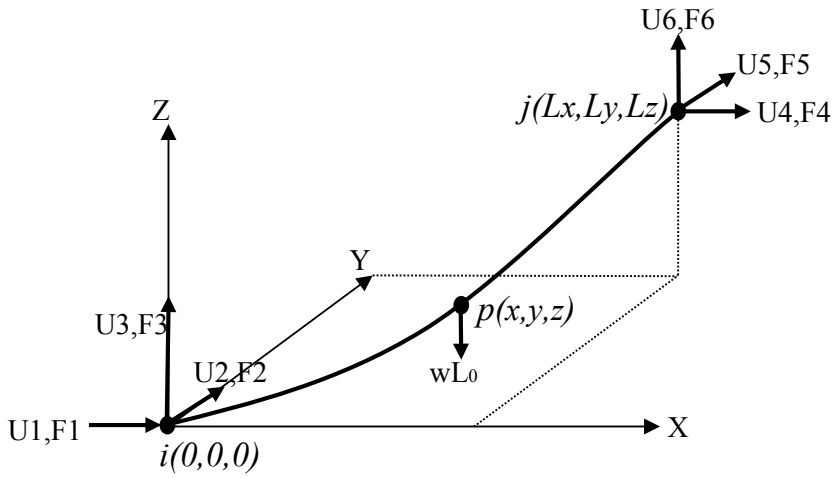

Fig. 2. 1 Nodal force and displacement vectors of an elastic catenary cable element

The cable tension T is related to the strain ε by Hook's law as

$$T=EA_0\varepsilon=EA_0(\frac{dp}{ds}-1) \tag{2.4}$$

where E = the elastic modulus; A_0 = the constant cross-sectional area in the unstrained profile.

The Lagrangian *s* and the Cartesian coordinates are related as show eq. (2.5)

$$x(s)=\int_0^s \frac{dx}{ds}ds,\ \ y(s)=\int_0^s \frac{dy}{ds}ds,\ \ z(s)=\int_0^s \frac{dz}{ds}ds \tag{2.5}$$

where

$$\begin{aligned}
\frac{dx}{ds}&=\frac{dx}{dp}\frac{dp}{ds}=-\frac{F_1}{T}(\frac{T}{EA_0}+1)\\
\frac{dy}{ds}&=\frac{dy}{dp}\frac{dp}{ds}=-\frac{F_2}{T}(\frac{T}{EA_0}+1)\\
\frac{dz}{ds}&=\frac{dz}{dp}\frac{dp}{ds}=-\frac{(F_3-ws)}{T}(\frac{T}{EA_0}+1)
\end{aligned} \tag{2.6}$$

and the boundary conditions at the *j* nodes:

$$\begin{aligned}
&x=0,\ \ y=0,\ \ z=0,\ \ p=0\ \ in\ \ s=0\\
&x=L_x,\ \ y=L_y,\ \ z=L_z,\ \ p=L\ \ in\ \ s=L_0
\end{aligned} \tag{2.7}$$

where L = the strained length of cable.

By integrating along the member in Cartesian coordinates x, y and z, and including boundary conditions, we have a 3D geometrical compatibility equation for the elastic catenary cable in eq. (2.8).

$$
\begin{aligned}
L_x &= -\frac{F_1 L_0}{EA_0} - \frac{F_1}{w}\left\{\ln(T_j + wL_0 - F_3) - \ln(T_i - F_3)\right\} \\
L_y &= -\frac{F_2 L_0}{EA_0} - \frac{F_2}{w}\left\{\ln(T_j + wL_0 - F_3) - \ln(T_i - F_3)\right\} \\
L_z &= -\frac{F_3 L_0}{EA_0} + \frac{wL_0^2}{2EA_0} + \frac{1}{w}(T_j - T_i)
\end{aligned} \tag{2.8}
$$

where $T_i = \sqrt{F_1^2 + F_2^2 + F_3^2}$, $T_j = \sqrt{F_1^2 + F_2^2 + (wL_0 - F_3)^2}$

Eq. (2.8) can be expressed as following form;

$$
L_x = L_x(F_1, F_2, F_3, L_0),\ L_y = L_y(F_1, F_2, F_3, L_0),\ L_z = L_z(F_1, F_2, F_3, L_0) \tag{2.9}
$$

By partial differential of eq. (2.9) with respect to nodal forces and L_0 leads to the following expression;

$$
\begin{aligned}
dL_x &= \frac{\partial L_x}{\partial F_1} dF_1 + \frac{\partial L_x}{\partial F_2} dF_2 + \frac{\partial L_x}{\partial F_3} dF_3 + \frac{\partial L_x}{\partial L_0} dL_0 \\
dL_y &= \frac{\partial L_y}{\partial F_1} dF_1 + \frac{\partial L_y}{\partial F_2} dF_2 + \frac{\partial L_y}{\partial F_3} dF_3 + \frac{\partial L_y}{\partial L_0} dL_0 \\
dL_z &= \frac{\partial L_z}{\partial F_1} dF_1 + \frac{\partial L_z}{\partial F_2} dF_2 + \frac{\partial L_z}{\partial F_3} dF_3 + \frac{\partial L_z}{\partial L_0} dL_0
\end{aligned} \tag{2.10}
$$

where $dL_x = dU_4 - dU_1, dL_y = dU_5 - dU_2, dL_z = dU_6 - dU_3$

or expressed in matrix form

$$\begin{Bmatrix} dL_x \\ dL_y \\ dL_z \end{Bmatrix} = \begin{bmatrix} f_{11} & f_{12} & f_{13} \\ f_{21} & f_{22} & f_{23} \\ f_{31} & f_{32} & f_{33} \end{bmatrix} \begin{Bmatrix} dF_1 \\ dF_2 \\ dF_3 \end{Bmatrix} + \begin{bmatrix} f_{14} \\ f_{24} \\ f_{34} \end{bmatrix} dL_0 \tag{2.11}$$

where f_{ij} is flexibility matrix given as follows

$$\begin{aligned}
f_{11} &= -(\frac{L_0}{EA_0} + \frac{1}{w}\ln\frac{T_j + F_6}{T_i - F_3}) + \frac{F_1^2}{w}\left[\frac{1}{T_i(T_i - F_3)} - \frac{1}{T_j(T_j + F_6)}\right] \\
f_{12} &= f_{21} = \frac{F_1 F_2}{w}\left[\frac{1}{T_i(T_i - F_3)} - \frac{1}{T_j(T_j + F_6)}\right] \\
f_{13} &= f_{31} = \frac{F_1}{w}\left[\frac{1}{T_j} - \frac{1}{T_i}\right] \\
f_{22} &= -(\frac{L_0}{EA_0} + \frac{1}{w}\ln\frac{T_j + F_6}{T_i - F_3}) + \frac{F_2^2}{w}\left[\frac{1}{T_i(T_i - F_3)} - \frac{1}{T_j(T_j + F_6)}\right] \\
f_{23} &= f_{32} = \frac{F_2}{w}\left[\frac{1}{T_j} - \frac{1}{T_i}\right]
\end{aligned} \tag{2.12}$$

$$\begin{aligned}
f_{33} &= -\frac{L_0}{EA_0} - \frac{1}{w}\left[\frac{F_6}{T_j} + \frac{F_3}{T_i}\right] \\
f_{14} &= -\frac{F_1}{EA_0} - \frac{F_1}{T_j} \\
f_{24} &= -\frac{F_2}{EA_0} - \frac{F_2}{T_j} \\
f_{34} &= -\frac{F_3}{EA_0} + \frac{wL_0}{EA_0} + \frac{wL_0 - F_3}{T_j}
\end{aligned}$$

The cable stiffness matrix k_{ij} can be obtained by inverting the flexibility matrix f_{ij} as follows (Kyung, 2002);

$$\begin{Bmatrix} dF_1 \\ dF_2 \\ dF_3 \end{Bmatrix} = \begin{bmatrix} k_{11} & k_{12} & k_{13} \\ k_{21} & k_{22} & k_{23} \\ k_{31} & k_{32} & k_{33} \end{bmatrix} \left(\begin{Bmatrix} dL_x \\ dL_y \\ dL_z \end{Bmatrix} - \begin{bmatrix} f_{14} \\ f_{24} \\ f_{34} \end{bmatrix} dL_0 \right) \tag{2.13}$$

and nodal force at node *j* are obtained from equilibrium equation as

$$F_4 = -F_1, \;\; F_5 = -F_2, \;\; F_6 = wL_0 - F_3 \tag{2.14}$$

From eq. (2.13) and (2.14) yields the following incremental equation of the elastic catenary cable element (Kyung, 2002; Kim and Kim, 2012).

$$\Delta F_c = k_c \Delta U_c + k_{cu} \Delta L_0 \tag{2.15}$$

where ΔF_c = the incremental nodal force vector; k_c = the stiffness matrix of elastic catenary cable element; ΔU_c = the incremental displacement vector; k_{cu} = the stiffness matrix related to the unstrained lengths of the cable element.

(2) Truss-cable element

The force-displacement relationship of the truss-cable elements is as follow;

$$T = \frac{EA_0}{L_0}(L - L_0) \tag{2.16}$$

where E and A_0 = the elastic modulus, cross-sectional area, respectively; L and L_0 and T = the strained and unstrained length, and tension of the truss element, respectively.

The cable tension in eq. (2.16) can be decomposed into its coordinate x, y and z as

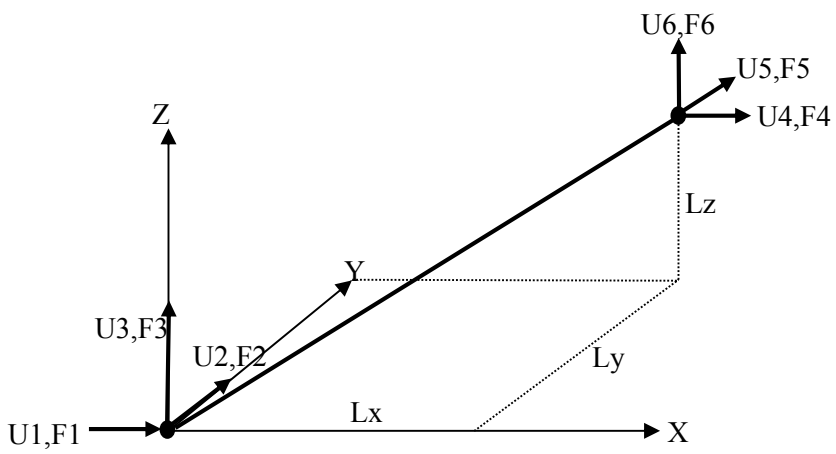

Fig. 2. 2 Nodal force and displacement vectors of a truss-cable element

$$
\begin{aligned}
F_1 &= -T\frac{L_x}{L} = -\frac{L_x}{L}\frac{EA_0}{L_0}(L-L_0) \\
F_2 &= -T\frac{L_y}{L} = -\frac{L_y}{L}\frac{EA_0}{L_0}(L-L_0) \\
F_3 &= -T\frac{L_z}{L} = -\frac{L_z}{L}\frac{EA_0}{L_0}(L-L_0)
\end{aligned}
\tag{2.17}
$$

where $L = \sqrt{L_x^2 + L_y^2 + L_z^2}$.

Eq. (2.17) can be expressed as following form;

$$
F_1 = F_1(L_x, L_y, L_z, L_0),\ F_2 = F_2(L_x, L_y, L_z, L_0),\ F_3 = F_3(L_x, L_y, L_z, L_0) \tag{2.18}
$$

An incremental equation can be derived from eq. (2.18) as

$$
\begin{aligned}
dF_1 &= \frac{\partial F_1}{\partial L_x}dL_x + \frac{\partial F_1}{\partial L_y}dL_y + \frac{\partial F_1}{\partial L_z}dL_z + \frac{\partial F_1}{\partial L_0}dL_0 \\
dF_2 &= \frac{\partial F_2}{\partial L_x}dL_x + \frac{\partial F_2}{\partial L_y}dL_y + \frac{\partial F_2}{\partial L_z}dL_z + \frac{\partial F_2}{\partial L_0}dL_0 \\
dF_3 &= \frac{\partial F_3}{\partial L_x}dL_x + \frac{\partial F_3}{\partial L_y}dL_y + \frac{\partial F_3}{\partial L_z}dL_z + \frac{\partial F_3}{\partial L_0}dL_0
\end{aligned}
\tag{2.19}
$$

where $dL_x = dU_4 - dU_1, dL_y = dU_5 - dU_2, dL_z = dU_6 - dU_3$

or expressed in matrix form (Kyung, 2002)

$$
\begin{Bmatrix} dF_1 \\ dF_2 \\ dF_3 \end{Bmatrix} = \begin{bmatrix} k_{11} & k_{12} & k_{13} \\ k_{21} & k_{22} & k_{23} \\ k_{31} & k_{32} & k_{33} \end{bmatrix} \begin{Bmatrix} dL_x \\ dL_y \\ dL_z \end{Bmatrix} + \begin{bmatrix} f_{14} \\ f_{24} \\ f_{34} \end{bmatrix} dL_0 \tag{2.20}
$$

Where

$$k_{11} = -\frac{EA_0 L_x^2}{L^3} - \frac{EA_0(L - L_0)}{L_0 L}$$

$$k_{12} = k_{21} = -\frac{EA_0 L_x L_y}{L^3}$$

$$k_{13} = k_{31} = -\frac{EA_0 L_x L_z}{L^3}$$

$$k_{22} = -\frac{EA_0 L_y^2}{L^3} - \frac{EA_0(L - L_0)}{L_0 L}$$

$$k_{23} = k_{32} = -\frac{EA_0 L_y L_z}{L^3}$$

$$k_{33} = -\frac{EA_0 L_z^2}{L^3} - \frac{EA_0(L - L_0)}{L_0 L}$$

$$k_{14} = \frac{EA_0 L_x}{L_0^2} \tag{2.21}$$

$$k_{24} = \frac{EA_0 L_y}{L_0^2}$$

$$k_{34} = \frac{EA_0 L_z}{L_0^2}$$

and nodal forces at node *j* are obtained from equilibrium equation as

$$F_4 = -F_1,\ \ F_5 = -F_2,\ \ F_6 = -F_3 \tag{2.22}$$

The incremental equation of equilibrium can be obtained for a truss-cable element considered unstrained lengths as unknowns (Kyung, 2002; Kim and Kim, 2012)

$$\Delta F_c = (k_{ce} + k_{cg})\Delta U_c + k_{cl}\Delta L_0 \tag{2.23}$$

where ΔF_c = the incremental nodal force vector; k_{ce} = the elastic stiffness matrix; k_{cg} = the geometric stiffness matrix of truss-cable element; ΔU_c = the incremental displacement vector; k_{cl} = the stiffness matrix related to the unstrained lengths of the cable element.

2.2 TCUD analysis method

Target configuration under dead loads (TCUD) method (Kim and Lee 2001; Kim and Kim 2012; Jung et al., 2013) is introduced. The TCUD is effective method to determine the unstrained length or tension of cable elements by Newton-Raphson iterative technique including the unstrained length of the cable element such as elastic catenary and truss-cable element in unknown parameters, and providing additional constraints condition which suppresses the undesirable displacement of the cable structure as boundary conditions. The incremental equilibrium equations of bridge structures are considered using eq. (2.15) and (2.23) adding unstrained lengths of the cable element as unknown, and using incremental tangential stiffness matrix in case of nonlinear or second-order framed structure (McGuire, w., et al., 2000; Gavin, H. P., 2014) as in eq. (2.24)

$$\Delta F_f = (k_{fe} + k_{fg})\Delta U_f \tag{2.24}$$

where ΔF_f = the incremental nodal force vector; k_{fe} = the elastic stiffness matrix of frame element; k_{fg} = the geometric stiffness matrix of frame element; ΔU_f = the incremental displacement vector

The direct assemblage of the tangential stiffness matrix leads to the following incremental form of equilibrium equation for the structural system (Kim and Kim 2012; Jung et al., 2013) as

$$\Delta F = K_t \Delta U + K_l \Delta L_0 \tag{2.25}$$

where $\Delta F(n\times 1)$ = the incremental unbalanced load vector composed of external load and internal member force; K_t $(n\times n)$ and K_l $(n\times m)$ = the tangential stiffness matrix and the unstrained length-related stiffness matrix due to m cable element, respectively; $\Delta U(n\times 1)$ = the incremental nodal displacement vector; $\Delta L_0(m\times 1)$ = the incremental unstrained length vector; *n* is the number of total degree of freedom and *m* the number of cable element.

As the total number of unknowns (n+m) in eq. (2.25), in order to solve this equation, is a required additional constraint condition. Fig. 2.3 shows examples of the additional constraints applied for cable-stayed suspension bridges. For this purpose, eq. (2.25) can be written (Kim and Kim 2012; Jung et al., 2013) as

$$\Delta F = K_{tu} \Delta U_u + K_{ts} \Delta U_s + K_l \Delta L_0 \tag{2.26}$$

where K_{tu} $(n\times(n\text{-}m))$ and K_{ts} $(n\times m)$ = partitioned stiffness matrices according to ΔU_u and ΔU_s, respectively. ΔU_u $((n\text{-}m)\times 1)$ = the unknown displacement vector to be determined by TCUD analysis; $\Delta U_s(m\times 1)$ = the constrained displacement vector defined by the designer to control the unwanted deformation of the bridge.

The second term in the right-hand side of eq. (2.26) cancels out and the other terms result in a nonsymmetrical stiffness formulation as

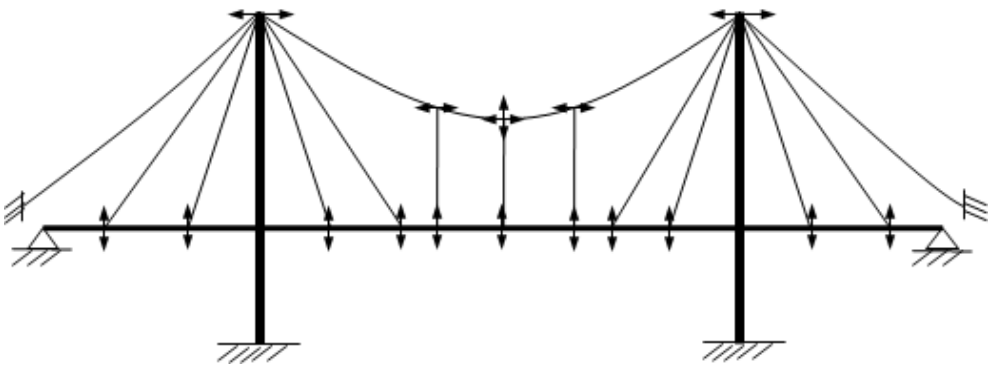

Fig. 2. 3 Geometric constraints in the TCUD method for cable-stayed suspension bridges

$$\begin{Bmatrix} \Delta F_u \\ 0 \end{Bmatrix} = \begin{bmatrix} K_{tu} & K_l \end{bmatrix} \begin{Bmatrix} \Delta U_u \\ \Delta L_0 \end{Bmatrix} \tag{2.27}$$

where total m constraint can be defined in a one-to-one correspondence with the m cable elements.

The generalized TCUD iterative algorithm can be represented (Kim et al., 2012) as follows

$$\begin{bmatrix} K_{tu}^{(i-1)} & K_{l}^{(i-1)} \end{bmatrix} \begin{Bmatrix} \Delta U_u^{(i)} \\ \Delta L_0^{(i)} \end{Bmatrix} = \begin{Bmatrix} \Delta F_u^{(i-1)} \\ 0 \end{Bmatrix}$$

$$\Delta F_u^{(i-1)} = W - F_f^{(i-1)} - F_c^{(i-1)} \quad \text{for i=1,2,...} \tag{2.28}$$

$$\begin{Bmatrix} U_u^{(i)} \\ L_0^{(i)} \end{Bmatrix} = \begin{Bmatrix} U_u^{(i-1)} \\ L_0^{(i-1)} \end{Bmatrix} + \begin{Bmatrix} \Delta U_u^{(i)} \\ \Delta L_0^{(i)} \end{Bmatrix}$$

$$\textit{initial condition}: \; U_u^{(0)} = 0, F_f^{(0)} = 0, F_c^{(0)} \neq 0 \tag{2.29}$$

where W = the dead load vector; $F_f^{(i)}, F_c^{(i)}$ = the equivalent internal force vectors for the frame and cable element, respectively.

This paper adopts the TCUD method following the flowchart as shown in Fig. 2.4.

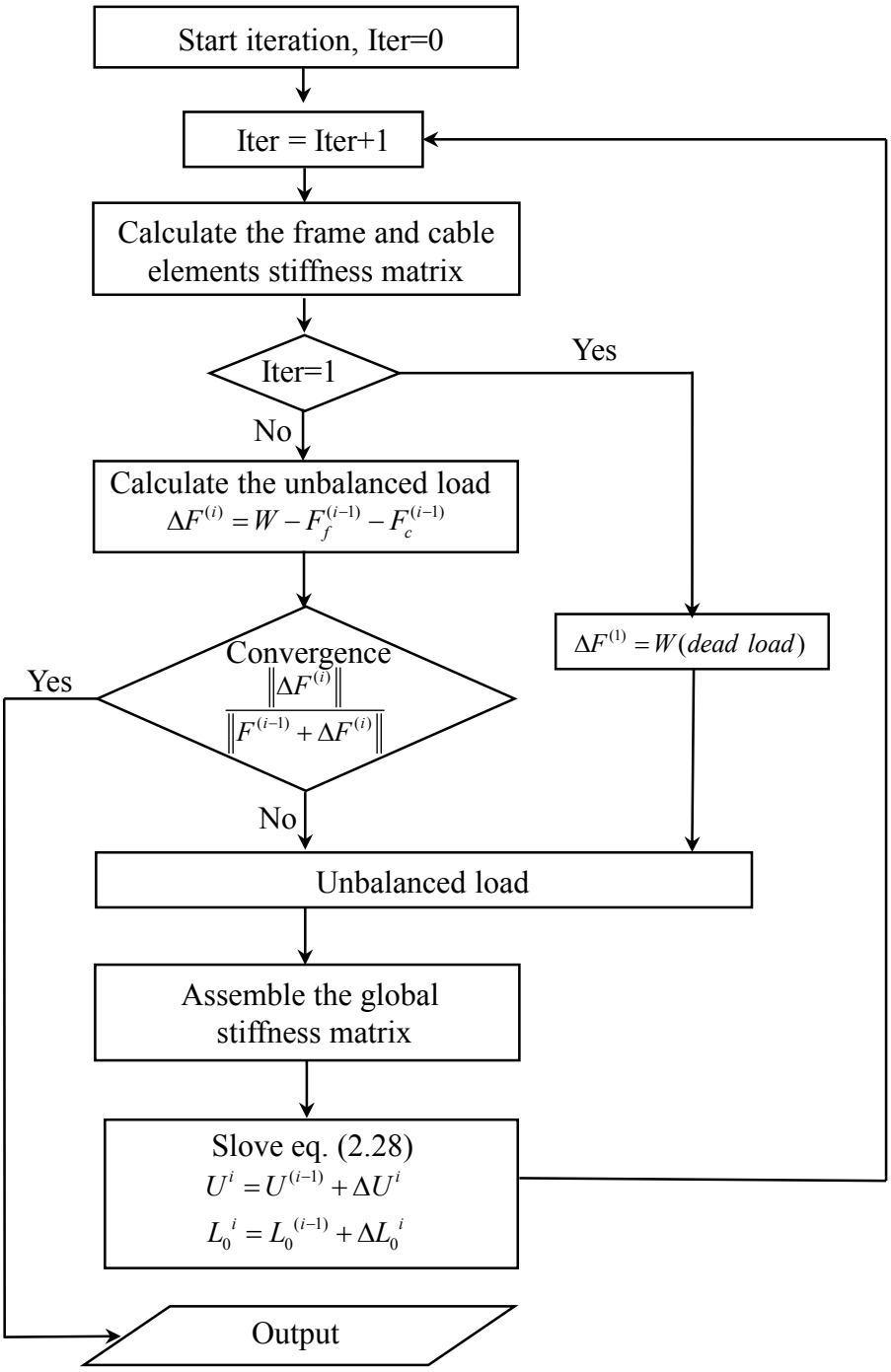

Fig. 2. 4 Flowchart of TCUD method

A cable-stayed suspension bridge as an example bridge has been studied in order to verify the cable element and the iteration procedure of TCUD method described in above section.

A cable-stayed suspension bridge as an example is taken from the study of Kim (2011) and Choi (2012), as shown in Fig. 2.5.

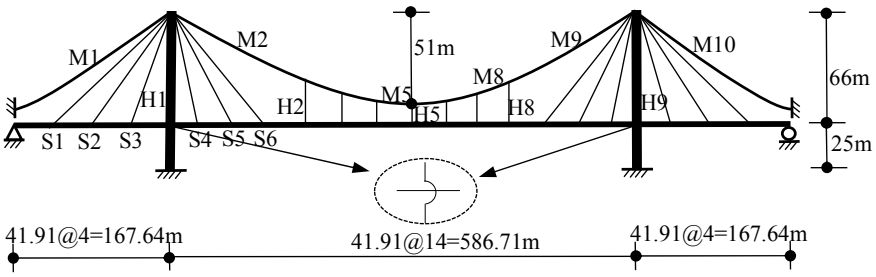

Fig. 2. 5 Analysis model of a cable-stayed suspension bridge

The example bridge has a span of 922.02 m with pylon height of 91m and the sag of 51 m. The bridge deck and pylons are modeled using 22 and 8 frame element, respectively. The bridge deck has 2 % camber for side spans and main span. The stay cables are modeled using 12 elastic catenary cable elements as a fan type cable system. The main cable and hangers are modeled using 10 and 9 elastic catenary cable elements and truss-cable elements, respectively. Those cable elements are considered one cable element. M, H, and S in Fig 2.5 are indicated number of main cable, hangers, and stay cables, respectively. Table 2.1 summarizes the material and sectional properties and the self-weight data.

Table 2. 1 Materal , sectional properties and self-weight data for a cable-stayed suspension bridge

Structural member	E(GPa)	A(m2)	I(m4)	W(kN/m)
Deck	207	0.320	1.13	87.5
Pylon(-25~0m)	207	0.300	0.500	7.06
Pylon(0~20.3m)	207	0.269	0.432	6.32
Pylon(20.3~40.6m)	207	0.228	0.345	5.36
Pylon(40.6~66m)	207	0.203	0.211	4.77
Stay cable exterior	207	0.042	-	3.22
Stay cable interior	207	0.016	-	1.24
Main cable	207	0.252	-	32.93
Hanger	207	0.042	-	1.24

In order to perform the initial configuration analysis by Newton-Rapson iteration technique, a trial value of both unstrained cable length of main cable and hangers and initial configuration of main cable is calculated by analytical method with nodal force equilibrium (Kim et al, 2002; Jung et al, 2013). On the other hand, the trial unstained length of stay cables are assumed straight line.

Fig. 2.6 shows the additional geometric constraints for a cable-stayed suspension bridge. The number of constraints applied is the same to the number of cable elements. The main cables suppress the horizontal movement and the hanger and stay cable prevent vertical movement of the deck at anchorage points.

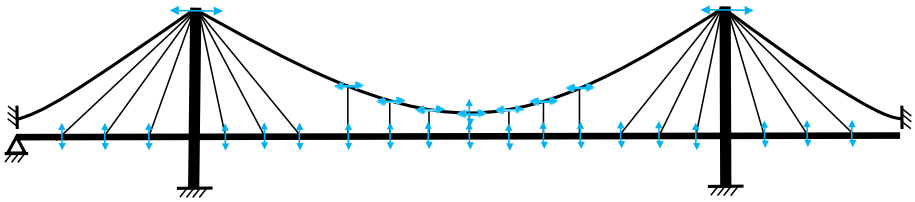

Fig. 2. 6 Additional geometric constraints for a cable-stayed suspension bridge

Table 2.2 shows summary of maximum displacements and internal forces in the frame elements. It can be noticed that the results analyzed by present study tool show good agreement with previous study.

Table 2. 2 The maximum displacements and internal forces in frame elements by TCUD method

Structural responses	Present study	Kim's study	Choi's study
Vertical displacement at the top of pylon(cm)	-15.47	-	-15.46
Max. positive bending moment of the deck(kN·m)	16222 (16245)	15000	15451
Max. negative bending moment of the deck(kN·m)	-11875 (-11895)	-11000	-11890

Note : The round bracket values denote the analyzed result with continuous beam analysis for the bridge deck only.

Table 2.3 shows the unstrained cable lengths of the main cable, hangers and stay cables by present study tool. This result indicated that the unstrained length of main cable, hangers, and stay cables are in good agreement with those previous studies.

Table 2. 3 Unstrained cable lengths of the main cable, hangers and stay cables by TCUD method

Cable No.	Present study(m)	Kim's study(m)	Choi's study(m)
M1	179.83	179.83	179.83
M2	171.99	171.98	171.99
M5	41.86	41.86	41.86
H1	65.81	65.77	65.81
H2	16.49	16.40	16.39
H5	3.00	2.98	3.00
S1	142.98	141.74	142.98
S2	107.46	106.37	107.59
S3	78.67	77.93	78.74
S4	75.27	77.96	75.10
S5	102.85	106.40	102.75
S6	138.20	141.81	137.93

Note : M - main cable, H - hanger, and S - stay cable

2.3 Configuration analysis procedure for a cable-stayed suspension bridge

The determination of initial equilibrium state of cable-stayed suspension bridges under dead load is very important in the process of structural analysis. The analysis process to determine the unstrained lengths or initial cable tension which satisfies a given design conditions under dead load is referred to as initial configuration analysis.

The road and railway long-span cable-stayed suspension bridge is taken as an example in this paper. In order to perform the configuration analysis of the example bridge, the elastic catenary cable and truss-cable element are derived considering the unstrained length as the unknown and Target configuration under dead loads (TCUD) method (Kim and Lee 2001; Kim and Kim 2012; Jung et al., 2013) is introduced in above section. With those element and method, the reasonable completed dead load state for the example bridge is performed according to the principle that the vertical displacement of the deck and longitudinal displacement of pylon close to zero under dead load. For the trial initial configuration of main cable is calculated by analytical method with nodal force equilibrium (Kim et al, 2002; Jung et al, 2013). The example adopted some measures in order to improve excessive vertical deflection occurs by the train load, as shown in Fig. 3.1. Those measures include installing several subsidiary piers and concrete deck at side span,

and taking short side span with partially earth-anchored stay cable. In this case, determination of reasonable completed dead load state is a lack of convenient method due to complex boundary conditions at side span. Therefore, practical method in terms of the deflection of deck and pylon close to zero has been applied to determine the initial equilibrium state for example bridge.

To do this, some assumptions are required as: 1) In the case of CSSBs, dead loads of the deck in cable-stayed parts and suspended part are supported by stay cables and hangers, respectively. 2) In the transition part, stay cables and hangers at the same point on the deck have a certain percentage of dead loads. 3) The horizontal tension of main cable is constant along the main cable. 4) The sag point at the middle of center span is given as design parameter. 5) The hangers in suspended part remain vertical in the initial shape finding analysis.

The configuration analysis procedure of CSSB under dead load can be divided into five steps as follow:

Step 1. Calculation of the vertical reaction forces of both stay cables and hangers at cable anchorage points using the method of continuous beam on rigid supports.

Step 2. Initial trial configuration of main cable is calculated by nodal force equilibrium method (Kim et al, 2002; Jung et al, 2013) under vertical reaction forces at the anchorage points of hangers, and obtained the unstained length of hangers and configuration of main cables.

Step 3. Determining the tension of stay cables in main span by TCUD based on the applied fixed boundary condition at the anchorage points of stay cable at the pylon, and also considering the initial tension of stay cables in side span as the horizontal and vertical force, as shown in Fig. 2.7.

Step 4. Calculation of the tension of stay cables in side span based on horizontal forces equilibrium at the pylon, as shown in Fig. 2.7.

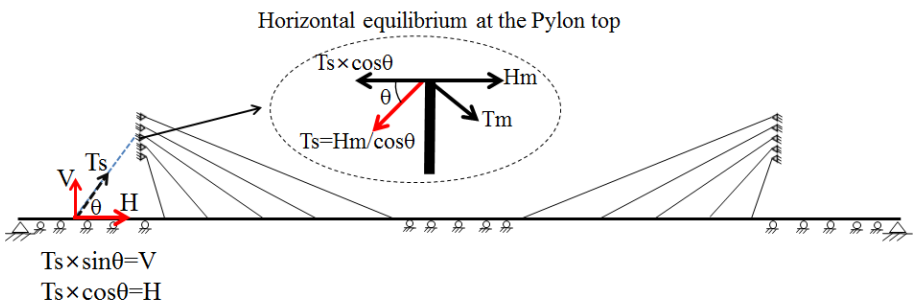

Fig. 2. 7 Analysis scheme of determinig the tension of stay cable in main span by TCUD

Step 5. Combined two bridge structure, and iterative calculation by Newton-Rapson is performed to meet the vertical displacement converge by adjusting the tension of stay cable in side span with nonlinear approach, as shown in Fig. 2.8.

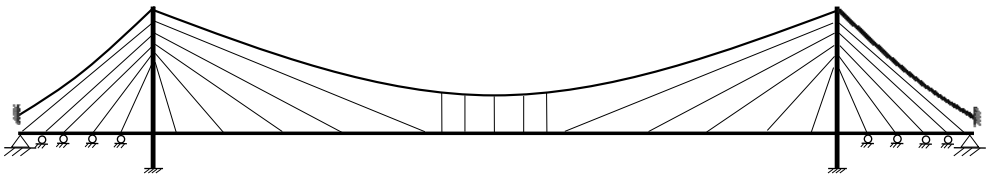

Fig. 2. 8 Combined two bridge structure for the configuration analysis

The convergence tolerance for the configuration analysis can be expressed as

$$\left|\frac{\delta v}{L}\right| \leq 10^{-4} \tag{2.30}$$

where δv = the maximum vertical displacement of all nodes; L = the main span length.

2.4 Buffeting analysis

The modal frequency domain approach is used to calculate the buffeting responses (Simiu and Scanlan, 1996). Wind direction and bridge axis is defined in Fig. 2.9.

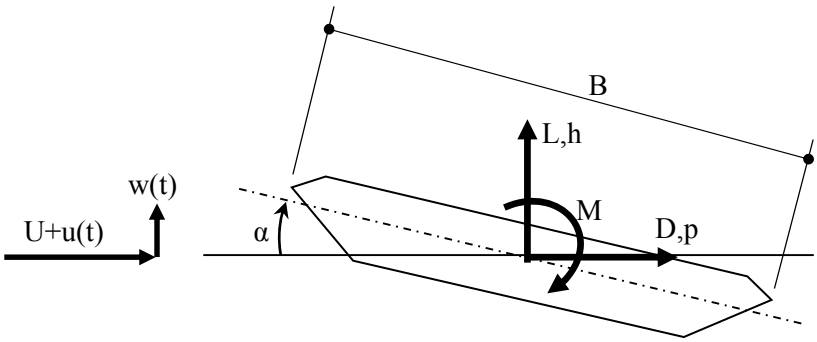

Fig. 2. 9 Bridge axis and wind component on the deck

Three displacement components of bridges can be expressed such as following forms:

$$
\begin{aligned}
&Vertical: \quad \mathrm{h(x,t)} = \sum_{i=1}^{N} h_i(x) B \xi_i(t) \\
&Lateral: \quad \mathrm{p(x,t)} = \sum_{i=1}^{N} p_i(x) B \xi_i(t) \\
&Torsion: \quad \alpha\mathrm{(x,t)} = \sum_{i=1}^{N} \alpha_i(x) \xi_i(t)
\end{aligned}
\tag{2.31}
$$

where x is the coordinate along the bridge deck span; and t = time; $h_i(x)$,$p_i(x)$, and

$\alpha_i(x)$ = modal values corresponding to vertical, lateral and torsional displacement components, respectively; ξ_i = generalized coordinate of the *i*th mode; N = number of modes; and B = deck width.

The governing equation of motion of ξ_i is

$$I_i\left[\ddot{\xi}_i + 2\zeta_i\omega_i\dot{\xi}_i + w_i^2\xi_i\right] = q_i(t) \tag{2.32}$$

where I_i and q_i = generalized mass and force of the bridge deck per unit length, respectively; ζ_i and ω_i = damping ratio-to-critical and the circular natural frequency of the *i*th mode, respectively.

The generalized force $q_i(t)$ is defined by

$$q_i(t) = \int_{deck} \left[(L_{se} + L_b)h_i B + (D_{se} + D_b)p_i B + (M_{se} + M_b)\alpha_i\right] dx \tag{2.33}$$

where L, D, and M indicate the lift, drag and pitching moment per unit span length. Self-excited force under sinusoidal motion of frequency ω can be expressed as

$$\begin{aligned} L_{se} &= \frac{1}{2}\rho U^2 B\left[KH_1^*\frac{\dot{h}}{U} + KH_2^*\frac{B\dot{\alpha}}{U} + K^2H_3^*\alpha + K^2H_4^*\frac{h}{B}\right] \\ D_{se} &= \frac{1}{2}\rho U^2 B\left[KP_1^*\frac{\dot{p}}{U} + KP_2^*\frac{B\dot{\alpha}}{U} + K^2P_3^*\alpha + K^2P_4^*\frac{p}{B}\right] \\ M_{se} &= \frac{1}{2}\rho U^2 B^2\left[KA_1^*\frac{\dot{h}}{U} + KA_2^*\frac{B\dot{\alpha}}{U} + K^2A_3^*\alpha + K^2A_4^*\frac{h}{B}\right] \end{aligned} \tag{2.34}$$

where ρ = air density; U = mean wind velocity; K = Bω/U = reduced frequency; ω = circular natural frequency (rad/s); over dots indicate the time derivative; H_i^*, P_i^*, and A_i^*, i = 1,…,4 are the flutter derivatives of the bridge deck section.

The buffeting forces due to a turbulent wind can be written as

$$
\begin{aligned}
L_b(x,t) &= \frac{1}{2}\rho U^2 B\left[2\chi_{Lu}C_L\frac{u(x,t)}{U}+\chi_{Lw}\left(\frac{dC_L}{d\alpha}+C_D\right)\frac{w(x,t)}{U}\right] \\
D_b(x,t) &= \frac{1}{2}\rho U^2 B\left(2\chi_{Du}C_D\frac{u(x,t)}{U}+\chi_{Dw}\frac{dC_D}{d\alpha}\frac{w(x,t)}{U}\right) \\
M_b(x,t) &= \frac{1}{2}\rho U^2 B^2\left(2\chi_{Mu}C_M\frac{u(x,t)}{U}+\chi_{Mw}\frac{dC_M}{d\alpha}\frac{w(x,t)}{U}\right)
\end{aligned}
\tag{2.35}
$$

where u(x,t) and w(x,t) = longitudinal and vertical wind velocity fluctuation component, respectively; C_L,C_D, and C_M = the lift, drag, pitching moment coefficients, respectively; $dC_L/d\alpha$ and $dC_M/d\alpha$ = the slopes of the load coefficient curves at angle α in Fig. 2.2, relatively; χ_{kl} = aerodynamic admittance function.

The single mode uncoupled equilibrium equation in (2.2) for the *i*th mode can be rewritten with a new frequency ω_{i0}, a new damping ratio γ_i, and a buffeting force q_{ib} (Simiu and Scanlan, 1996) as

$$
\ddot{\xi}_i + 2\gamma_i\omega_{i0}\dot{\xi}_i + \omega_{i0}^2\xi_i = \frac{q_{ib}(t)}{I_i} \tag{2.36}
$$

and

$$\omega_{i0} = \omega_i^2 - \frac{\rho B^4 l}{2I_i}\omega^2 (H_3^* G_{h_i\alpha_i} + H_4^* G_{h_i h_i} + A_3^* G_{\alpha_i\alpha_i} + A_4^* G_{\alpha_i h_i}) \tag{2.37}$$

$$2\gamma_i\omega_{i0} = 2\xi_i\omega_i - \frac{\rho B^4 l}{2I_i}\omega (H_1^* G_{h_i h_i} + H_2^* G_{h_i\alpha_i} + P_1^* G_{p_i p_i} + A_1^* G_{\alpha_i h_i} + A_2^* G_{\alpha_i\alpha_i}) \tag{2.38}$$

The modal integrals G_{risi} are obtained by

$$G_{r_i s_i} = \int_{deck} r_i(x) s_i(x) \frac{d_x}{l},\ r_i, s_i = h_i, p_i \text{ or } \alpha_i \tag{2.39}$$

For the buffeting force $q_{ib}(t)$ defined as

$$q_{ib}(t) = \frac{1}{2}\rho U^2 B^2 l \int_{deck} \left[L_b(t) h_i(x) B + D_b(t) p_i(x) B + M_b(t) \alpha_i(x) \right] dx \tag{2.40}$$

Defining the Fourier transform of ξ_i (t) to be

$$\overline{\zeta}_i(\omega) = \lim_{T\to\infty} \int_0^T \xi_i(t) e^{-j\omega t} dt \tag{2.41}$$

and taking the Fourier transform of (2.36) yields the new system of equations such that

$$\left[\omega_{i0}^2 - \omega^2 + 2j\gamma_i\omega_{i0}\omega \right] \overline{\xi}_i = \frac{\rho U^2 \mathrm{B}^2 l}{2I_i} \int_{deck} \left[\varphi(x) \frac{\overline{u}(x,\omega)}{U} + \psi(x) \frac{\overline{w}(x,\omega)}{U} \right] \frac{dx}{l} \tag{2.42}$$

where

$$\varphi(x) = 2\left[\chi_{Lu} C_L h_i(x) + \chi_{Du} C_D p_i(x) + \chi_{Mu} C_M \alpha_i(x)\right] \tag{2.43}$$

$$\psi(x) = (\frac{dC_L}{d\alpha} + C_D)\chi_{Lw} h_i(x) + \frac{dC_M}{d\alpha}\chi_{Mw}\alpha_i(x) \tag{2.44}$$

Multiplying (2.42) by its complex conjugate and by 2/T, the result

$$\lim_{T\to\infty}\frac{2}{T}\left[(\omega_{i0}^2 - \omega^2)^2 + (2j\gamma_i\omega_{i0}\omega)^2\right]\overline{\xi}_i\overline{\xi}_i^* = (\frac{\rho U^2 \mathrm{B}^2 l}{2I_i})^2 \int\int_{deck} J(x_a, x_b, \omega)\frac{dx_a}{l}\frac{dx_b}{l} \tag{2.45}$$

where

$$\begin{aligned} J(x_a, x_b, \omega) = \lim_{T\to\infty}\frac{2}{T}\frac{1}{U^2}&\left[\varphi(x_a)\overline{u}(x_a,\omega) + \psi(x_a)\overline{w}(x_a,\omega)\right]\times \\ &\left[\varphi(x_b)\overline{u}^*(x_b,\omega) + \psi(x_b)\overline{w}^*(x_b,\omega)\right] \end{aligned} \tag{2.46}$$

For the power spectral density of ξ_i is defined as

$$S_{\xi_i\xi_i}(\omega) = \lim_{T\to\infty}\frac{2}{T}\overline{\xi}_i\overline{\xi}_i^* \tag{2.47}$$

in which the power spectrum for the *i*th generalized coordinate can be obtained (Simiu and Scanlan, 1996) as

$$S_{\xi_i \xi_i}(\omega) = \frac{(\frac{\rho U^2 \mathrm{B}^2 l}{2I_i})^2}{\left[1-(\frac{\omega}{\omega_{i0}})^2\right]^2 + \left[2\gamma_i \frac{\omega}{\omega_{i0}}\right]^2} \left[R_\varphi S_u(\omega) + R_\psi S_w(\omega)\right] \frac{1}{U^2} \qquad (2.48)$$

where

$$R_\varphi = \iint_{deck} \varphi(x_a)\varphi(x_b) e^{-C|x_a - x_b|/l} \frac{d_{xa}}{l} \frac{d_{xb}}{l} \qquad (2.49)$$

$$R_\psi = \iint_{deck} \psi(x_a)\psi(x_b) e^{-C|x_a - x_b|/l} \frac{d_{xa}}{l} \frac{d_{xb}}{l} \qquad (2.50)$$

where C = exponential decay function of the wind velocity fluctuation between two separate point a and b along the bridge deck; $S_u(\omega)$ and $S_w(\omega)$ = power spectral density functions of the wind velocity fluctuations u and w, respectively.

The mean square of the generalized response can be obtained accordingly:

$$\sigma_{\xi_i}^2 = \int_0^\infty S_{\xi_i \xi_i}(\omega) d\omega \qquad (2.51)$$

and the global responses with respect to vertical, lateral and torsional directions can be combined from single-modal responses due to the squared root of the sum of the squares (SRSS) principle as follows:

$$\sigma_h(x) = sqrt(\sum_{i=1}^{N} h_i^2 B^2 \sigma_{\xi_i}^2), \sigma_p(x) = sqrt(\sum_{i=1}^{N} p_i^2 B^2 \sigma_{\xi_i}^2), \sigma_\alpha(x) = sqrt(\sum_{i=1}^{N} \alpha_i^2 \sigma_{\xi_i}^2) \qquad (2.52)$$

The maximum response for the *i*th mode can be calculated as a peak factor times *i*th RMS response. The peak factor k_p is defined (Strømmen, 2010) as

$$k_p = \sqrt{2 \times \ln[f_x(0) \times T]} + \frac{0.577}{\sqrt{2 \times \ln[f_x(0) \times T]}} \tag{2.53}$$

where

$$f_x(0) = \frac{1}{2\pi} \times \frac{\int_0^\infty \omega^2 S_x(\omega) d\omega}{\int_0^\infty S_x(\omega) d\omega} \tag{2.54}$$

and T is set to be 10 min in a full scale.

Chapter 3

Investigated bridge

3.1 Bridge description

The cable-stayed suspension bride (CSSB) is a road and railway bridge as an example bridge. The CSSB has a main span of 1408 m and two side spans of 378 m as shown in Fig. 3.1(a). The main span consists of the cable-stayed portion of 1096m and the suspension portion of 312m. In the side span, four intermediate piers are installed in order to increase in-plane flexural rigidity of bridge. The cable system consists of the main cables, hangers and stay cables. The distance of two main cables is 13.5m, the cable sag to span ratio is 1/6.5, and the hanger is spaced at 24m. The stay cables are anchored to the deck at 15m intervals in side spans and 24m in the main span. The deck shown in Fig. 3.1(b) is a streamlined box girder with 58.5 m wide and 5.2 m high. The main span and side span decks consist of steel and pre-stressed concrete, respectively. The pylon is A-shape concrete leg with a transverse beam, and its height is 322 m as shown in Fig. 3.1(c). Total 9 cross sections for concrete decks of side span and 11 cross sections for steel decks of main span are defined. The sectional and material properties are listed in Table 3.1.

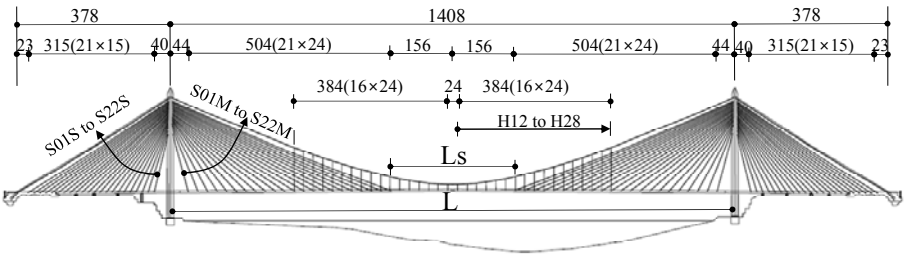

(a) Side view (plan)

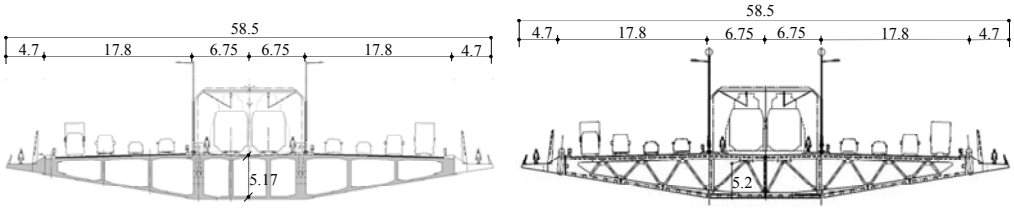

General section of concrete box in side span

General section of steel box in main span

(b) Girder cross-section

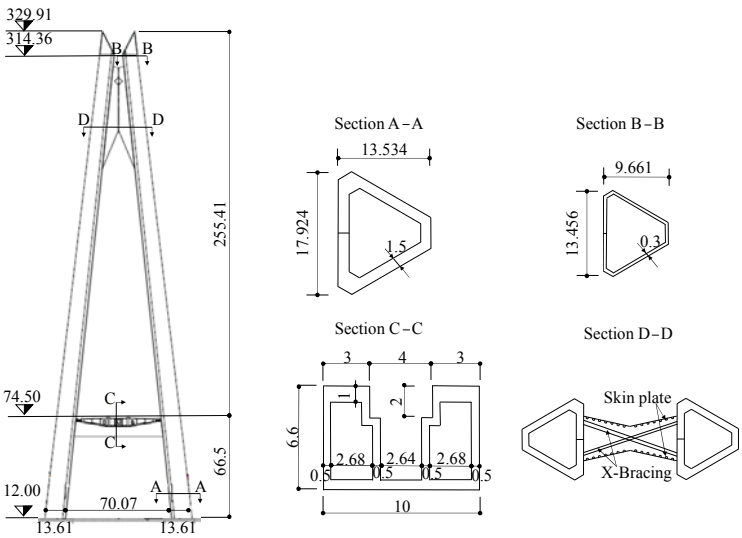

(c) Pylon

Fig. 3. 1 Layout of investigated bridge with a main span of 1408 m (unit: m)

Table 3. 1 The cross-sectional properties of cable-stayed suspension bridge

Structural members	E (MPa)	A (m^2)	I_x (m^4)	I_y (m^4)	I_z (m^4)	m (ton/m)	Im (ton·m^2/m)	Remark
Girder side span	2.2×10^4	51.21 ~65.07	471.89 ~612.35	8399.3 ~10248	155.67 ~201.2	154.65 ~294.3	25878 ~45347	
Girder main span	2.1×10^5	3.04 ~7.48	25.92 ~33.27	756.4 ~1632.2	11.76 ~27.07	43.45 ~98.82	11013 ~25975	
Pylon-bottom	2.2×10^4	72.77	2405.8	1431.9	1871.2	181.91	-	A-A
Pylon-top	2.2×10^4	35.87	737.46	385.9	551.94	89.68	-	B-B
Pylon-transverse	2.2×10^4	35.87	737.46	385.9	551.94	62.60	-	C-C
Pylon-top bracing	2.1×10^5	35.87	737.46	385.9	551.94	0.53	-	D-D
Main cable side span	2.0×10^5	35.87	-	-	-	2.785	-	
Main cable main span	2.0×10^5	35.87	-	-	-	2.580	-	
Hangers	2.05×10^5	0.004 ~0.014	-	-	-	0.036 ~0.119	-	H12 to H28
Stay cable side span	1.95×10^5	0.012 ~0.023	-	-	-	0.110 ~0.206	-	S01S to 22S
Stay cable main span	1.95×10^5	0.010 ~0.021	-	-	-	0.089 ~0.194	-	S01M to 22M

Notes: E – elastic modulus; A - sectional area; I_x - torsional moment inertia; I_y - lateral moment inertia; I_z - vertical moment inertia; m – mass per unit length; Im – mass moment of inertia per unit length.

3.2 Initial equilibrium state for the example bridge

The reasonable completed dead load state of the example bridge is determined using the proposed practical method as mentioned in Chapter 2. In the configuration analysis, it is assumed that hanger of H12 to H22 in the transition part has an equal dead load distribution rate, as shown in Fig. 3.2.

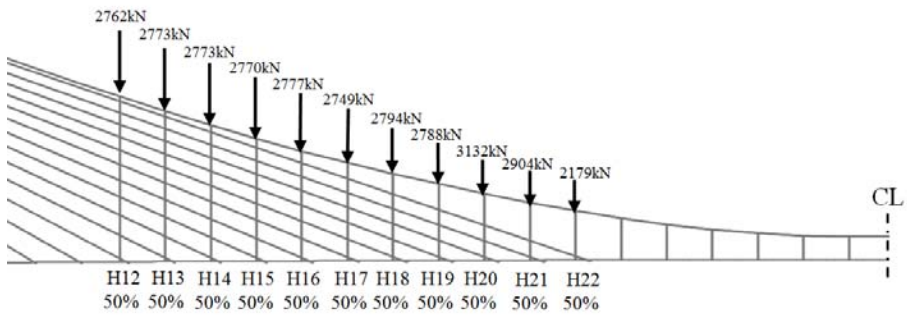

Fig. 3. 2 A dead loads distribution rate for hangers in the transition part

The tensions of stay cables and hangers are compared with initial design value as reference. The comparison results are shown in Fig. 3.3 and 3.4. Fig. 3.3 shows the equivalent tension of stay cables by this study compared with the initial design value. As shown in Fig. 3.3, the results at the near to pylon and the center of mid-span by this study are a little larger than initial design value. The distribution of equivalent tension of hangers is close to that of initial design value, as shown in Fig.

3.4. The results show that the practical method works well for the completed dead load state of the example bridge.

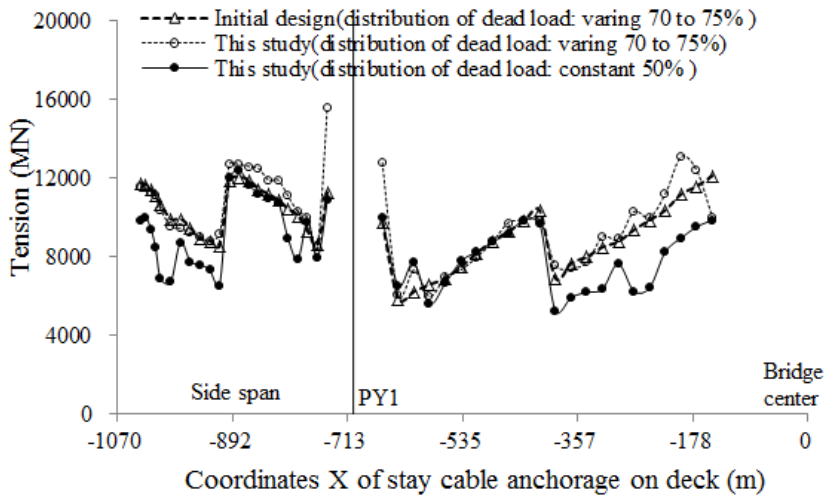

Fig. 3. 3 Distribution of equivalent tensions of stay cables in example bridge

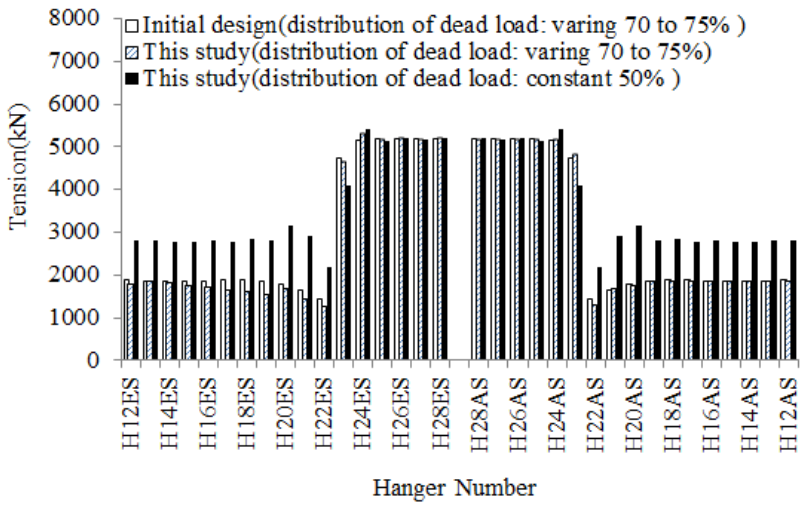

Fig. 3. 4 Distribution of equivalent tensions of hangers in example bridge

3.3 Initial equilibrium state for the parametric study analysis models

In order to investigate the structural behaviors considering different suspension-to-span ratio for cable-stayed suspension bridges, seven bridge models with the same design conditions of the example bridge are designed based on added or removed stay cables and hanger in both structural parts, the cable-stayed parts and suspended part, as shown in Fig. 3.5. Table 3.2 listed seven bridge analysis models which are designed to modify the example CSSB model in section 3.1.

Table 3. 2 Analysis cases for parametric study

Analysis case	Suspension portion length(m)	Suspension-to-span ratio
Ls/L=0.00	0(Cable-stayed br.)	0.00
Ls/L=0.22	312(As-built)	0.22
Ls/L=0.45	647	0.45
Ls/L=0.56	792	0.56
Ls/L=0.66	936	0.66
Ls/L=0.77	1080	0.77
Ls/L=1.00	1408(Suspension br.)	1.00

Notes: Ls - Length of suspension portion, L- Length of main span

Ls/L=0.00 as a partially earth-anchored cable-stayed bridge, the pylon height should be changed in order to enhance the efficiency of stay cables due to the increase inclining angles of stay cables. However, the pylon height has fixed for the

purposes of comparison with cable-stayed suspension bridges. Furthermore, a pure suspension model of Ls/L=1.00, the concrete deck of side spans are required with a view of back stay for cable-stayed bridges but not effective in structural viewpoint. However, the same design conditions of side spans have applied like other bridge models for the comparison purposes. Also, the distance of two main cables is 49.6m and vertical hangers are attached along the edge of the bridge deck in analysis case of Ls/L=1.00.

Detailed illustrations for the arrangement of the stay cables and hangers in seven bridge models are shown as follows:

Analysis model of Ls/L=0.00 has 112 pairs of stay cables, where 11 pairs of them are partially earth-anchored in each side span. Ls/L=1.00 has 56 pairs of hangers in the center of main span. In model Ls/L=0.2 has 88 pairs of stay cables where 5 pairs of them are partially earth-anchored in each side span, and 12 pairs of hangers in the center of main span. 15 pairs of stay cables in both side span and main span and 26 pairs of hangers in main span are installed in Ls/L=0.45. In the case of Ls/L=0.56 to Ls/L=0.77, the pairs of stay cables installed descend as 12 to 6 by 3 in both side span and main span while the pairs of hangers on main span ascend from 32 to 44 by 6. This is illustrated in Fig. 3.5.

(a) Ls/L=0.00, Ls=0m

(b) Ls/L=0.22, Ls=312m

(c) Ls/L=0.45, Ls=647m

(d) Ls/L=0.56, Ls=792m

(e) Ls/L=0.66, Ls=936m

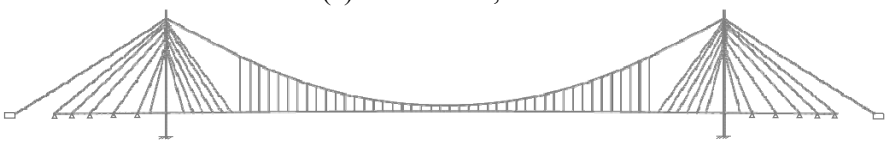

(f) Ls/L=0.77, Ls=1080m

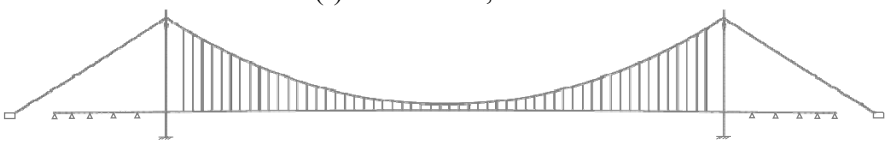

(g) Ls/L=1.00, Ls=1408m

Fig. 3. 5 Finite element models for parameter study

Seven bridge analysis models are developed as a simplified three-dimensional (3-D) FE models. The deck and pylon members are modeled by a 3-D frame element (Kim et al. 2004) and stay cables, main cables and hangers are modeled by elastic catenary cable element (Irvine, 1981) , as shown in Fig 3.2.

Initial equilibrium state under completed dead load is found by practical methods mentioned in Chapter 2, and the results are compared as follows.

Fig. 3.6 shows the distribution of axial forces in the deck. At the near to pylon of deck are large compressive forces in all the models. In the deck of the earth-anchored analysis cases of Ls/L=0.00 and Ls/L=0.22 are in compression and tension at the same times. The model Ls/L=0.00 has a large number of earth-anchored stay cables, and the peak of the tension in the deck is significantly larger. As the suspension-to-span ratio increases, both compressive forces and tension in the deck decreases, which improves the structural stability and saves materials.

Fig 3.7 illustrates vertical bending moment of the deck. All of the bridge analysis models represent a similar trend with a small difference in value. The maximum and minimum vertical bending moment of the deck is found at the near to pylon and subsidiary piers of side spans.

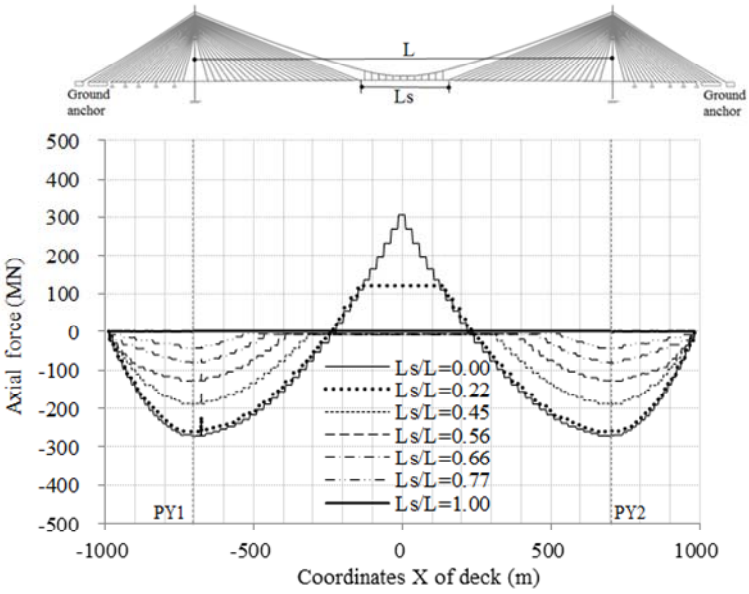

Fig. 3. 6 Distribution of axial forces in deck under dead load

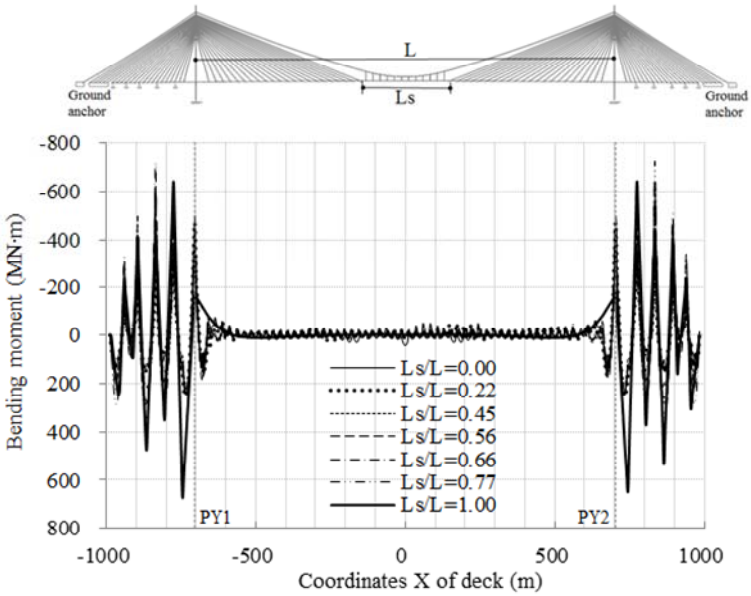

Fig. 3. 7 Distribution of vertical bending moment of deck under dead load

Table 3.3 gives the horizontal tension of main cable. As the increase of suspension-to-span ratio, the horizontal tension of main cable also increases. This is because the distributed dead load of the deck is transferred to main cables by hangers is increased. The horizontal tension of main cable for bridge model of Ls/L=0.22 is 41% compared to bridge model of Ls/L=1.00 as a pure suspension bride.

Table 3. 3 Comparison of Horizontal tension in main cables under dead load

Analysis case	Horizontal tension(MN)	Ratio
Ls/L=0.00	-	-
Ls/L=0.22	120.1	0.41
Ls/L=0.45	208.0	0.71
Ls/L=0.56	235.0	0.80
Ls/L=0.66	257.0	0.88
Ls/L=0.77	274.0	0.94
Ls/L=1.00	292.0	1.00

Notes: Ls - Length of suspension portion, L- Length of main span

The tension of stay cable in main span increases from pylons to bridge center or the end of side span in the analysis case from Ls/L=0.00 to Ls/L=0.77, as shown in Fig 3.8. The tension of stay cable in side span decreases as the increase of suspension-to-span ratio under dead load. Because, as previously mentioned, the longer suspension part enlarges a load distribution on main cable so that it reduces load distribution of stay cables in main span. Accordingly, the tension of stay cable in main span is reduced, and also reduces the tension of stay cables in side spans

with the same rate.

As shown in Fig. 3.9, the tension of the hanger is constant in the main span in the analysis cases from Ls/L=0.22 to Ls/L=1.00. But the largest tension is found at the longest hanger in Ls/L=1.00 as a pure suspension bride which is largest tension than others due to different load condition.

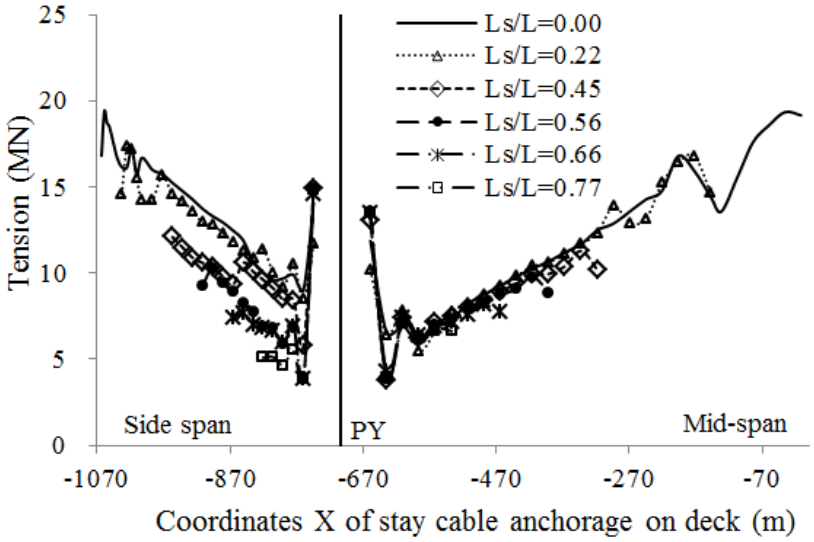

Fig. 3. 8 Distribution of cable forces in stay cables under dead load

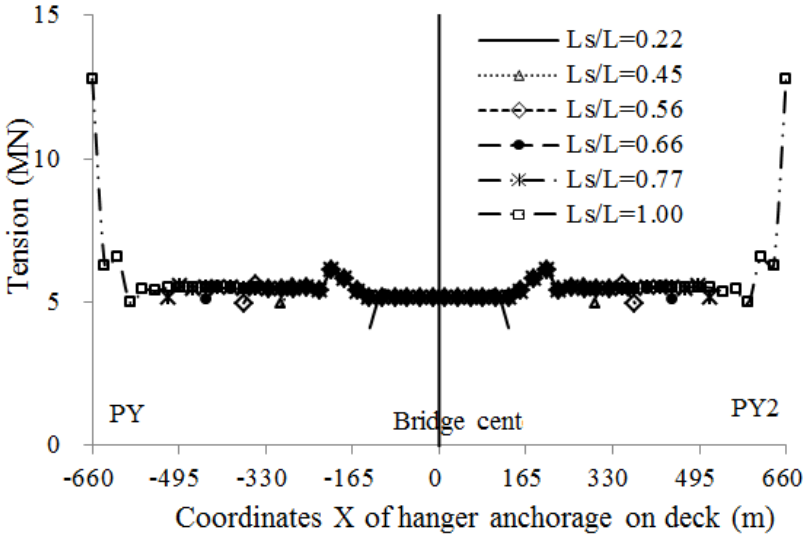

Fig. 3. 9 Distribution of cable forces in hangers under dead load

Chapter 4

Design parameter study on structural performance of cable-stayed suspension bridge under live load and wind load

Considering train load in long-span cable-supported bridges, the bridge has to satisfy the rigorous vertical deflection criteria under service load. The cable-stayed suspension bridge (CSSB) can improve the vertical stiffness by additional stay cable, and becomes an alternative structure. In order to comprehensively understand and a realistically predict the structural behavior of CSSB, parametric study is carried out with seven bridge analysis models considering different suspension-to-span ratio. The scheme of suspension-to-span ratio (Ls/L) shows in Fig. 4.1. Investigated bridge analysis models are developed as a simplified three-dimensional (3-D) FE models, as shown in Fig 3.5.

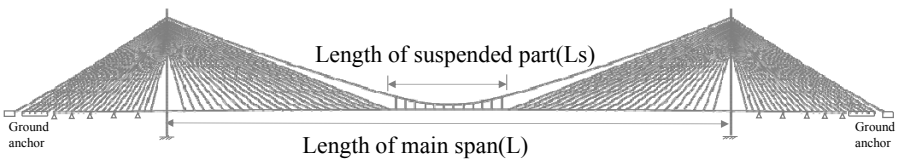

Fig. 4. 1 The scheme of suspension-to-span ratio (Ls/L)

For the parametric study, two design parameters, the suspension-to-span ratio and length of transition part are considered and studied for their effects on the structural behavior under live loads consisting of trains and road vehicles and wind load.

The design live road is consist of a uniform lane load *w* and truck load based on the Korean Highway Bridge Design Code (Limit State Design) – Cable Supported Bridges (KBDC, 2015) as shown in Fig 4.2.

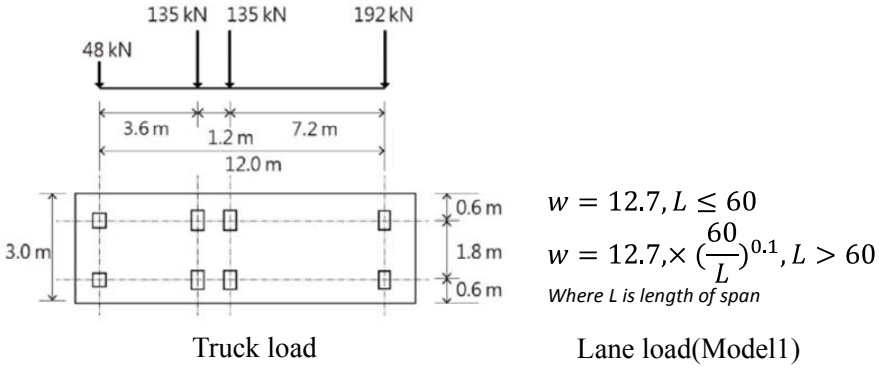

Fig. 4. 2 Road model in KBDC 2015

For the design train load consists of a uniformly distributed load 80kN/m and 4 point loads of 250 kN based on LM 71 of Eurocodes1 (CEN, 2003), as shown Fig. 4. 3.

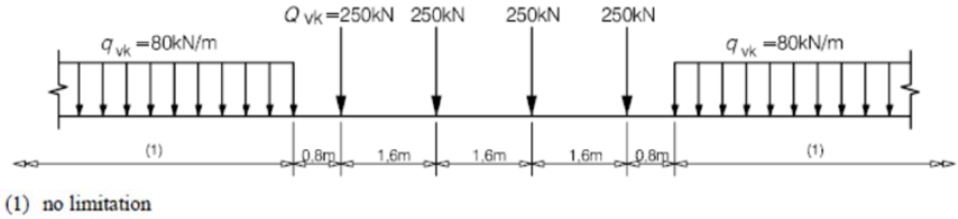

Fig. 4. 3 Train load model LM71 in EC1-EN1991-2

In the analysis, two live load cases LC1 and LC2 are considered as shown in Fig 4.4. In the load case LC1, the road vehicle loads in the mid-span and the train loads in 400m length at the center of mid-span are loaded in order to consider the maximum deflection at the center of main span. In the second case, the only one side quarter of mid-span is loaded to consider the maximum longitudinal slope of the deck.

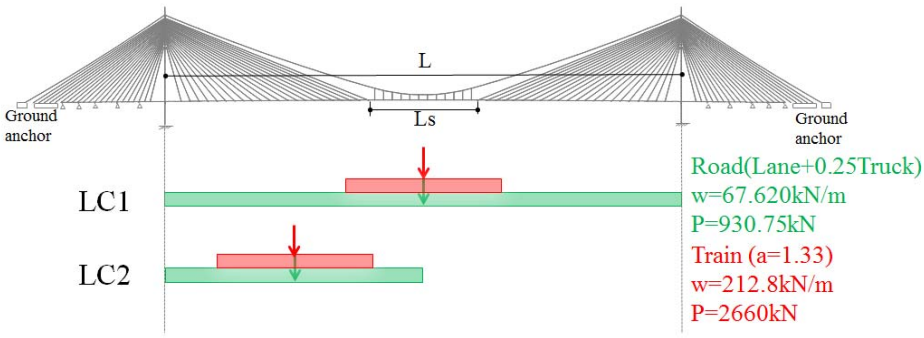

Fig. 4. 4 Live load cases

For all live load cases, 2 train track and 10 traffic lane are loaded together. For

road vehicle, a uniform lane load of w=67.620 kN/m and truck load as a concentrated load of 930.75 kN considering multi-lane reduction factor are considered based on the Korea Bridge Design Code (Limit State Design) for cable-supported bridge (KBDC, 2015). For train load, a uniformly distributed loads 212.8 kN/m and 4 point loads as a concentrated load of 2660 kN with α=1.33.

For the aerostatic stability analysis, the aerostatic drag (D), lift (L), and pitching moment (M) components of wind load are considered to be acted on the bridge deck under wind attack angles of 0°, as shown in Fig. 2.7. The following three components of wind load are as follow

$$\begin{aligned} D(\alpha) &= 0.5\rho V^2 B C_D(\alpha) \\ L(\alpha) &= 0.5\rho V^2 B C_L(\alpha) \\ M(\alpha) &= 0.5\rho V^2 B^2 C_M(\alpha) \end{aligned} \tag{4.1}$$

where α = wind attack angle; ρ = the air density; V = wind velocity; B = width of deck; C_D, C_L, and C_M = aerostatic coefficients of drag, lift, and pitching moment, respectively.

The aerostatic coefficients are obtained from wind tunnel test (Greisch, 2013), as listed in Table 4.1. Wind load action on the cables and pylons only considered the drag component, and the corresponding drag coefficient is 0.7 for cables and ranging from 0.824 to 1.038 for pylons.

Table 4. 1 Aerostatic coefficients

Members	C_D (0°)	C_L (0°)	C_M (0°)	C_D' (-2°~2°)	C_L' (-2°~2°)	C_M' (-2°~2°)	Note
Deck	0.0521	-0.2964	-0.0118	-0.2029	5.7339	1.3904	Wind tunnel
Main cable	0.7	-	-	-	-	-	Circular shape
Stayed cable	0.7	-	-	-	-	-	
Hanger	0.7	-	-	-	-	-	

The design wind velocity (V_z) depending on the height of z is given by power law (KBDC, 2015) as follow

$$V_z = 1.925 \times (\frac{Z}{500})^{0.12} \times V_{10},\ \mathrm{Z} \geq \mathrm{Z}_b \tag{4.2}$$

where V_{10} = wind velocity at a height of 10m; Z_b =5m.

4.1 Suspension-to-span ratio effects under live load

Based on the initial equilibrium state of seven bridge analysis models from Chapter 3, nonlinear static analysis was conducted for those models and displacement and internal forces were obtained. After that the responses is compared with seven bridge analysis models and discussed.

(1) Responses of deck

The vertical displacement of analysis case $L_S/L=0.22$ due to load case LC1, as shown in Fig. 4.5. The maximum vertical displacement of 3.26m at mid-span of deck under train load is larger than road vehicle load, and the difference of maximum vertical displacement is about 58%. These figures clearly indicate that the loading effect of train is dominant in the vertical deflection.

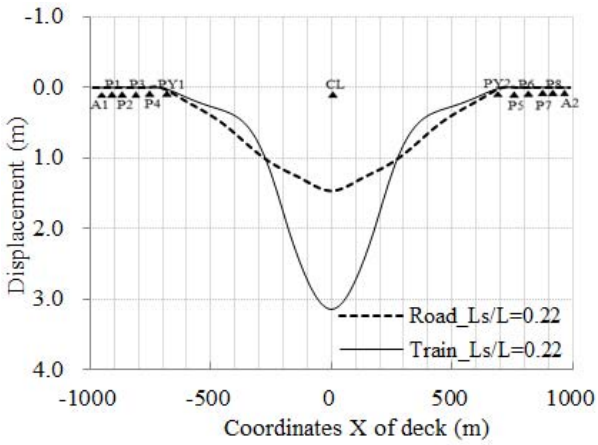

Fig. 4. 5 Vertical displacement of deck under LC1 for Ls/L=0.22

The vertical displacement of analysis models are compared with two live load cases. Load cases LC1 and LC2 as show in Fig 4.5 and 4.6, respectively. With the increase of suspension-to-span ratio, the vertical displacement at the center of mid-span of deck and at the quarter of mid-span gradually increases under two live load cases, as shown in Fig 4.6 and Fig 4.7. The minimum value of the vertical displacement of deck is found at the Ls/L=0.22(with suspended part length being 312m) under load case of LC1 and LC2.

Table 4.2 shows the vertical displacement of deck under combined maximum responses of LC1 and LC2. With the increase of suspension-to-span ratio, the maximum vertical displacement at the center of mid-span of deck gradually increases. The most effective in restricting the live load deformation occurs at the suspension-to-span ratio of 0.22, and the ratio of mid-span to maximum vertical displacement (L/δ_{max}) is 316.

Table 4. 2 The vertical displacement of deck under combined maximum response of LC1 and LC2

Analysis case	L/2(m)	δmax(m)	L/δmax
Ls/L=0.00	7.287	7.728	193
Ls/L=0.22	4.450	4.450	316
Ls/L=0.45	6.100	6.100	231
Ls/L=0.56	6.480	6.480	217
Ls/L=0.66	7.730	7.730	191
Ls/L=0.77	7.920	8.190	172
Ls/L=1.00	8.810	9.160	154

Notes: Ls - Length of suspension portion, L- Length of main span

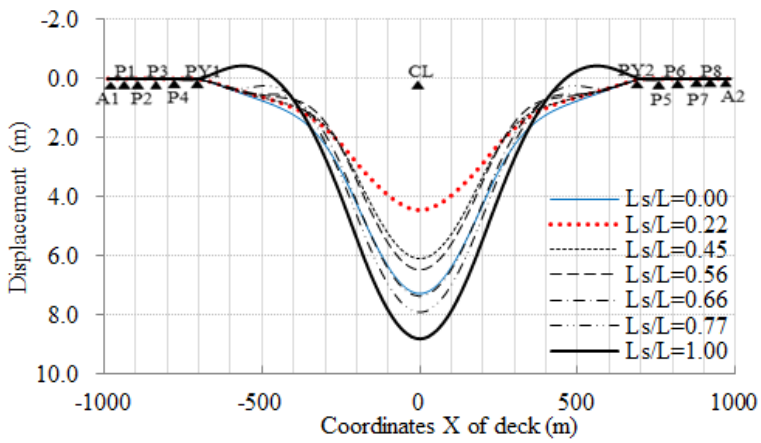

Fig. 4. 6 The vertical displacement of deck under LC1

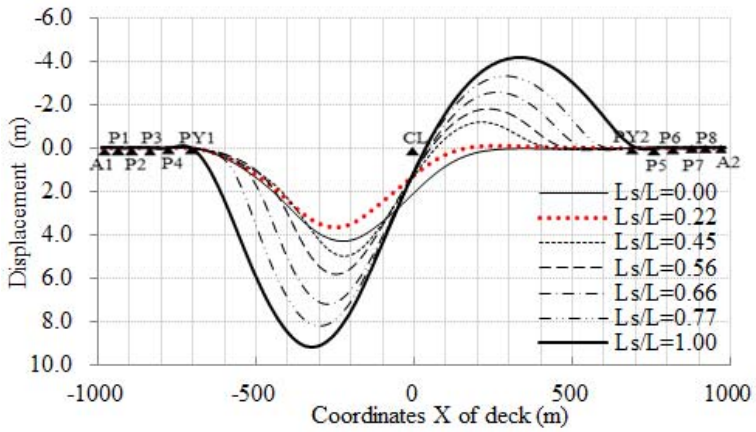

Fig. 4. 7 The vertical displacement of deck under LC 2

The maximum longitudinal slope of deck under LC2 including initial slope of deck is shown in Fig. 4.8. The maximum longitudinal slope of deck in Ls/L=0.22 is smallest and within the allowable deformation angle. The maximum longitudinal slope of deck gradually increases with the increase of suspension-to-span ratio due

to the decreased vertical rigidity.

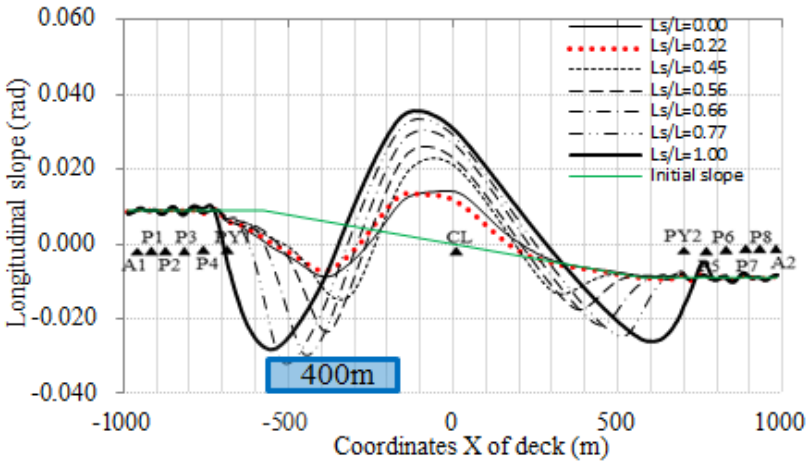

Fig. 4. 8 The maximum longitudinal slope of deck under LC 2

Table 4.3 shows the averaged slope of deck over the length of the train (400m) under LC2. With the increase of suspension-to-span ratio, the maximum longitudinal slope of deck gradually increases.

Table 4. 3 The maximum longitudinal slope of the deck under LC2

Analysis case	Maximum (rad)	Minimum (rad)	Averaged in the length of train (rad)	Allowable (rad)
Ls/L=0.00	0.0114	-0.0088	-0.0023	
Ls/L=0.22	0.0132	-0.0072	-0.0003	
Ls/L=0.45	0.0170	-0.0149	-0.0038	±0.016
Ls/L=0.56	0.0223	-0.0235	-0.0049	
Ls/L=0.66	0.0273	-0.0298	-0.0065	
Ls/L=0.77	0.0313	-0.0321	-0.0053	
Ls/L=1.00	0.0341	-0.0282	0.0000	

Notes: Ls - Length of suspension portion, L- Length of main span

Fig. 4.9 shows the vertical bending moment of deck under LC2. In the deck, the maximum negative vertical bending moment, 1450 MN·m, is found at the Ls/L=1.00 as a pure suspension bridge. Along with the increase of suspension-to-span ratio, the maximum negative vertical bending moment of deck at the junction sharply increases due to the stiffness difference of suspended part and cable-stayed parts. It indicates that transition part have to be set up to improve the stiffness transition of the deck between the cable-stayed part and suspended part.

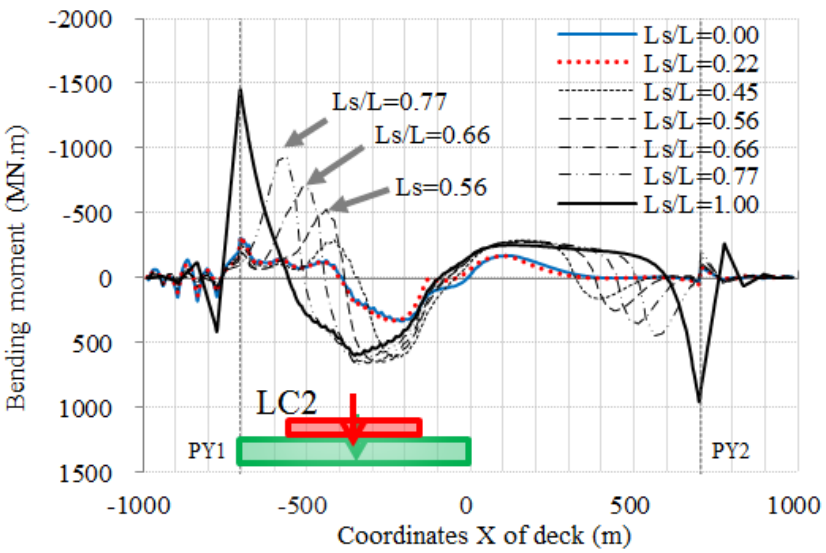

Fig. 4. 9 The vertical bending moment of deck under LC 2

In terms of two aspects of maximum vertical deformation and longitudinal slope of deck, the effective suspension-to-span ratio is about 0.22 to 0.56, this is to improve vertical rigidity for serviceability under train load.

(2) Responses of pylon

The responses of pylon are shown under combined maximum value of live load cases of LC1 and LC2, as listed in Table 4.4. As the suspension-to-span ratio changes from 0.22 to 1.00, the longitudinal displacement at the top of pylon under live load cases increases, which indicates that the vertical rigidity of the bridge structure becomes smaller. The maximum longitudinal displacement at top of pylon equal to 1.117m is found at the Ls/L=0.00 as a pure cable-stayed bridge. The minimum bending moment of pylon base equal to -524 MN·m occurs at the analysis model of Ls/L=0.00, and the difference between analysis model of Ls/L=0.00 and Ls/L=1.00 is about 59%.

Table 4. 4 Responses of pylon under combined maximum value of LC1 and LC2

Analysis case	Longitudinal displacement at top of pylon(m)	Ratio	Bending moment of pylon base(MN·m)	Ratio
Ls/L=0.00	1.117	1.56	-524	0.41
Ls/L=0.22	0.496	0.69	-665	0.52
Ls/L=0.45	0.54.	0.76	-917	0.71
Ls/L=0.56	0.517	0.72	-923	0.72
Ls/L=0.66	0.596	0.83	-1046	0.81
Ls/L=0.77	0.641	0.89	-1103	0.86
Ls/L=1.00	0.717	1.00	-1285	1.00

Notes: Ratio is calculated by using the displacement or bending moment responses of Ls/L=1.00 as a reference

(3) Responses of main cables

Table 4.5 gives the cable tension of main cable under combined maximum value of LC1 and LC2. The maximum horizontal tension of main cable at the center of mid-span gradually increases due to the increased vertical load transmission to the main cable by hangers with the increase of suspension-to-span ratio. The minimum horizontal tension of main cable at mid-span is found at Ls/L=0.22 and 33% lower than that of Ls/L=1.00 as a pure suspension bridge. The live load-to-dead load ratio of horizontal tension of main cable for all of analysis cases are mostly in the range of 0.29 to 0.47.

Table 4. 5 Horizontal tension of main cable under combined maximum value of LC1 and LC2

Analysis case	Main cable tension at mid-span(MN)		Ratio
	Dead load	Maximum live load	(Live load/Dead)
Ls/L=0.00	-	-	-
Ls/L=0.22	120.1	57.0	0.47
Ls/L=0.45	208.0	80.6	0.39
Ls/L=0.56	235.0	79.4	0.34
Ls/L=0.66	257.0	86.2	0.34
Ls/L=0.77	274.0	86.8	0.32
Ls/L=1.00	292.0	85.0	0.29

Notes: the ratio is expressed as each result of live load divided by dead load

(4) Responses of stay cables

The distribution of the maximum tension of stay cables shows under combined maximum values of LC1 and LC2, as found in Fig. 4.10. Along with the increase

of suspension-to-span ratio, the maximum tension of stay cables at the mid-span is gradually increasing. As the suspension-to-span ratio changes from 0.45 to 0.77, the maximum tension of stay cable under live loads are found at the longest stay cable near to junction.

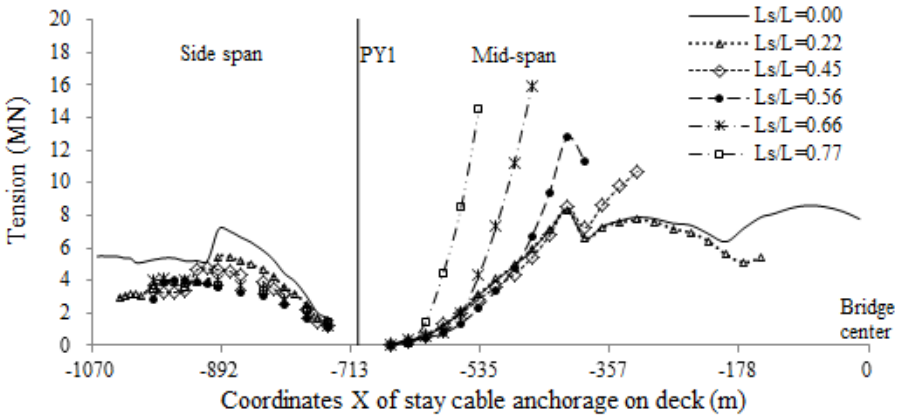

Fig. 4. 10 Tension of stay cables under combined maximum response of LC1 and LC2

(5) Responses of hangers

The distribution of the maximum tension of hanger is found at the longest hanger near to junction, as shown in Fig. 4.11. It means that the fatigue problem might occur due to the stiffness difference of suspended part and cable-stayed parts in mid-span of cable-stayed suspension bridge. Therefore, the stress amplitude of the longest hanger at the junction should be verified under fatigue load, and some structural measures should be determined for overcoming the problem of stiffness

transition between cable-stayed parts and suspended part.

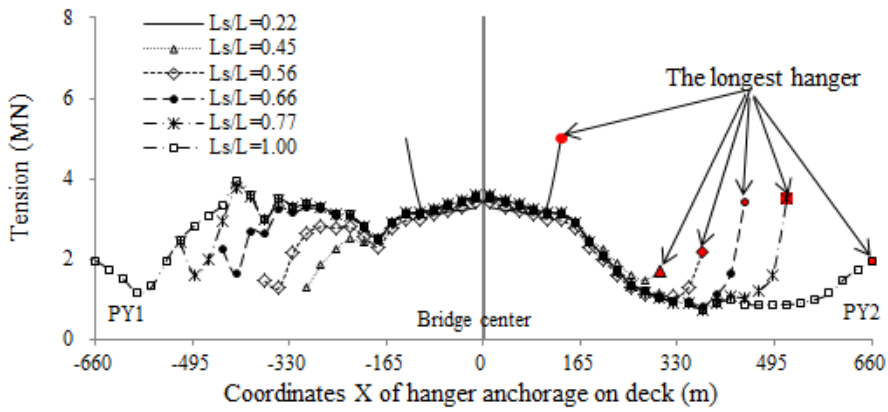

Fig. 4. 11 Tension of hangers under combined maximum response of LC1 and LC2

4.2 Effect of transition part under live load

A sudden change of stiffness at junction between stay-cable parts and suspended part cause sharply increase of negative bending moment on deck and the tension amplitude of the longest hanger near to the junction, which can lead to fatigue problem. As a structural improvement suggestion to mitigate the severe stiffness change on the junction part, additional hangers on the cable-stayed part is considered. These hangers are called crossing hangers. The scheme of transition part-to-cable-stayed part ratio (L_t/L_c) shows in Fig. 4.12. In order to investigate the effect of the transition part, the ratio of transition part to cable-stayed part is changed from 0 to 0.45, by adding crossing hangers in the cable-stayed part based on the structural system of Ls/L=0.22, as shown in Fig. 4.13. One of the design parameters for transition parts is the dead load distribution ratio for each pair of stay cables and hangers at the same point on the deck. In order to investigate the effect of the load distribution ratio in the transition parts, four different load distribution ratios are considered in parameter study, as shown in Fig. 4.14.

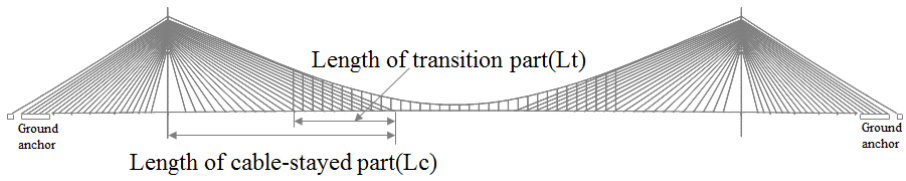

Fig. 4. 12 The scheme of transion part-to-cable-stayed part ratio (Lt/Lc)

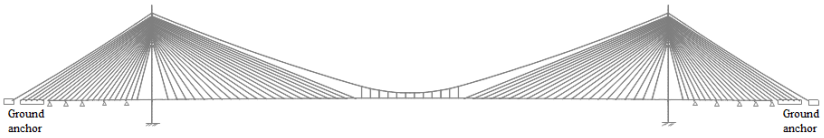

(a) Lt/Lc =0(No transition part)

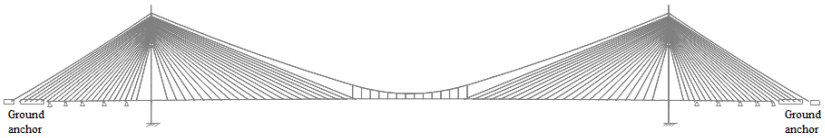

(b) Lt/Lc =0.02; 1 crossing hangers

(c) Lt/Lc =0.14; 4 crossing hangers

(d) Lt/Lc =0.32; 8 crossing hangers

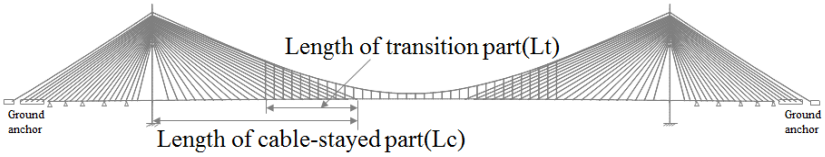

(e) Lt/Lc =0.45; 11 crossing hangers

Fig. 4. 13 FE analysis model for the verified effect of transition ratio

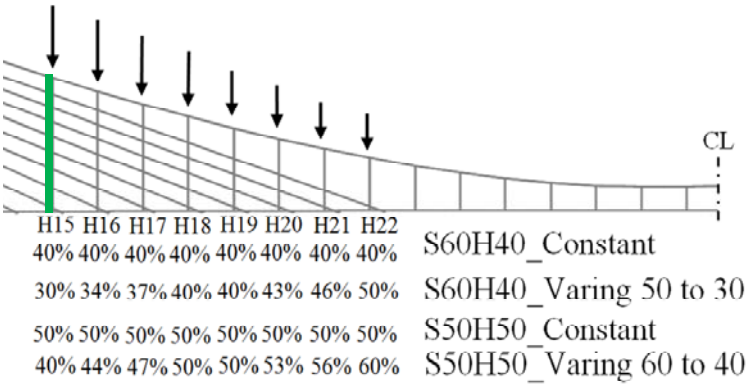

Fig. 4. 14 Analysis case of the load distrinution ratio at the transion parts

A train load, which has a strong effect on a tension of stay cables and hangers, is considered in the fatigue analysis. Moving load analysis is carried out based on a linearized finite displacement analysis by a commercial program of Midas Civil. The transition parts ratio and dead load distribution at the transition parts are studied with respects of the amplitude of longest hanger tension and secondary stress of main cable, and recommend value for these parameters on condition of this parametric study results.

(1) Effect of transition part ratio

Fig 4.15 gives the amplitude of hanger tensions according to the variation of transition part under equal dead load distribution ratio for cable-stayed parts and suspended part. As the transition part increases, the amplitude of the longest hanger tension reduces.

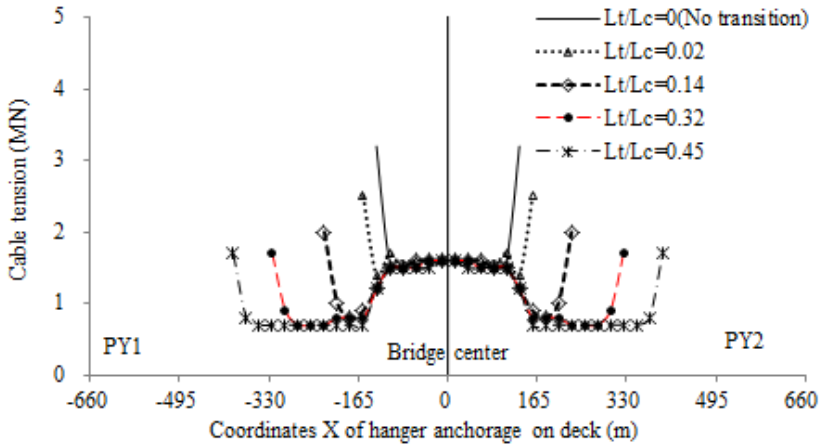

Fig. 4. 15 Effect of transition part for the amplitude of hanger tension

Fig 4.15 gives the amplitude of hanger tensions according to the variation of transition part. As the transition part increases, the amplitude of the longest hanger tension reduces.

In order to evaluate the longest hanger fatigue strength, the fatigue damage due to train load investigates based on the equivalent stress method in EN 1991-2. The simplified λ-method in Eurocode is an adaption of the general equivalent stress range concept corrected by various λ-factors. The verification of fatigue strength is expressed as:

$$\lambda_{Ff} \times \lambda \times \Delta\sigma_{LM71} \leq \frac{\Delta\sigma_c}{\lambda_{Mf}} \tag{4.3}$$

where λ_{Ff} = the partial safety factor for fatigue loading, λ_{Mf} = the partial safety factor for fatigue strength, $\Delta\sigma_{LM71}$ = the stress range associated to load model 71, and λ = the fatigue damage equivalent factor related to $2 \cdot 10^6$ cycles

With increased transition ratio, the fatigue damage of the longest hanger decreases and ensured the fatigue strength, as listed in Table 4.6.

Table 4. 6 The fatigue damage for the longest hanger at the transition parts

Analysis case	Stress range of the longest hanger $\Delta\sigma_{71}$(Mpa)	Equivalent stress range $\Delta\sigma_{E,2}$(Mpa)	Fatigue damage D<1.0
Lt/ Lc =0.00	238	145	1.2
Lt/ Lc =0.02	186	113	0.3
Lt/ Lc =0.14	149	91	0.1
Lt/ Lc =0.32	127	77	0.03
Lt/ Lc =0.45	127	77	0.03

Fig 4.16 gives the secondary stress (Lee and Kim, 2015) of main cable at the cable bands of first and center position under equal dead load distribution ratio at the transition parts. The maximum secondary stress of main cable at the position of center band is largest and within the allowable stress. As the transition part increases, the secondary stress of main cable at the position of center band reduces.

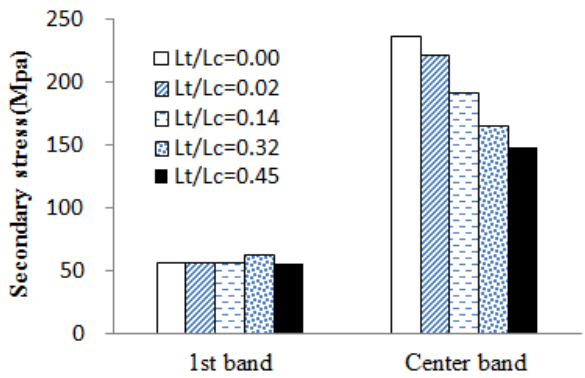

Fig. 4. 16 Secondary stress of main cable at cable bands with transiton ratio

(2) Effect of dead load distribution ratio in the transition parts

The maximum tension amplitude of the longest hangers for analysis cases considered the different dead load distribution ratio, as listed in Table 4.7. S60H40_Constrant, which is applying a constant dead load distribution ratio to 40% for hangers in transition parts, is smallest (1.31Mpa) and within the allowable fatigue strength.

Table 4. 7 The fatigue damage for the longest hanger at the transition parts

Analysis case	Amplitude of tension(MN)	Ratio	Fatigue damage D<1.0
S60H40_Constant	1.31	0.85	0.01
S60H40_Varing(50to30%)	1.48	0.96	0.01
S50H50_Constant	1.35	0.88	0.01
S50H50_Varing(60to40%)	1.54	1.00	0.02

Fig 4.17 gives the secondary stress of main cable at the cable bands of first and center position under different dead load distribution ratio at the transition parts. The maximum secondary stress of main cable at the position of center band is largest and within the allowable stress. Based on the secondary stress of main cable, analysis models of S50h50_Constant is promising to reduce the secondary stress of main cable.

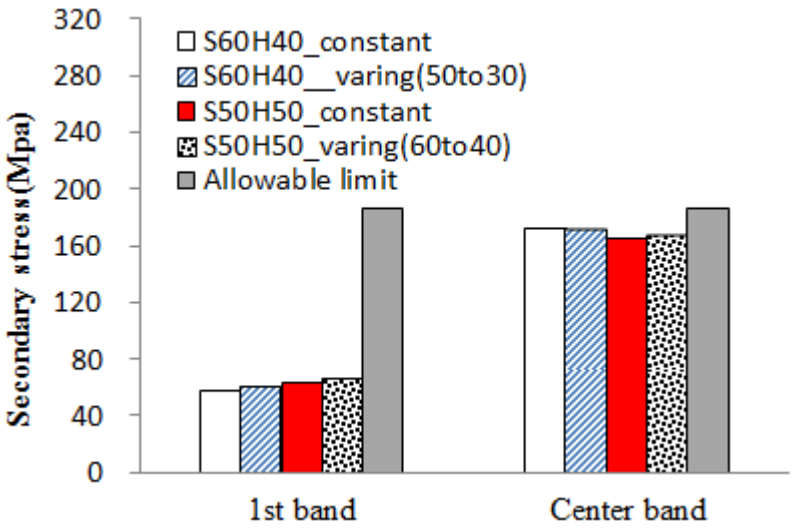

Fig. 4. 17 Secondary stress of main cable at cable bands with different load distribution ratio

In conclusion, a set-up of transition part can reduce the amplitude of hanger tension and secondary stress of main cable. The result shows that 32% of transition part-to-cable-stayed part ratio (L_t/L_c) is more effective to mitigate tension amplitude of the longest hanger. However, the tension amplitude of longest hanger turns to increase when transition part exceeds 32%. This characteristic should be considered to design of transition part in cable-stayed suspension bridges. In order to reduce the secondary stress of main cable, equal dead load distribution of each pair of stay cables and hangers at the same point on the deck is effective.

4.3 Dynamic characteristics

The seven bridges analysis models with various suspension-to-span ratio have conducted a free vibration analysis to obtain modal parameters and structural geometric nonlinearity is also considered.

Fig. 4.18 shows comparison of main natural frequencies for those bridge analysis models. In Fig. 4.18, the notation of V, L, and T indicates the mode of Vertical, Lateral, and Torsional, respectively. Also, the notation of S and AS indicates the symmetric and asymmetric, respectively. The 1st modal frequencies of vertical, lateral, and torsional for cable-stayed suspension bridges, which indicate the bridge analysis model of Ls/L=0.22 to Ls/L=0.77, are all between the bridge model of Ls/L=0.00 and Ls/L=1.00, but its natural frequencies much greater than bridge model of Ls/L=1.00m due to the cable-stayed part in bridge model of Ls/L=0.22 to Ls/L=0.77 helps to improve the vertical and torsional rigidity. However, the 1st symmetric torsional frequency of deck gradually decreases with increase of suspended portion in main span due to the vertical cable plane positioned inside of the bridge deck, as shown in Fig. 3.1.(b).

Under same main span, structural rigidity of Ls/L=0.22 is greater than other bridge models. It means that the suspension-to-span ratio of 0.22 is effective for the increase of overall rigidity of structure.

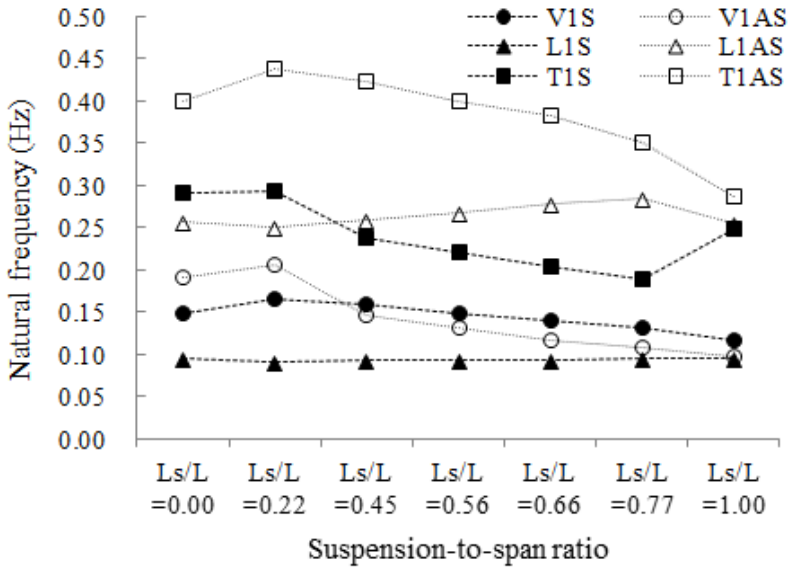

Fig. 4. 18 Comparison of natural frequencies of seven sample bridge models

4.4 Effect of suspension-to-span ratio on the aerostatic stability

In order to fully understand the wind stability of cable-stayed suspension bridges, the effects of suspension-to-span ratio on the aerostatic stability are investigated, and its favorable values are discussed.

The seven bridges analysis models with various suspension-to-span ratio have conducted nonlinear static analysis under the wind attack angle of 0°, and the deck maximum vertical, lateral and torsional displacements at the center of main span with increasing wind speed are compared.

Fig. 4.19~4.21 shows lateral displacements, vertical displacement, and rotational angle of the deck at the center of mid-span of the seven bridges analysis models, respectively. The displacement curves under different suspension-to-span ratio are approximately equivalent, which indicates that suspension-to-span ratio has little effect on the aerostatic stability in this example bridge case. However, the lateral displacement of the deck increases with the decrease of suspension-to-span ratio under the same wind velocity, as shown in Fig. 4.19. Both the vertical displacement and torsional angle of bridge deck increase with suspension-to-span ratio increase under the same wind velocity, as shown in Fig. 4.20~4.21. When the wind velocity is over 120 m/s, the torsional displacement of bridge analysis case of Ls/L=0.77becomes prominent.

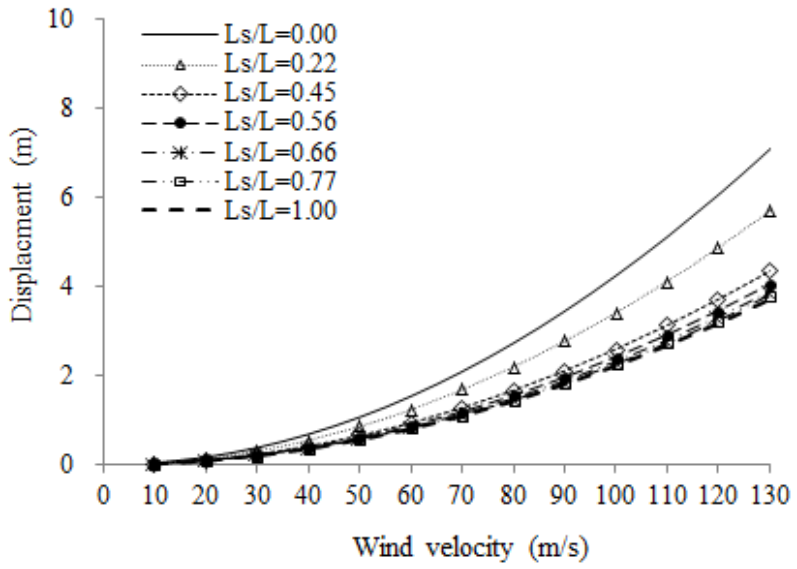

Fig. 4. 19 The lateral displacement of the deck at the center of mid-span

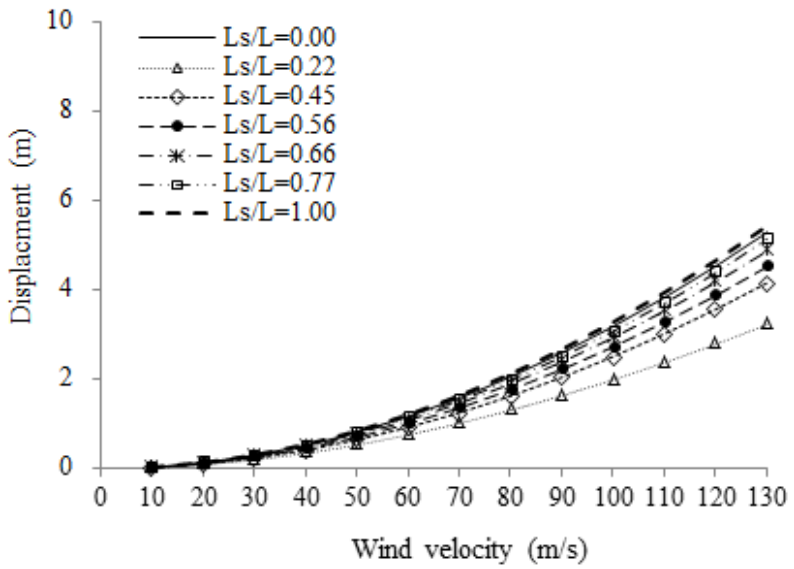

Fig. 4. 20 The vertical displacement of the deck at the center of mid-span

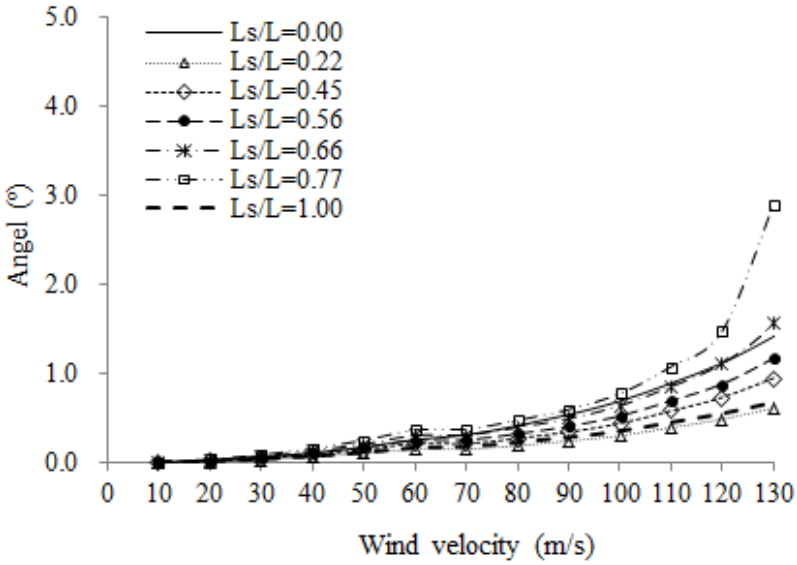

Fig. 4. 21 The torsional displacement of the deck at the center of mid-span

4.5 Summary and discussion

Parametric study is carried out. Two design parameters such as suspension-to-span ratio and length of transition part are considered and studied for their effects on the structural behavior under live loads consisting of trains and road vehicles. The overall results are as follows.

1. The effective suspension to span ratio is 22~56% from the point of view of improvement of vertical displacement by train load.
2. Increasing the suspension-to-span ratio provides extremely high negative bending moment of deck at the junction between cable-stayed parts and suspended part. The tension of longest hanger also rapidly increases due to the stiffness difference between two structural systems. In order to mitigate the rapid stiffness change, transition part is required to install crossing hanger at the cable-stayed parts.
3. Increase of the transition part can mitigate the rapid change of tension of the longest hanger near to the junction. This mitigation effect is valid up to the transition part of 32%. However, as the transition part exceeds 32%, tension amplitude of the longest hanger rather tends to increase.
4. An equally distributed dead load in transition parts is efficient to reduce the secondary stress of main cable.

5. The vertical and torsional stiffness of cable-stayed suspension bridges is relatively larger than suspension bridge (Ls/L=1.00) based on the dynamic characteristics analysis. It results from the effect of cable-stayed part. For the structural rigidity in this example bridge case, suspension-to-span ratio of 0.22% is greater than that of conventional bridges, such as cable-stayed bridges and suspension bridges.
6. The suspension-to-span ratio has little effect on the aerostatic stability in this example bridge case

Chapter 5

Aerodynamic stability of a cable-stayed suspension bridge in construction

In the long-span cable-supported bridges, aerodynamic stability is a major design issue. Particularly, it is important to assure aerodynamic stability in construction stage which has lower stiffness relative to completed stage. Especially for the case of CSSB with train load, the hangers can set in the middle of the deck unlike to the normal case when it is set center of the deck to reduce the excessive vertical deflection, as shown in Fig 5.1. In this case, the highly decrease the torsional stiffness of deck offered by the cable system (Gimsing et al, 2011), and the evaluation of the wind stability is required during erection of deck in construction stage.

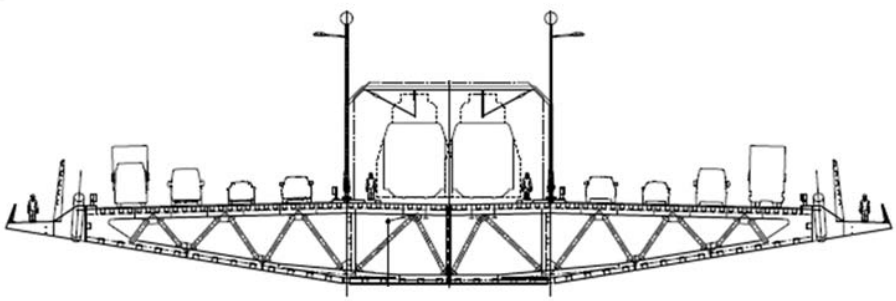

Fig. 5. 1 System with two vertical cable planes positioned the central area

Cable-stayed suspension bridges can be constructed by series construction sequence which erected the deck of cable-stayed parts and afterwards suspension part, as shown in Fig. 5.2(a).

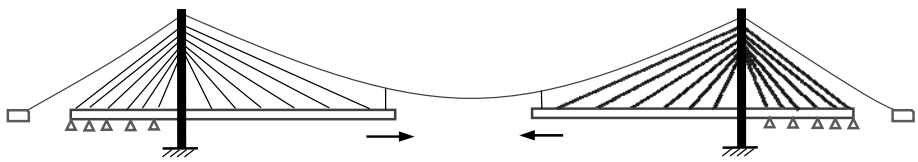

(a) Series construction sequence; erecting in the main span from pylons

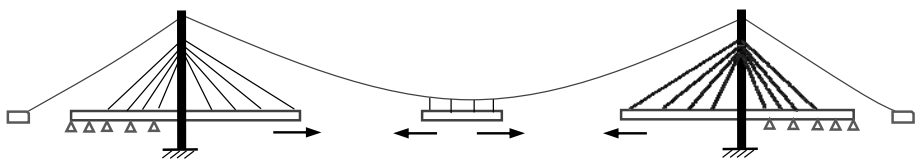

(b) Simultaneous construction sequence; erecting in the main span simultaneously from mid-span and pylons

Fig. 5. 2 Construction scheme of cable-stayed suspension bridges

Erecting the deck starting from two pylons to mid-span is effective for aerodynamic stability ensured the torsional stiffness of deck by the pylons. When the erection of main cable is completed, above construction scheme can be erected without aerodynamic stability improvement measures since deck of suspended part is attached to deck of cable-stayed parts. However, reducing the construction time can be necessary due to demand of owner and environmental restrictions. From a structural point of view, cable-stayed suspension bridges can be reduced the

construction period by erecting in the main span deck simultaneously from suspended part and cable-stayed parts after completed erection of main cables, as shown in Fig. 5.2(b).

However, it is required both to verify the aerodynamic stability on the construction phase of suspended deck and to find the potential improvement measures in the aerodynamic stability for the erection of the deck in suspended part.

Therefore, it is necessary to investigate applicable aerodynamic stability enhancement measures.

In this paper, X-Type bracing, Rigid beam and Strut system are considered as structural stabilization measures from the literature survey (Honda et al., 1998; Nakamura, 2006; Kubo, 2007; Xiang and Ge, 2007).

This study investigates the aerodynamic stability during construction of a cable-stayed suspension bridge. The considered example bridge can be found in Chapter 3. Erecting the bridge decks of this example bridge structure can be used two construction plans such as series construction sequence and simultaneous construction sequence, as shown in Fig. 5.2. With two construction plans, aerodynamic stability on the erection of main span decks is investigated in condition of completed erection of pylons and side span decks.

Since the bridge structure is subjected to a large displacement during construction, the structural geometry and internal forces of members should be reasonably simulated for the investigation of aerodynamic stability for specific construction steps. The SNUSUS (Kim, 1993), an in-house program developed in

Structural Design Laboratory at Seoul National University (SNU) for a construction step analysis of suspension bridge, is utilized for this purpose. The main cables, hangers, and stay cables are modeled with an elastic catenary cable element (Irvine, 1981), which is rigorously formulated based on an unstrained length. The girders and pylons are modeled with a 3-D frame element (Kim, 1993; Kim et al. 2004). The structural system can be changed by a series of construction commands and the static analysis is performed considering the geometric nonlinear properties of the strain-hardening structure.

The initial equilibrium state for the completed structure is established by practical method as mentioned in chapter 3. Overall geometry and internal forces introduced were confirmed to be in a reasonable range.

The construction stage is simulated by a backward analysis from the initial equilibrium state by eliminating structural components in a reverse order of erection sequences. When an equilibrium status is realized for a construction stage, a free vibration analysis is followed to obtain modal parameters for further buffeting analysis of the structural stage. The aerodynamic stability of the structures in construction is evaluated by BUFFET2 (Kim, 2004; 2013), a buffeting analysis program developed by Structural Design Laboratory at SNU, with the modal and structural information delivered from SNUSUS. The design wind velocity for construction stage is determined to be 40.66 m/s at the deck level of 75m for sea wind. The von Karman spectra are used to describe the wind velocity fluctuations (von Karman, 1948).

$$\frac{f \cdot S_u(f)}{\sigma_u^2} = \frac{4 \cdot \hat{f}_u}{(1+70.8 \cdot \hat{f}_u^2)^{5/6}} \tag{5.1a}$$

$$\frac{f \cdot S_n(f)}{\sigma_n^2} = \frac{4 \cdot \hat{f}_n \cdot (1+755.2 \cdot \hat{f}_u^2)}{(1+283.2 \cdot \hat{f}_u^2)^{11/6}}, \; n=v,w \tag{5.1b}$$

where $\hat{f}_u = f \cdot {}^{xf}L_n / V$, f = natural frequency; ${}^{xf}L_n$ = the integral length scale of the relevant turbulence component of u, v, and w in the x_f wind direction.

The turbulence intensities and integral length scales are assumed to be 10% and 5% and 183 m and 15 m for the u and w components, respectively. The coherence of wind velocity fluctuations between two separated points are modeled with function as (Simiu and Scanlan, 1996)

$$Coh(x_A, x_B, f) = exp(-\frac{cf\,|x_B - x_A|}{V(z)}) \tag{5.2}$$

in which, the constant c is taken as 8.

The scientific and Technical Centre for Building (CSTB) at Nantes wind tunnel performed wind tunnel tests with a 1:100 scaled model of investigated bridge (Greisch, 2013). The aerostatic coefficients are listed in Table 5.1.

The self-excited drag force is evaluated based on the quasi-steady theory. The self-excited lift and pitching moment are calculated based on the flutter derivatives derived from Theodorsen function in terms of the reduced wind velocity U/nB,

where n is the natural frequency of the bridge deck. The quasi steady theory applies to the drag component ($P_1^* = -2C_D / K$). The aerodynamic admittance of the bridge deck section is taken as unity in all cases in a conservative aspect. The modal damping ratio is assumed to be 0.32% in all considered mode. Only the aerodynamic forces acting on the bridge deck are included for the buffeting analysis.

Table 5. 1 Static coefficient for bridge members

Members	C_D (0°)	C_L (0°)	C_M (0°)	C_D' (-2°~2°)	C_L' (-2°~2°)	C_M' (-2°~2°)	Note
Deck	0.0323	-0.2369	-0.0024	-0.1432	5.4496	1.3789	Wind tunnel
Main cable	0.7	-	-	-	-	-	Circular shape
Stayed cable	0.7	-	-	-	-	-	
Hanger	0.7	-	-	-	-	-	

5.1 Description of construction scheme

Two construction plans such as series construction sequence (Construction Plan 0) and simultaneous construction sequence (Construction Plan 1) can be used erecting the bridge decks of this example bridge structure, as shown in Fig 5.3 and 5.4. Based on completed erection of pylons and the side span decks, seven erection stages were selected for each construction plan. Expected construction period of each construction plan is calculated by ideal construction sequence and is compared. The notation of ES, D, P0, and P1 in Fig 5.3~5.4 are indicated erection stage, deck segment number and each construction plan, respectively.

For Construction Plan 0, the deck of main span erection proceeds from cable-stayed parts to suspension part. The erection phase was divided into 7 stages, and described as follows:

Erection stage (ES) 1: The pair of deck segments D0 to D12 and 24 stay cables in each cable plan are installed.

ES2: The pair of decks D20 and the stay cables S20 are installed.

ES3: The main cable completed. The pair of decks d21 and the hangers H21 is installed.

ES4: The pair of decks D23 and the hangers H23 is installed.

ES5: The pair of decks D25 and the hangers H25 is installed.

ES6: The pair of decks D28 and the hangers H28 is installed.

ES7: The key segment D99 is installed.

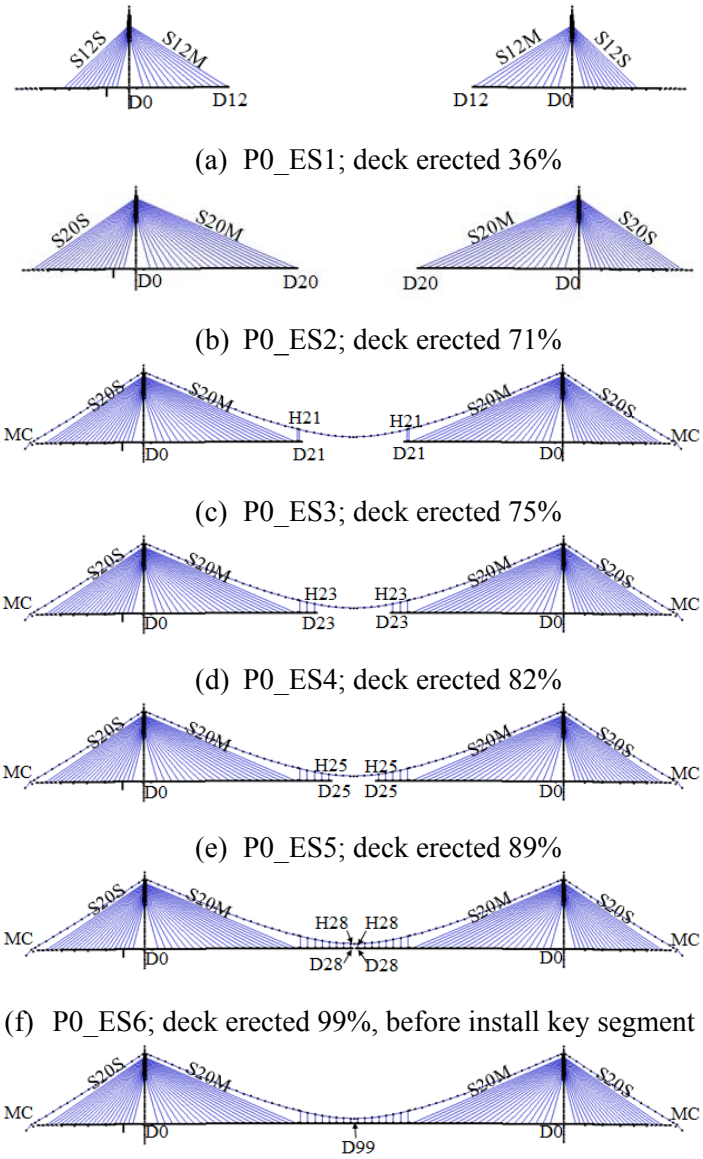

(a) P0_ES1; deck erected 36%

(b) P0_ES2; deck erected 71%

(c) P0_ES3; deck erected 75%

(d) P0_ES4; deck erected 82%

(e) P0_ES5; deck erected 89%

(f) P0_ES6; deck erected 99%, before install key segment D99

(g) P0_ES7; deck erected 100%, closure

Fig. 5. 3 FE models of erection sequence in construction Plan 0

For Construction Plan 1, erecting the decks of main span precedes simultaneously form cable-stayed parts and suspension part after completed erection of main cables. The erection phase was divided into 7 stages, and described as follows:

ES 1: The pair of deck segments D0 to D15 and 30 stay cables in each cable plan are installed.

ES 2: The pair of decks D16 and stay cables S16 are installed in the cable-stayed parts, and the pair of decks D28 and hangers H28 are installed in suspended part.

ES 3: The pair of decks D17 and stay cables S17 are installed in the cable-stayed parts, and the pair of decks D26 to D27 and the pair of hangers H26 to H27 is installed in suspended part.

ES 4: The pair of decks D18 and stay cables S18 are installed in the cable-stayed parts, and the pair of decks D25 and hangers H25 are installed in suspended part.

ES 5: The pair of decks D19 and stay cables S19 are installed in the cable-stayed parts, and the pair of decks D23 to D24 and the pair of hangers H23 to H24 is installed in suspended part

ES 6: The pair of decks D20 and stay cables S20 are installed in the cable-stayed parts, and the pair of decks D22 and the pair of hangers H21 to H22 are installed in suspended part.

ES 7: The key segment D21 is installed.

(a) P1_ES1; deck erected 54%

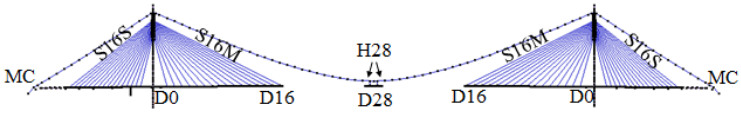

(b) P1_ES2; deck erected 61%

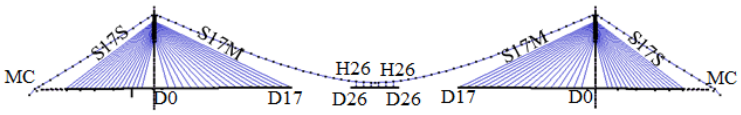

(c) P1_ES3; deck erected 72%

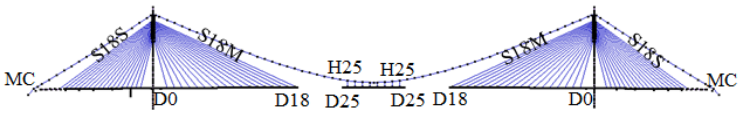

(d) P1_ES4; deck erected 79%

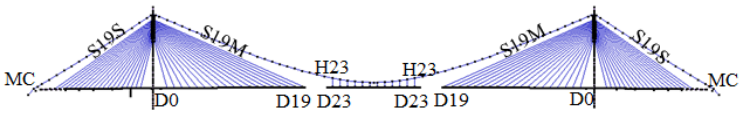

(e) P1_ES5; deck erected 89%

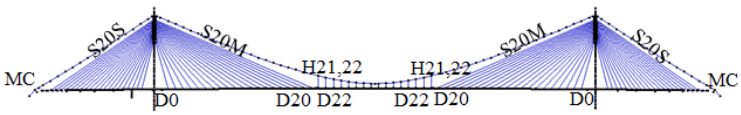

(f) P1_ES6; deck erected 96%, before install key segment D21

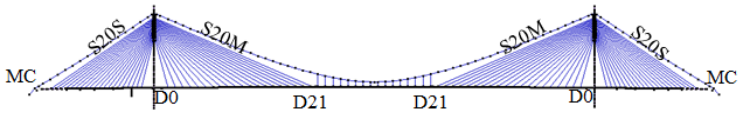

(g) P1_ES7; deck erected 100%, closure

Fig. 5. 4 FE models of erection sequence in construction Plan 1

Based on the each construction plan, construction period for the erection of main span decks is calculated, as listed in Table 5.2 and 5.3. When calculated construction duration, the cable-stayed parts is assumed to use free cantilever method by derrick crane and 1cycle of 10days for erection of the deck (i.e., lift and erect of deck segment is 1day, install stay cable is 3days, welded deck segment is 6days). Otherwise, the suspension part is considered to use strand jack method for the lifting of deck segment and 1cycle of 7days for erection of the deck (i.e., lift and erect of deck segment, install hanger is 1day, welded deck segment is 6days).

Fig. 5.5 and 5.6 show deck erection method to estimate the construction period.

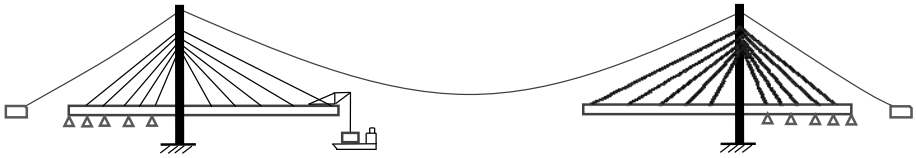

Fig. 5. 5 Deck erection by derrick crane

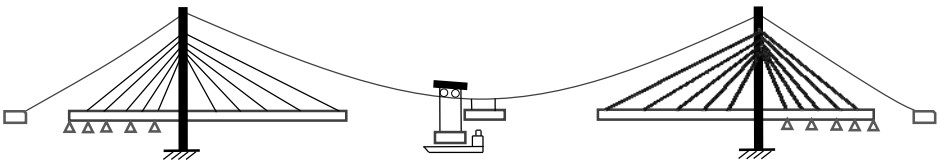

Fig. 5. 6 Deck erection by lifting gantry

Table 5. 2 The estimated construction durations for Plan 0

Erection sequence	Activity	Duration (Days)	Cumulative (Days)
P0_ES1	D00 D01 to D10, S01 to S10	128 (=8day+10block×10day)	108
P0_ES2	D11 to D20, S11 to S20	100 (=10block×10day)	208
P0_ES3	D21, H21	7 (=1block×7day)	215
P0_ES4	D22 to D23, H22 to H23	14 (=2block×7day)	229
P0_ES5	D24 to D25, H24 to H25	14 (=2block×7day)	243
P0_ES6	D26 to D28, H26 to H28	21 (=3block×7day)	264
P0_ES7	D99, key segment	7 (=1block×7day)	**271**

Note: D** - deck segment number, S**- stay cable number, and H**-hanger number

Table 5. 3 The estimated construction durations for Plan 1

Erection sequence	Activity	Duration (Days)	Cumulative (Days)
P1_ES1	D00 D01 to D15, S01 to S15	158 (=8day+15block×10day)	158
P1_ES2	D16, S16 D28, D99, and H28	10 (=1block×10day)	168
P1_ES3	D17, S17 D26 to D27, H26 to H27	14 (=2block×7day, 1block×10day)	182
P1_ES4	D18, S18 D25, H25	10 (=1block×10day, 1block×7day)	192
P1_ES5	D19, S19 D23 to D24, H23 to H24	14 (=2block×7day, 1block×10day)	206
P1_ES6	D20, S20 D22, H21 to H22	10 (=1block×10day, 1block×7day)	216
P1_ES7	D21, key segment	7 (=1block×7day)	**223**

Note: D** - deck segment number, S**- stay cable number, and H**- hanger number

Table 5.4 shows comparing construction period for the erection of main span bridge decks based on the completed erection of pylons and the decks of side spans. The result shows that construction Pl can be reduced 48 days compared with construction Plan 0.

Table 5. 4 The estimated construction durations for construction plans

Construction plan	Construction period of deck(Day)	Reduced day
Plan0	271	-
Plan1	223	48

5.3 Aerodynamic stability of construction Plan 0 (P0)

Based on the construction Plan0, aerodynamic stability in construction stages is investigated by buffeting analysis focus on the torsional displacement of suspended decks.

(1) Aerodynamic stability of construction stage of P0_ES2

The construction stage of P0_ES2, which is the longest cable-stayed parts, is erected pair of deck d00 to d20 and pair of stay cables S01 to S20. Fig. 5.7 shows FE analysis mode of P0_ES2.

Fig. 5. 7 FE analysis model of P0_ES2

Fig. 5.8 shows some dominant vibration modes. The 1st torsional frequency for P0_ES2 is 0.486 Hz.

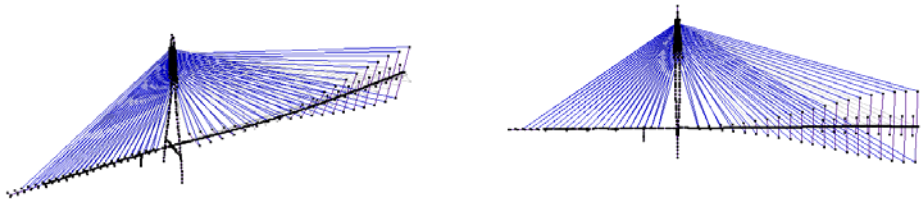

Fig. 5. 8 The 1st torsional mode shapes for P0_ES2(f = 0.486Hz)

Fig. 5.9 gives the buffeting analysis results for construction stage of P0_ES2. The result shows that the maximum rigid body rotational displacement of deck under buffeting is dominant than mean wind load. Under the combined effect of mean wind and buffeting load, the maximum rigid body rotational displacement of deck rises as the wind velocity is increased. The maximum rigid body rotational displacement of deck is 0.8° at design wind speed of 41m/s and divergence not occurred.

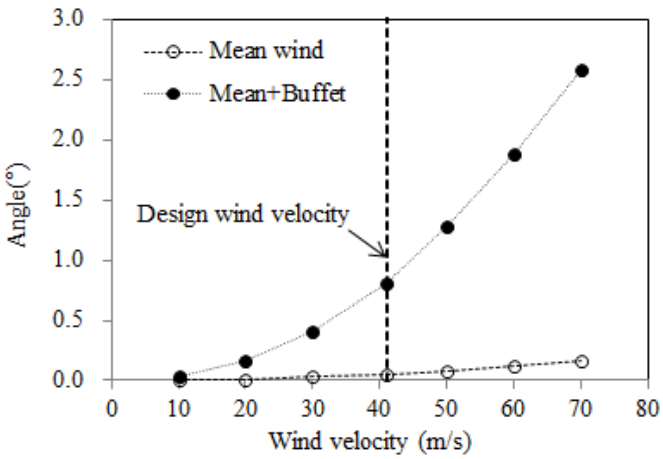

Fig. 5. 9 The maximum torsional displacement at the tip of the deck for P0_ES2

(2) Aerodynamic stability of construction stage of P0_ES6

Erection stage of P0_ES6, which is before closing of the bridge at the main span center, is erected pair of deck d00 to d28, pair of stay cables S01 to S20, and pair of hangers H21 to H28, as shown in Fig. 5.10.

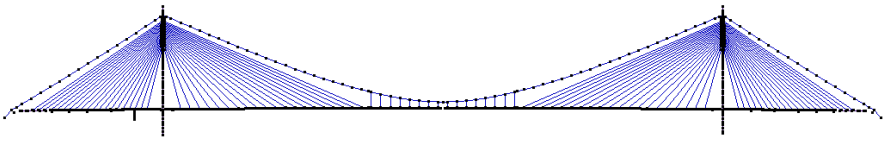

Fig. 5. 10 FE analysis model of P0_ES6

Fig. 5.11 shows some dominant vibration modes. The 1st torsional frequency for P0_ES6 is 0.319 Hz.

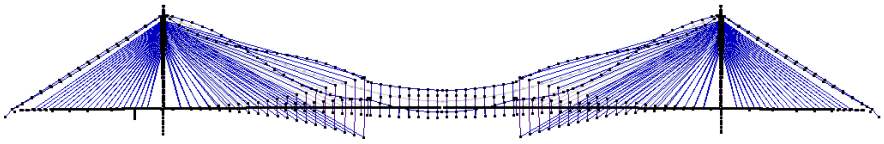

Fig. 5. 11 The 1st torsional mode shapes for P0_ES6(f = 0.319Hz)

Fig. 5.12 shows the buffeting analysis results for construction stage of P0_ES6. The result shows that the maximum torsional displacement of deck under buffeting is dominant than mean wind load. Under the combined effect of mean wind and

buffeting load, the maximum torsional displacement of deck rises as the wind velocity is increased. The maximum torsional displacement of deck is 1.7° at design wind speed of 41m/s and divergence not occurred.

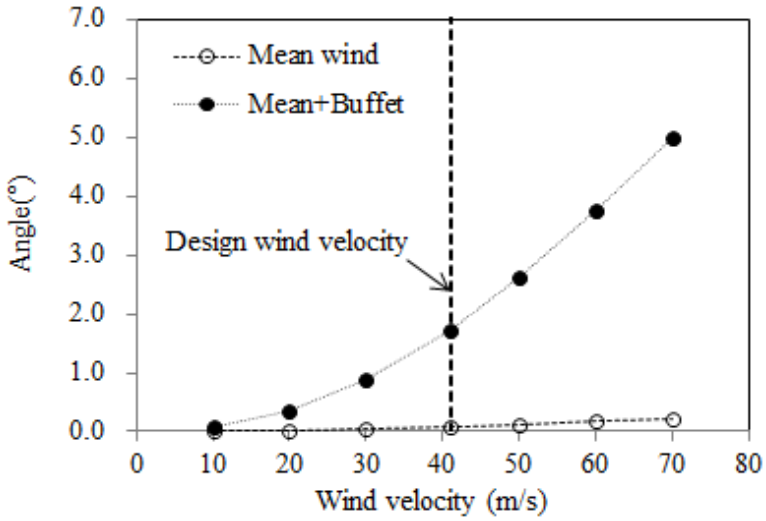

Fig. 5. 12 The maximum torsional displacement at the tip of the deck for P0_ES6

Under critical construction stage of P0_ES2 and P0_ES6, the divergence of torsional displacement of deck during erection stages is not found in design wind speed of 41m/s. therefore, aerodynamic stability of construction Plan 0 is investigated with seven erection stages, as shown in Fig. 5.3.

(3) Aerodynamic stability of construction Plan 0

Fig 5.13 shows the dominate frequency of torsion, lateral, and vertical of the

deck in each erection phase for construction Plan 0. As far as deck erection increases, the dominant frequency of torsion, lateral, and vertical tends to be reduced. This indicates that overall rigidity of bridge structure becomes smaller. Especially, torsional frequency declines dramatically in the deck erection of suspended part.

Fig. 5.14~5.16 shows the maximum torsional displacement, lateral displacement, and vertical displacement at the tip of cantilever deck under wind load, respectively.

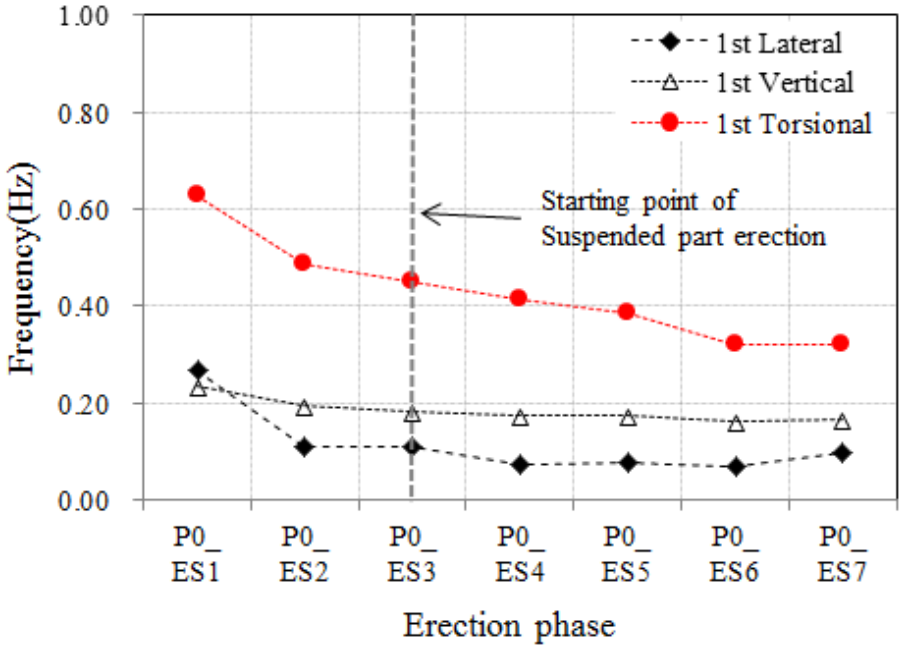

Fig. 5. 13 The dominant frequency of deck for construction Plan 0

The maximum torsional displacement at the tip of cantilever tends to rises as the increase of deck erection, as shown in Fig. 5.14. The largest maximum torsional displacement of deck can be found 1.7° under combined results of mean wind and buffeting at the erection stage of P0_ES6. The largest maximum lateral displacement of deck can be found at the erection stage of P0_ES6 and its value is 1.941m, as shown in Fig. 5.15. On the other hand, the maximum vertical displacement of deck decreases at the initial erection stage due to controlling effect of the longitudinal displacement at the top of pylons by main cables. The largest maximum vertical displacement of deck can be found at the erection stage of P0_ES4 and its value is 2.205m, as shown in Fig. 5.16.

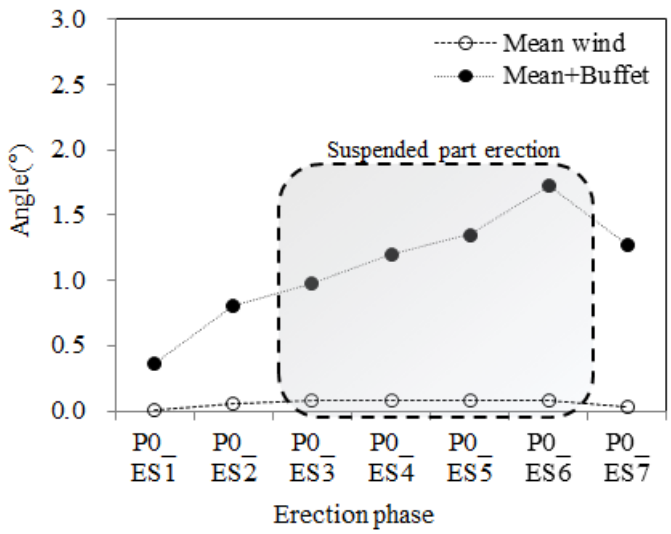

Fig. 5. 14 The maximum torsional displacement at the tip of cantilever deck in construction Plan 0

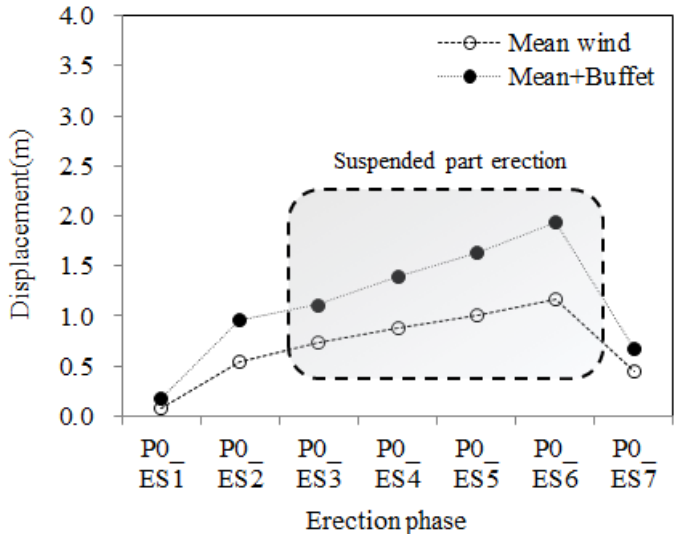

Fig. 5. 15 The maximum lateral displacement at the tip of cantilever deck in construction Plan 0

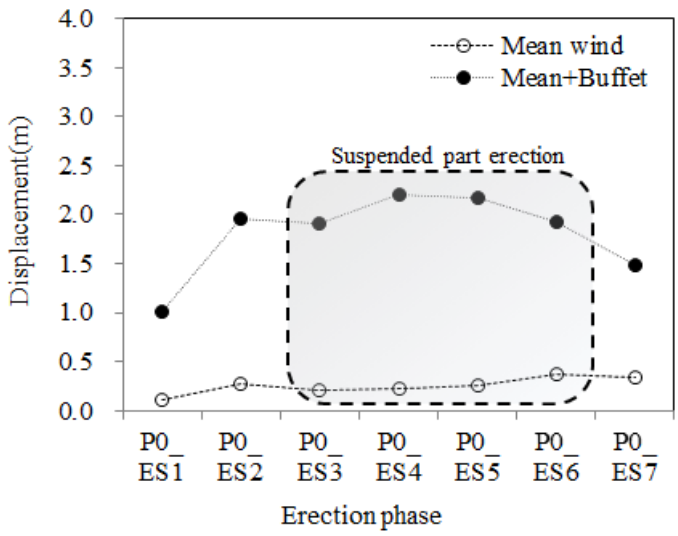

Fig. 5. 16 The maximum vertical displacement at the tip of cantilever deck in construction Plan 0

Fig 5.17 shows the distribution of stay cables tensions under combined Dead (D) load and Wind (W) load for erection stages in construction Plan 0. The tension of stay cables is biggest after their installation. In all cases, the tensions of stay cables under loading case of D+W are limited to allowable equivalent tension of each stay cables.

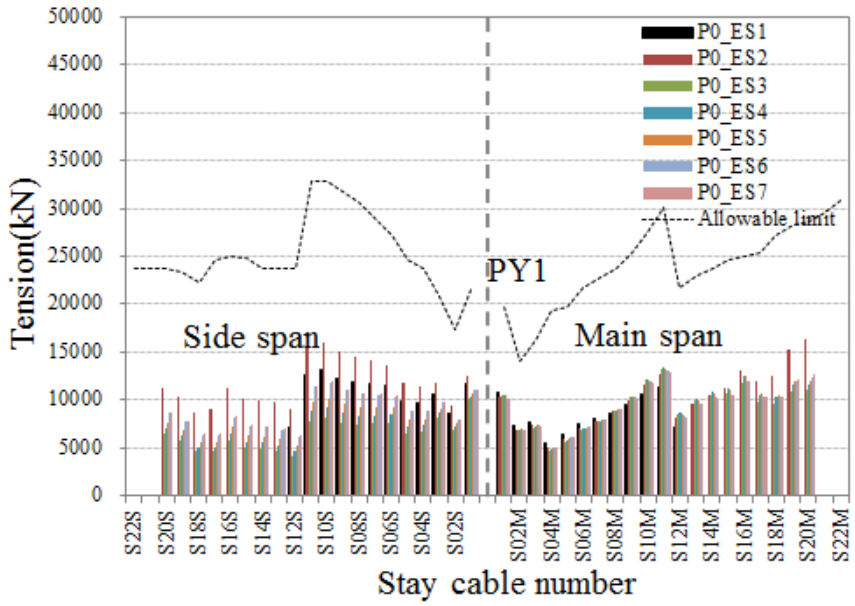

Fig. 5. 17 Distribution of stay cables tension under D+W in construction Plan 0

Fig 5.18 shows the tension variation of hanger H12 under loading case of D+W for each erection stage in construction Plan 0. The maximum tension of hanger after erection stage of P0_ES7 is exceeded the allowable equivalent tension. In order to secure the aerodynamic stability, Hanger of H21 needs to be increased

of cross-sectional area or adjust its length of cable after their installation in erection stage of P0_ES3 and P0_ES7. The maximum hanger tension increase up to 14571 kN for H21.

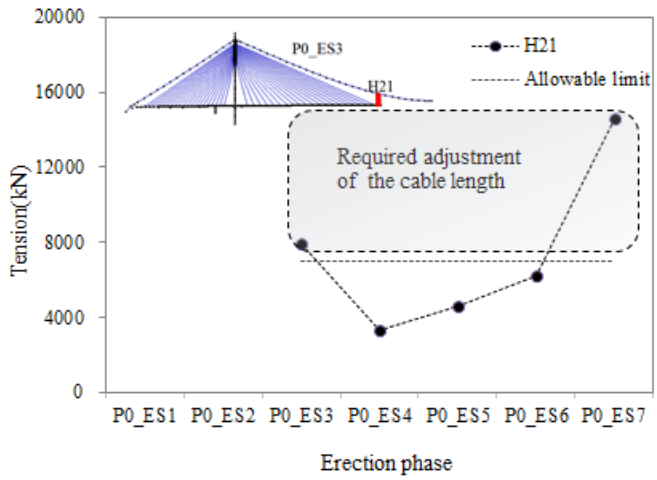

Fig. 5. 18 The tension variation of hanger H12 under D+W in construction P0

(4) Summary of aerodynamic stability for construction Plan 0

The feasibility of suggested construction plan of deck in terms of aerodynamic stability is examined. The torsional deformation under construction stage of suspension part is less than 2 degree, which is stable. Aerodynamic stability problems are not expected for the construction Plan 0 except the longest hanger of H21. Hanger of H21 needs to be increased of cross-sectional area or adjust its length of cable after erection phase of P0_ES3 and P0_ES7 to secure the aerodynamic stability in construction Plan 0.

5.4 Aerodynamic stability of construction Plan 1(P1)

Based on the construction Plan1, by erecting in the main span deck simultaneously from suspended part and cable-stayed parts, aerodynamic stability in construction stages is investigated by buffeting analysis focus on the erection of suspended decks.

(1) Aerodynamic stability of construction stage of P1_ES2

The construction stage of P1_ES2 is erected both pair of deck d00 to d16 and pair of stay cables S01 to S16 for cable-stayed parts and pair of deck d28 and pair of hangers H28 for suspended part. Fig. 5.19 shows FE analysis mode of P1_ES2.

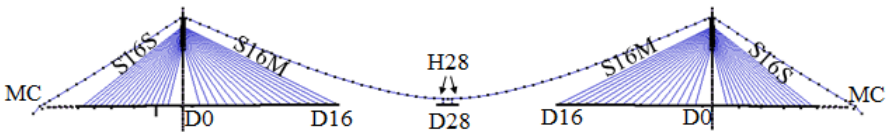

Fig. 5. 19 FE analysis model of bare structure for P1_ES2:0 Bare structure

Fig. 5.20 gives the buffeting analysis results with 41m/s of design wind speed at deck level are reported for construction stage of P1_ES2. The maximum torsional displacement of suspended deck is 26° under wind speed of 41m/s. Such excessive torsional deformation may cause problems with the structural safety and derailment of construction equipment.

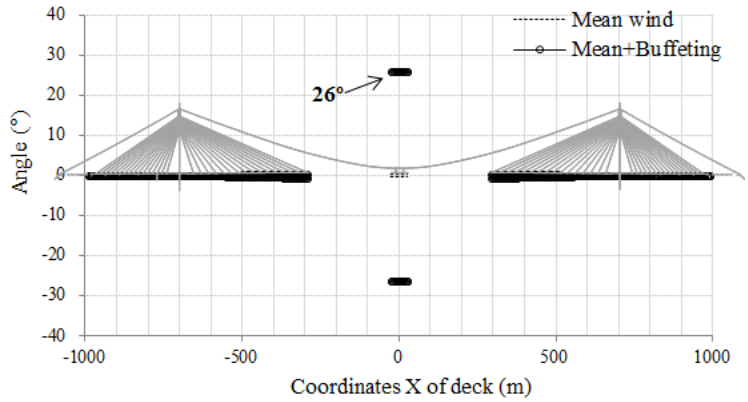

Fig. 5. 20 The torsional displacement of deck for P1_ES2:0 Bare structure

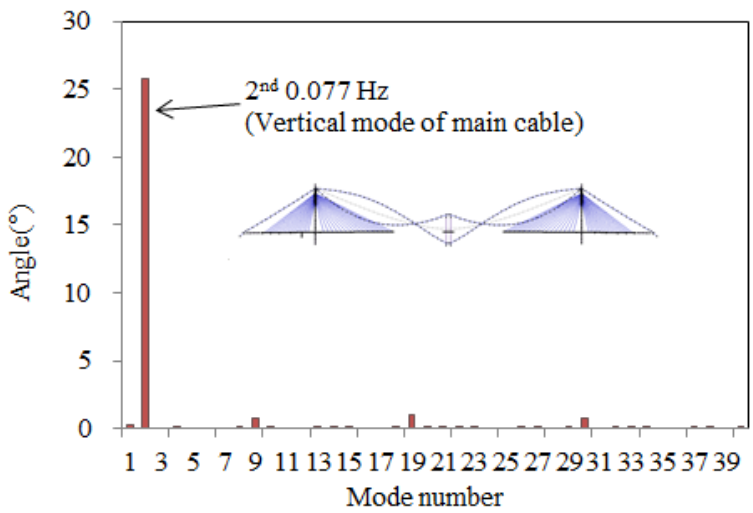

Fig. 5. 21 Mode contribution of torsional displacement of deck for P1_ES2:0 Bare structure

In order to analyze the main reason for the excessive torsional deformation of the suspended deck, the responses contributions of modes are investigated. Fig. 5.21 shows that the most contribution mode for the torsional deformation of suspended deck is the 1st vertical mode of main cable. Therefore, it is required structural measures to reduce the torsional deformation of suspended deck by controlling the 1st vertical mode of the main cable.

To overcome the above problem, several structural measures are proposed in this paper such as X-Type bracing, Rigid beam and Strut system from the literature survey (Honda et al., 1998; Nakamura, 2006; Kubo, 2007; Xiang and Ge, 2007).

(2) Increasing torsional stiffness by X-Type bracing for erection phase of P1_ES2

In order to increase the torsional stiffness of the bridge deck, some hangers connect each cable with the opposite side of the deck. These hangers are called X-Type bracing(X-B) as shown in Fig. 5.22.

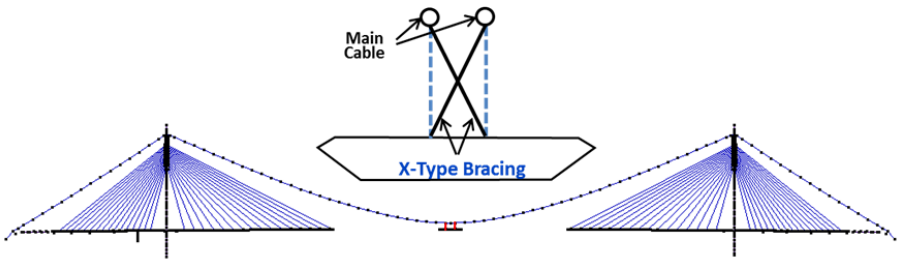

Fig. 5. 22 Increasing torsional stiffness by X-Type bracing for P1_ES2

The result of buffeting analysis is reported in Table 5.5. The maximum rigid body rotational displacement of the deck of suspended part is compared to the bare structure in condition of combined result of mean wind and buffeting.

The rigid body rotational displacement of suspended deck by applied X-Type bracing can be reduces around 44% compared to bare structure of P1_ES2.

Table 5. 5 Influence of X-Type bracing on the maximum displacement at the tip of suspended decks for P1_ES2

Structure	Torsional disp. (Deg.)	Lateral disp. (m)	Vertical disp. (m)
P1_ES2:0 Bare structure	26.2	7.028	2.955
P1_ES2:1 X-Type bracing	14.7	7.900	2.952

(3) Improving torsional stiffness by Rigid beam for erection phase of P1_ES2

The torsional stiffness of the bridge deck maybe enhanced by Rigid beam for the construction phase of P1_ES2, as shown in Fig. 5.23.

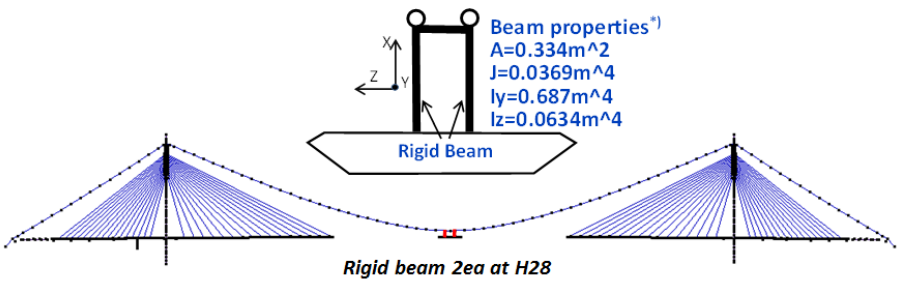

Fig. 5. 23 Improving torsional stiffness by Rigid beam for P1_ES2

In case of applying Rigid beam, the rigid body rotational displacement of suspended deck can reduce and its maximum value is 0.5 °, which shows a 98% reduction compared by bare structure of P1_ES2, as listed in Table 5.6.

Table 5. 6 Influence of Rigid beam on the maximum displacement at the tip of suspended decks for P1_ES2

Structure	Torsional disp. (Deg.)	Lateral disp. (m)	Vertical disp. (m)
P1_ES2:0 Bare structure	26.2	7.028	2.955
P1_ES2:1 X-Type bracing	14.7	7.900	2.952
P1_ES2:2 Rigid beam	0.5	5.710	2.723

(4) Enhancement torsional stiffness by Strut system for erection phase of P1_ES2

In order to improve the torsional stiffness of suspended deck, strut system (Strut) is installed on main cables as show in Fig 5.24.

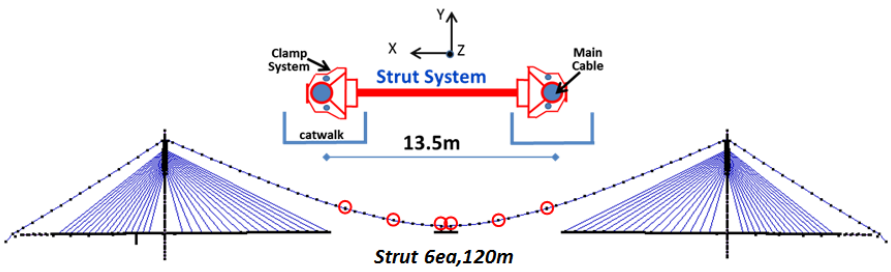

Fig. 5. 24 Improving torsional stiffness by Strut system for P1_ES2

By adapting Strut system in the main cables, the maximum rigid body rotational deformation is 0.5° at the suspended deck, around 98% lower than that of bare structure of P1_ES2, as listed in Table 5.7.

Table 5. 7 Influence of Strut system on the maximum displacement at the tip of suspended decks for P1_ES2

Structure	Torsional disp. (Deg.)	Lateral disp. (m)	Vertical disp. (m)
P1_ES2:0 Bare structure	26.2	7.028	2.955
P1_ES2:1 X-Type bracing	14.7	7.900	2.952
P1_ES2:2 Rigid beam	0.5	5.710	2.723
P1_ES2:3 Strut system	0.5	6.044	2.888

From above results, both Strut system and Rigid beam are effective to control the torsional displacement of suspended deck and these measures can reduce around 98% compared with bare structure of P1_ES2.

To examine the applicability of several stabilization measures for erection stages in construction Plan 1, erection stage of P1_ES6, which has the longest suspended part, is investigated with respect to the torsional deformation of suspended deck and cable tensions by buffeting analysis.

(5) Aerodynamic stability of construction stage of P1_ES6

The construction stage of P1_ES6 is erected both pair of deck d00 to d20 and pair of stay cables S01 to S20 for cable-stayed parts and pair of deck d28 and both

pair of deck d22 to d28 and pair of hangers H21 to H28 for suspended part. Fig. 5.25 shows FE analysis mode of P1_ES6.

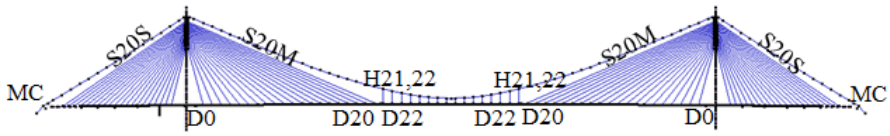

Fig. 5. 25 FE analysis model of bare structure for P1_ES6:0 Bare structure

Fig. 5.26 gives mode contribution of torsional displacement of deck for P1_ES6:0Bare structure. The most contribution mode for the torsional deformation of suspended deck is 1st vertical mode of main cable. The maximum torsional deformation of suspended deck is 9.9 ° at the design wind velocity of 41m/s.

As shown in Fig. 5.27, distribution of stay cable tensions for erection stage of P1_ES6 is smaller than the allowable equivalent tension of each stay cable.

Otherwise tension of the longest hanger H21 is 11277 kN, which is exceeded 61% than the allowable equivalent tension of 7007 kN, as shown in Fig. 5.28. Meanwhile, structural stabilization measures are needed for erection phase of suspended deck under wind effects. Likewise, it is necessary to verify the hanger stability under examination of the applicability of stabilization measures for erection stages.

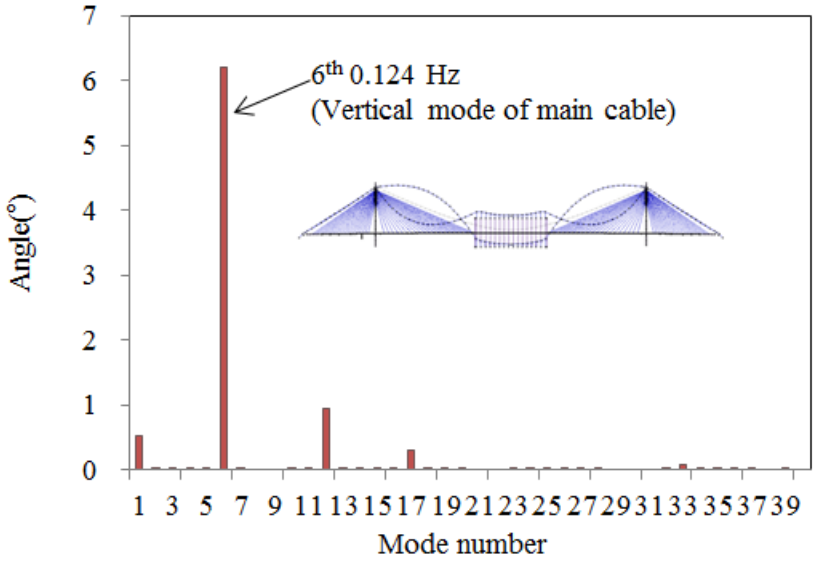

Fig. 5. 26 Mode contribution of torsional displacement of deck for P1_ES6:0 Bare structure

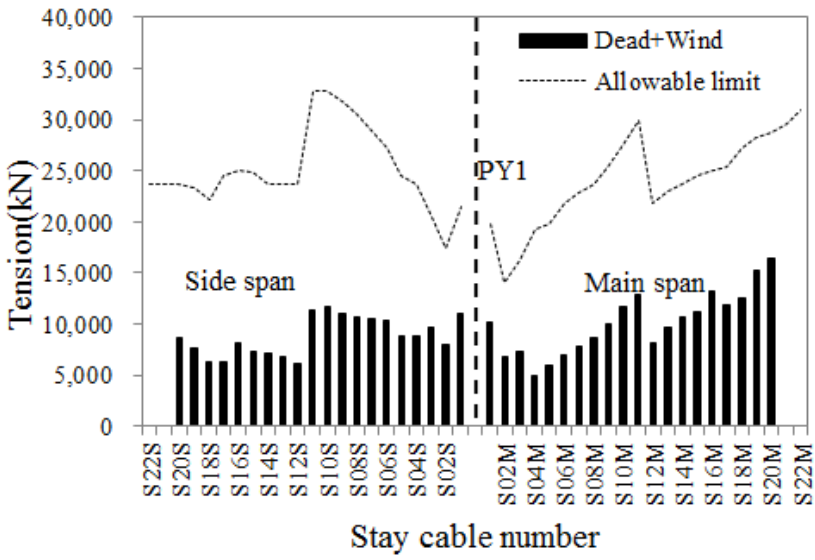

Fig. 5. 27 Distribution of stay cable tensions for P1_ES6

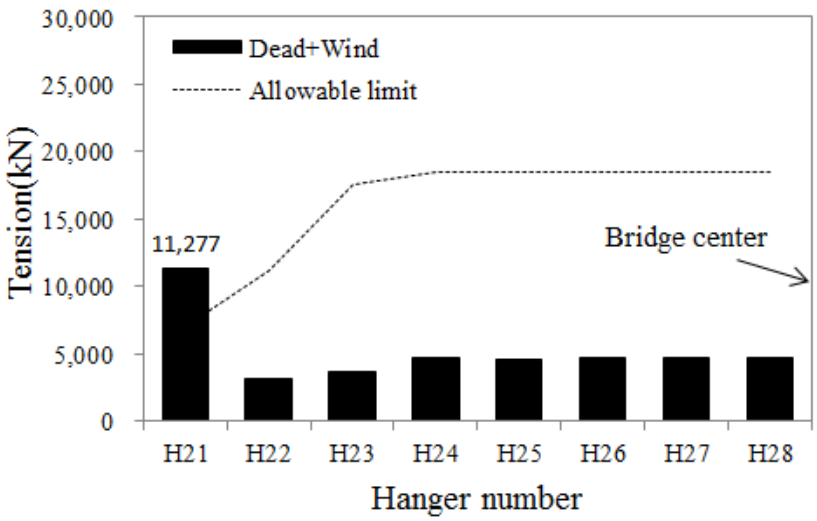

Fig. 5. 28 Distribution of hanger tensions for P1_ES6

(6) Aerodynamic stability for erection stage of P1_ES6 with X-Type bracing

Erection stage of P1_ES6 is applied the X-Type bracing in order to increase the torsional stiffness of the suspended deck, as shown in Fig. 5.29.

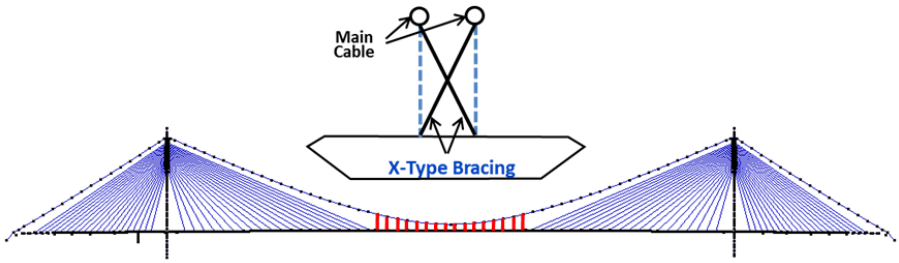

Fig. 5. 29 Improving torsional stiffness by X-Type bracing for P1_ES6

The result of buffeting analysis is reported in Table 5.8. The maximum torsional displacement of deck at the suspended part is compared to the bare structure on condition of combined mean wind and buffeting responses. Controlling of the torsional displacement of suspended deck by X-Type bracing is effective and reduced around 34% compared than bare structure.

Table 5. 8 Influence of X-Type bracing on the maximum displacement at the tip of suspended decks for P1_ES6

Structure	Torsional disp. (Deg.)	Lateral disp. (m)	Vertical disp. (m)
P1_ES6:0 Bare structure	9.9	6.019	2.753
P1_ES6:1 X-Type bracing	6.6	6.426	2.750

The tension in the hangers is smaller than the allowable equivalent tension of each hanger under combined effect of D and W except the longest hanger of H21, as shown in Fig. 5.30.

For the X-Type hangers, tension of the X-Type hanger in H21X to H26X exceeds the allowable equivalent tension. So those X-Type hangers are required to adjust its length of cable for each erection phase, as shown in Fig 5.31.

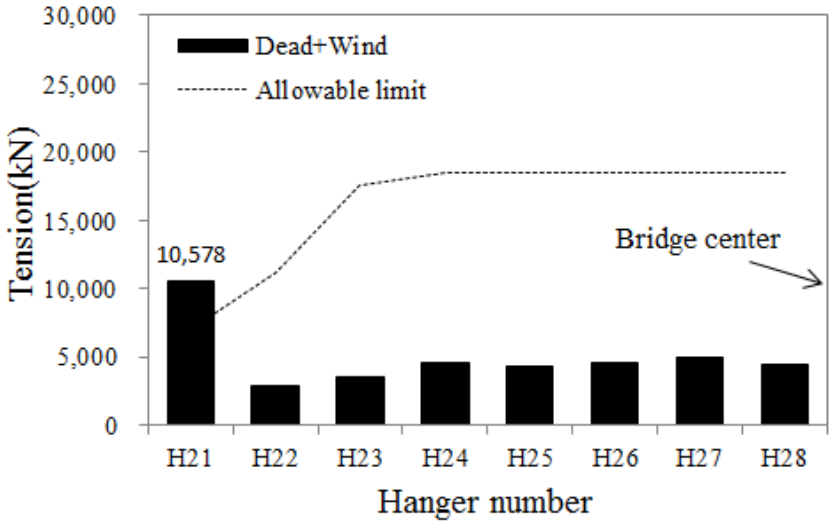

Fig. 5. 30 The tension of hangers under D+W for P1_ES6:1 X-Type bracing

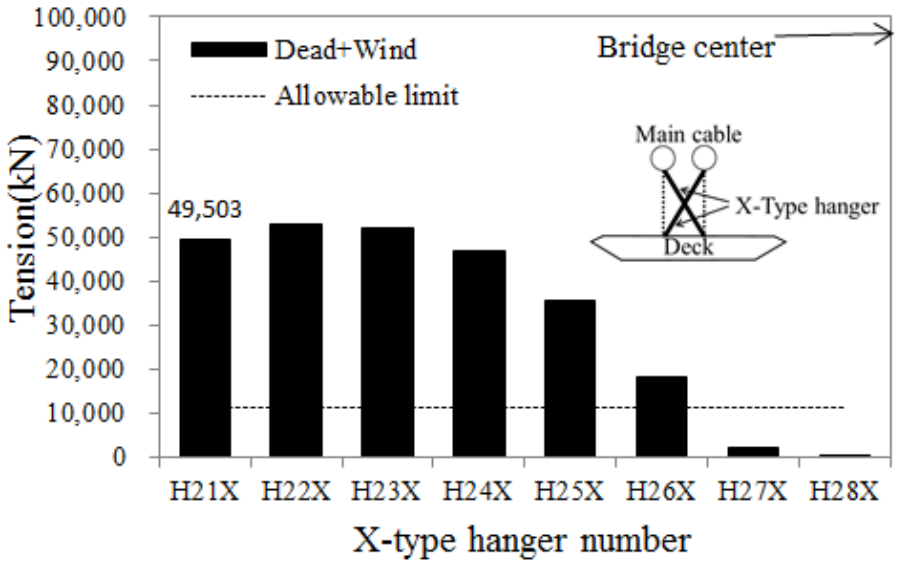

Fig. 5. 31 The tension of X-Type hangers under D+W for P1_ES6:1 X-Type bracing

(7) Aerodynamic stability for erection stage of P1_ES6 with Rigid beam

In order to increase the torsional stiffness of the bridge deck, hangers of H24 and H 28 are replaced with four Rigid beam for erection stage of P1_ES6 as shown in Fig. 5.32.

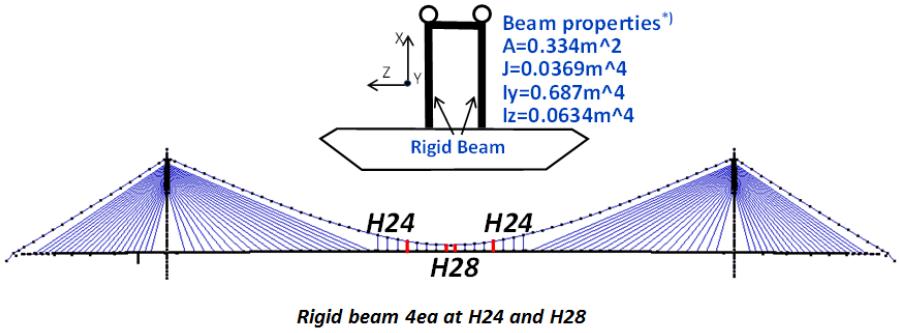

Fig. 5. 32 Increasing torsional stiffness by Rigid beam for P1_ES2

The torsional displacement of suspended deck by applied Rigid beam can be reduce around 92% compared to bare structure of P1_ES6, as listed in Table 5.9.

Table 5. 9 Influence of Rigid beam on the maximum displacement at the tip of suspended decks for P1_ES6

Structure	Torsional disp. (Deg.)	Lateral disp. (m)	Vertical disp. (m)
P1_ES6:0 Bare structure	9.9	6.019	2.753
P1_ES6:1 X-Type bracing	6.6	6.426	2.750
P1_ES6:2 Rigid beam	0.8	5.174	2.671

As shown in Fig. 5.33, tension of the longest hanger H21 is 10021 kN under combined result of D+W, which is exceeded 43% than the allowable equivalent tension of 7007 kN. It means that the longest hanger of H21 near to junction of the cable-stayed parts and suspended parts is required to increase the cross-sectional area or adjust its length of cable after installation in erection phase.

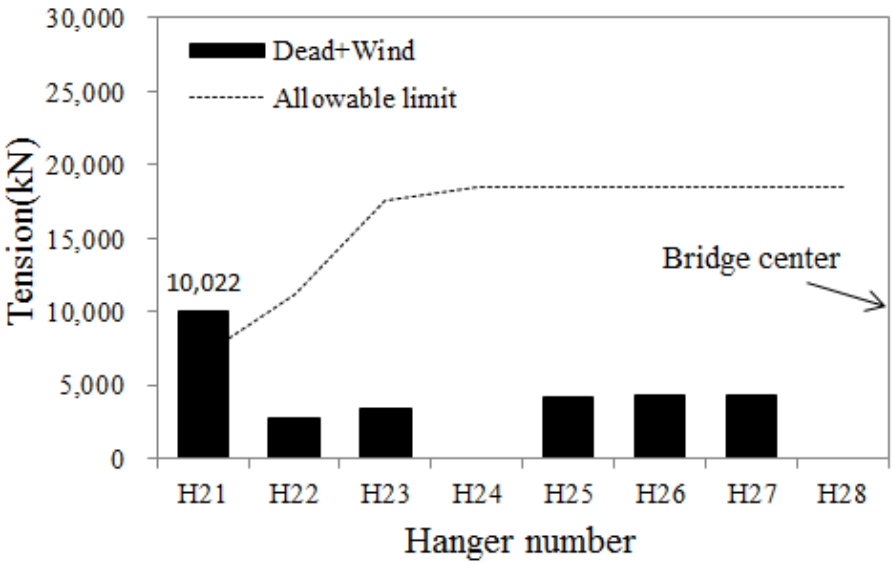

Fig. 5. 33 The tension of hangers under D+W for P1_ES6:2 Rigid beam

(8) Aerodynamic stability for erection stage of P1_ES6 with Strut system

Six strut systems are installed on main cables to improve the torsional stiffness of the bridge deck, as show in Fig. 5.34.

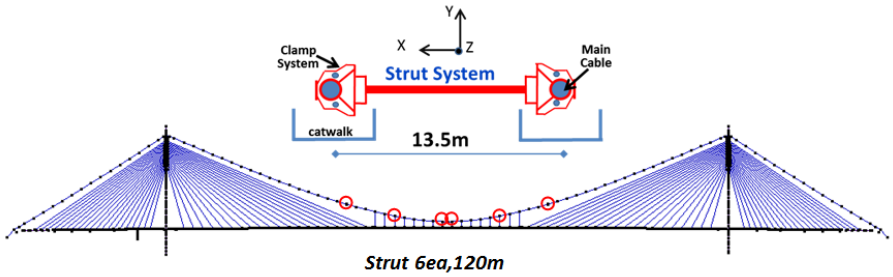

Fig. 5. 34 Enhancement of torsional stiffness by Strut system for P1_ES6

The torsional displacement of suspended deck by applied Strut system can be reduce around 92% compared to bare structure of P1_ES6, as listed in Table 5.10.

Table 5. 10 Influence of Strut system on the maximum displacement at the tip of suspended decks for P1_ES6

Structure	Torsional disp. (Deg.)	Lateral disp. (m)	Vertical disp. (m)
P1_ES6:0 Bare structure	9.9	6.019	2.753
P1_ES6:1 X-Type bracing	6.6	6.426	2.750
P1_ES6:2 Rigid beam	0.8	5.174	2.671
P1_ES6:3 Strut system	0.8	5.689	2.738

As shown in Fig. 5.35, tension of the longest hanger H21 is 9888 kN under combined result of D+W, which is exceeded 41% than the allowable equivalent tension of 7007 kN. It means that the longest hanger of H21 is required to increase the cross-sectional area or adjusts its length of cable after installation in erection phase.

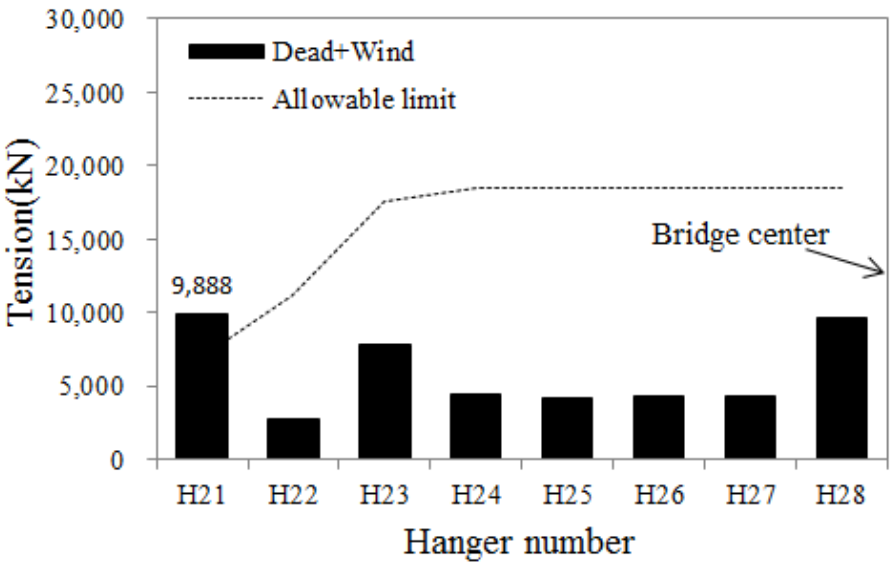

Fig. 5. 35 The tension of hangers under D+W for P1_ES6:3 Strut systems

From effect of the structural stabilization measures in erection stage of P1_ES6, both Strut system and Rigid beam are effective to control the torsional displacement of suspended deck and those measures can reduce around 92% compared with bare structure of P1_ES6. But Rigid beam limited usage can be adapted for short hanger part. However, strut system has less limitation compared to Rigid beam. Therefore, aerodynamic stability for construction Plan 1 is investigated with six Strut system installed on the main cables in order to stabilize the torsional deformation of suspended deck.

(9) Aerodynamic stability of construction Plan 1

Fig. 5.36 and 5.37 show the dominant frequency of torsion, lateral, and

vertical of the deck in each erection phase of cable-stayed parts and suspended part, respectively. Along with deck erection increases, the dominant frequency of torsion, lateral, and vertical tends to be reduced, which indicates that overall rigidity of bridge structure becomes smaller, as shown in Fig. 5.36.

For the dominant frequency of deck at the suspended part, the 1st vertical frequency increases as erection of suspended deck is increased. However, the 1st torsional frequency of deck in each erection phase is reduced and the 1st lateral frequency of deck in each erection phase is constant, as shown in Fig. 5.37.

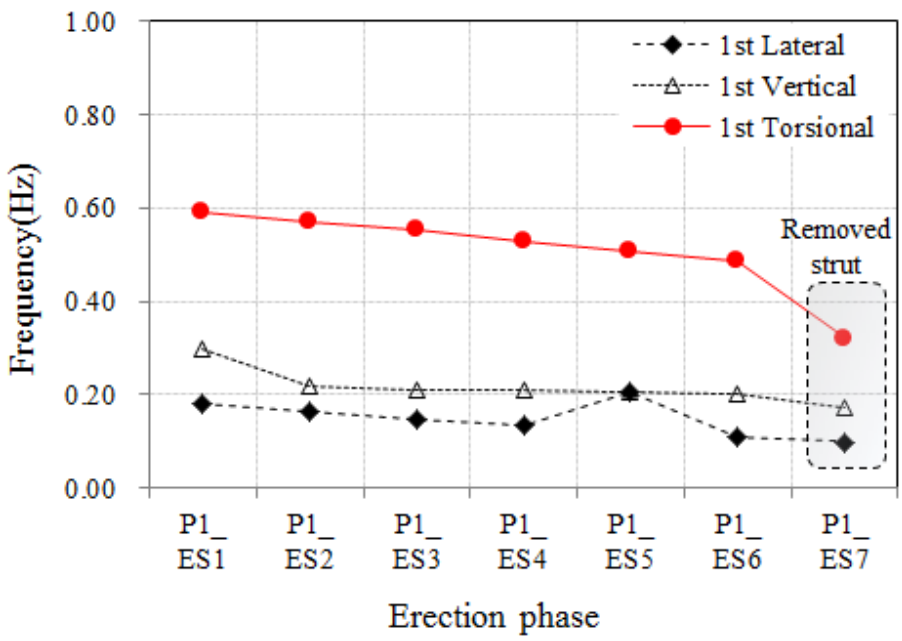

Fig. 5. 36 The dominant frequency of cable-stayed deck for construction Plan 1

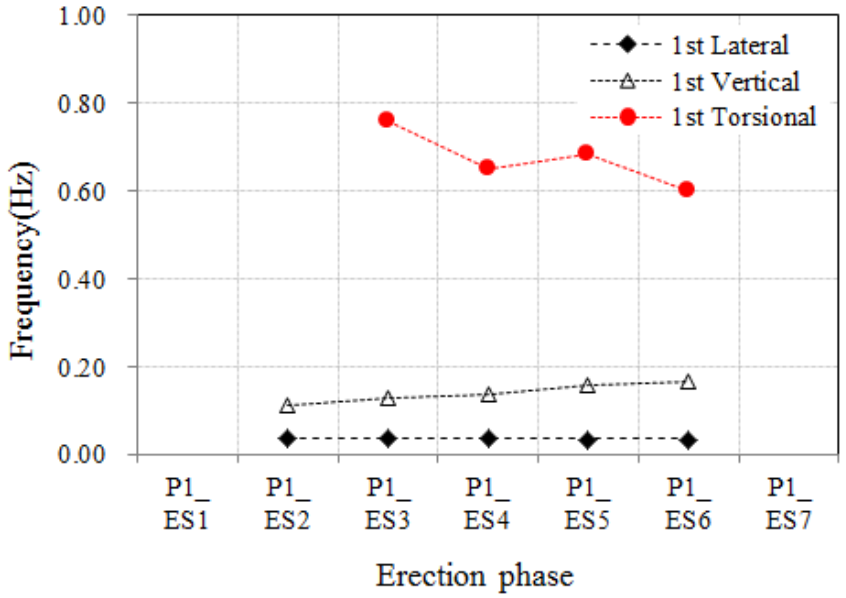

Fig. 5. 37 The dominant frequency of suspended deck for construction Plan 1

Fig 5.38~5.40 show the maximum torsional displacement, lateral displacement, and vertical displacement at the tip of cantilever deck under wind load, respectively. The maximum torsional displacement at the tip of cantilever tends to rises as the increase of deck erection, as shown in Fig. 5.38. The largest maximum torsional displacement of deck at the suspended part can be found 0.8° under combined results of mean wind and buffeting at the erection stage of P1_ES6. The maximum lateral displacement of deck about 6m is constant in the erection phases for construction Plan 1, as shown in Fig. 5.39. On the other hand, the maximum vertical displacement of deck can be found at the initial erection stage of P1_ES2 and its value is 2.89m, as shown in Fig 5.40.

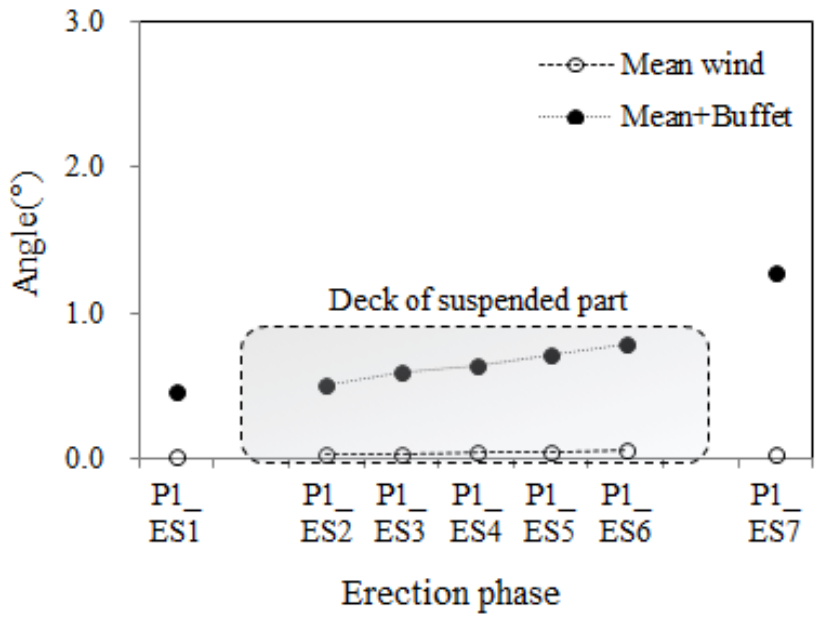

Fig. 5. 38 The maximum torsional displacement of deck in construction Plan 1

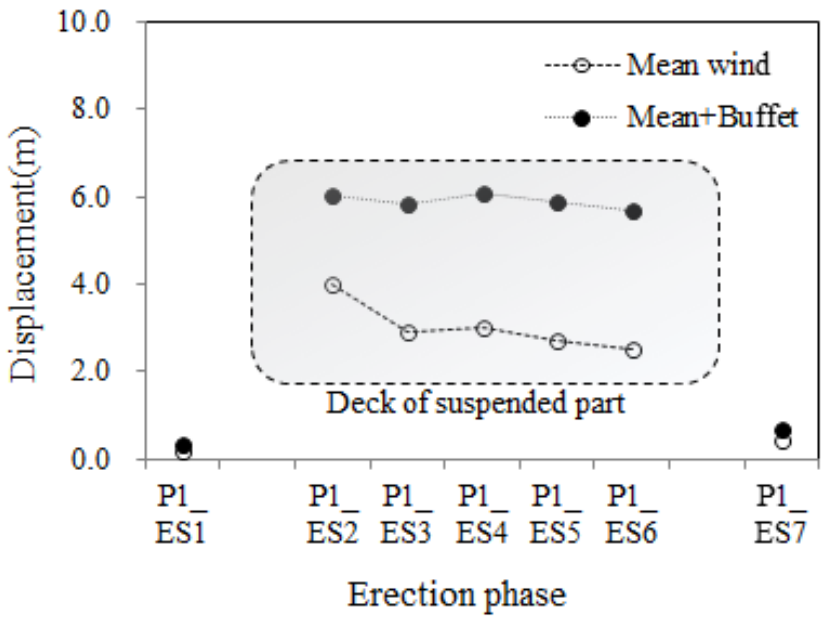

Fig. 5. 39 The maximum lateral displacement of deck in construction Plan 1

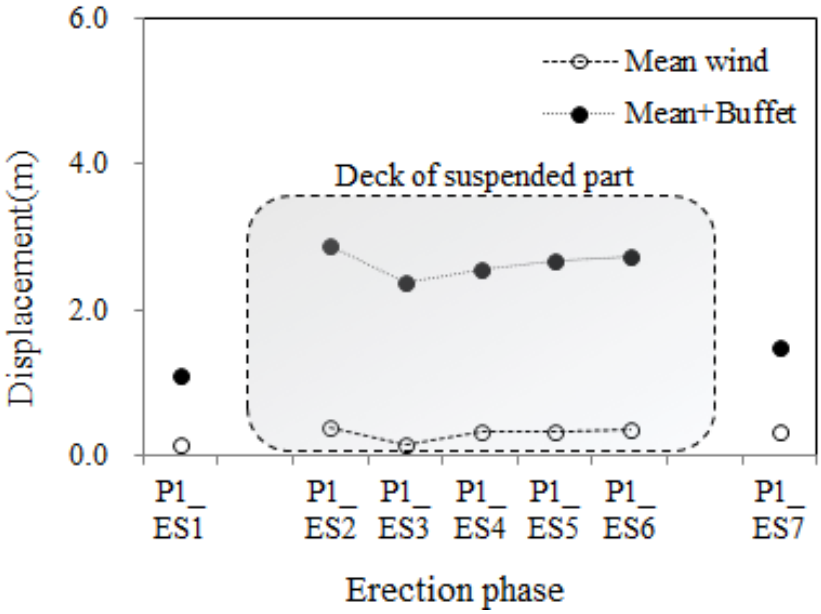

Fig. 5. 40 The maximum vertical displacement of deck in construction Plan 1

Fig 5.41 shows distribution of stay cable tensions under combined dead load and wind load for erection stages in construction Plan 1. In all cases, the tensions of stay cables under loading case of dead load and wind load are limited to allowable equivalent tension of each stay cables.

Fig 5.42 shows distribution of hanger tensions under loading case of D+W for each erection stage in construction Plan 1. The longest hanger of H21 exceeded the allowable equivalent tension after their installation in erection stage of P1_ES6. In order to secure the aerodynamic stability, hanger of H21 needs to increase the cross-sectional area or adjust its length of cable after their installation in erection stage of P1_ES6. The maximum hanger tension increase is up to 14558 kN for H21.

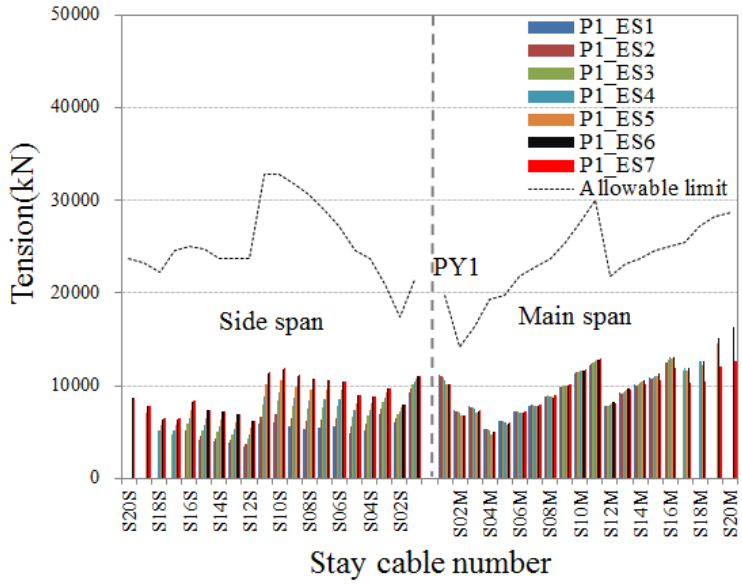

Fig. 5. 41 Distribution of stay cables tension under D+W in construction Plan 1

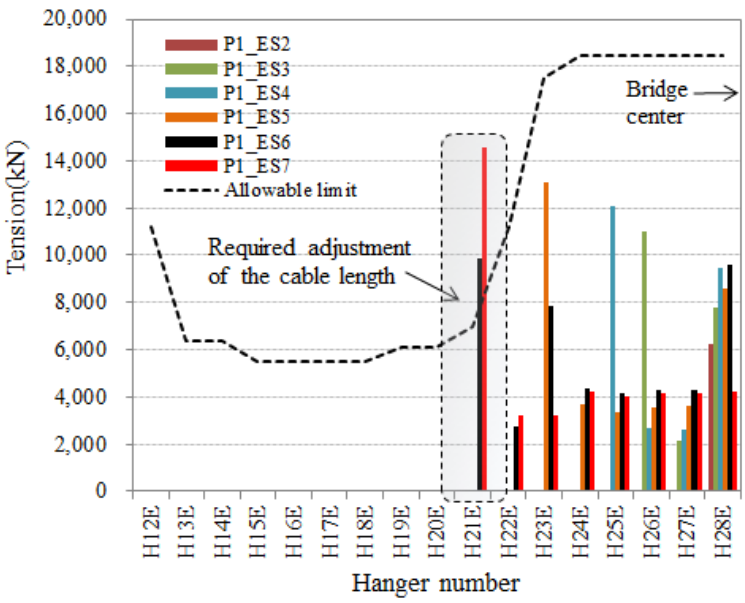

Fig. 5. 42 Distribution of hangers tension under D+W in construction Plan 1

(10) Parameter study of strut system for construction Plan 1

To adapt Strut system, parametric study is carried out with various layouts on the main cable considering the number of its uses and with stiffness sensitivity.

To describe the effect of the number of Strut system, four different layout of Strut system on the main cable are considered in erection stage of P1_ES2 for this study, as shown in Fig. 5.43.

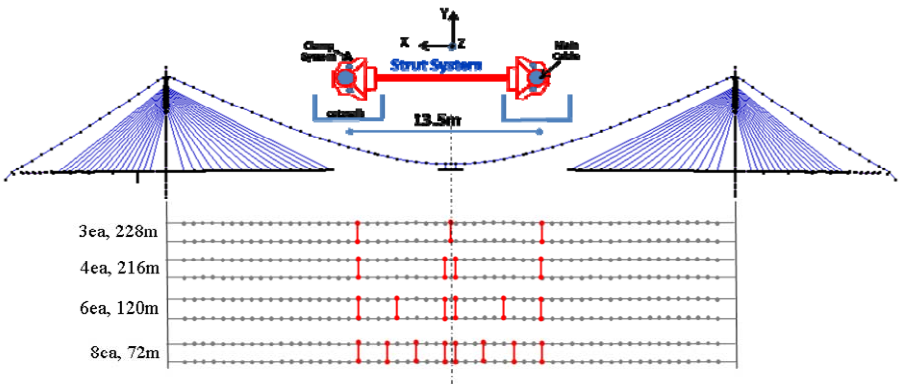

Fig. 5. 43 Layout of Strut system on the main cable

As shown in Fig. 5. 44, an increase of the number of Strut system is efficient to reduce the torsional displacement of suspended deck. The case of applying three Strut system with interval of 228m on the main cable produces the biggest torsional displacement of the suspended deck under combined results of mean wind and buffeting. After applying four Strut systems, the torsional deformation of suspended deck is converged. For the structural safety in erection phases, four to

six of Strut systems are recommended for this example bridge.

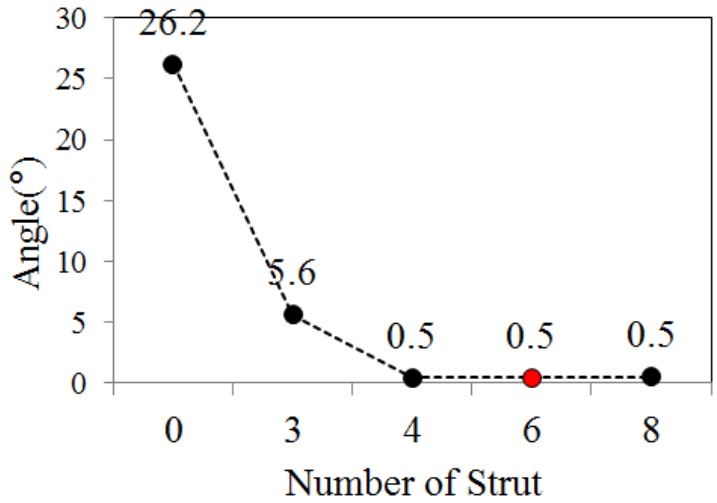

Fig. 5. 44 Torsional displacement of suspeded deck with number of Strut

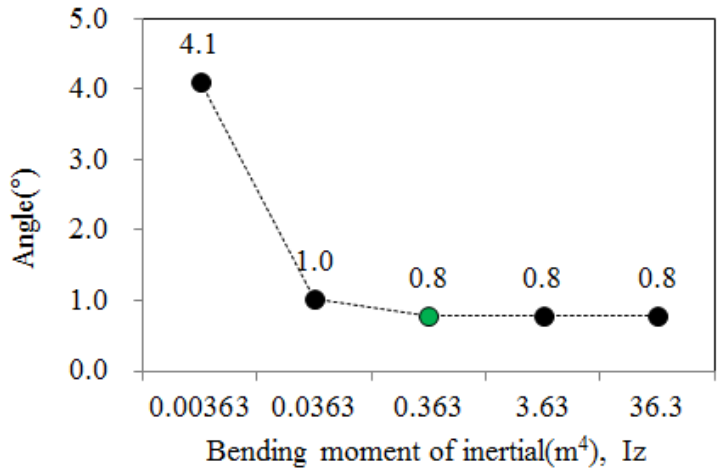

Fig. 5. 45 Torsional displacement of suspeded deck with various moment of inertia Iz

When the vertical stiffness multiple of the Strut system changes from 0.01 to 100 in erection stage of P1_ES6, the torsional displacement of suspended deck is shown in Fig. 5.45. The bending moment of inertia Iz in the Strut system is the most sensitive for the torsional displacement of suspended deck and the minimum value of Iz=0.36 m^4 is required for the structural safety in erection phases, as shown in Fig. 5.45.

(11) Aerodynamic stabilizing method by lifting gantry for construction Plan 1

The lifting gantry, which is the construction equipment for the suspended deck, is examined as an aerodynamic stability enhancement measure. The stiffness of the lifting gantry is considered by calculating the equivalent stiffness with applied actual cross-section, as listed in Table 5.11.

Table 5. 11 Equivalent stiffness for lifting gantry

Structure	Area (m^2)	J (m^4)	Iy (m^4)	Iz (m^4)
Lifting gantry	0.2862	0.0857	0.0103	0.0401

Fig 5.46 shows the position of lifting gantry for each erection phase of deck in suspended part.

Fig 5.47~5.48 show the maximum torsional displacement at the tip of cantilever deck under wind load and distribution of hanger tensions under loading case of D+W for each erection stage with lifting gantry in construction Plan 1,

respectively. The largest maximum torsional displacement of deck at the suspended part can be found 1.9° under combined results of mean wind and buffeting at the erection stage of P1_ES5, as shown in Fig. 5.47.

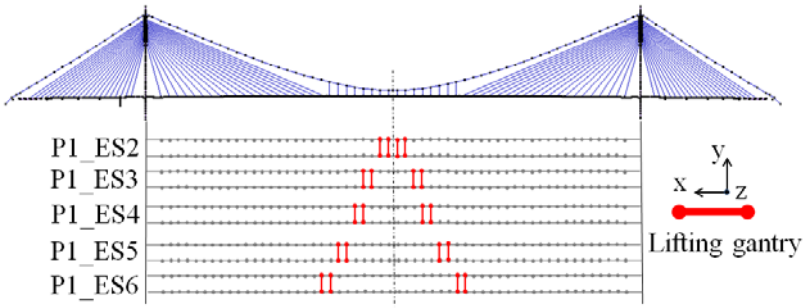

Fig. 5. 46 The position of the lifting gantry for the erection phase of deck in construction plan1

The longest hanger of H21 exceeded the allowable equivalent tension after their installation in erection stage of P1_ES6. In order to secure the aerodynamic stability, hanger of H21 needs to increase the cross-sectional area or adjust its length of cable after their installation in erection stage of P1_ES6. The maximum hanger tension increase is up to 8810kN for H21.

From above results, the lifting gantry can be applicable for aerodynamic stabilizing measures to mitigate the torsional deformation of suspended deck during construction stage.

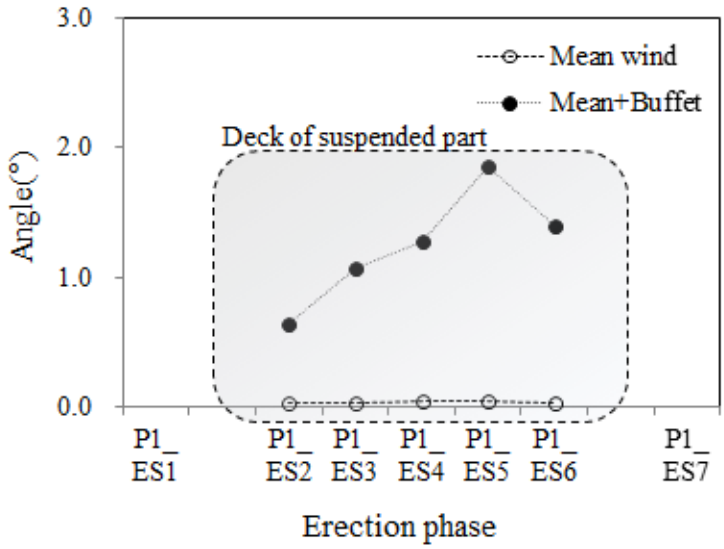

Fig. 5. 47 The maximum torsional displacement of deck with lifting gantry in construction Plan 1

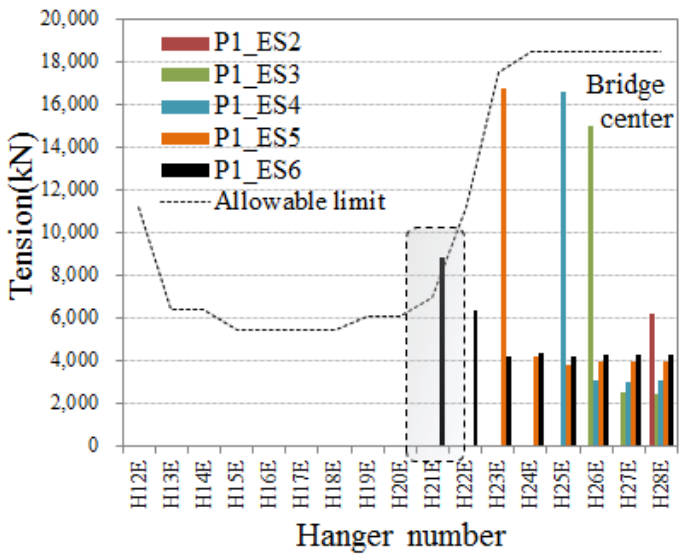

Fig. 5. 48 Distribution of hangers tension under D+W with lifting gantry in construction Plan 1

(12) Summary of aerodynamic stability for construction Plan 1

Aerodynamic stability problems are expected for the suspended deck in construction Plan 1. In order to improve the torsional rigidity of suspended deck, three different structural measures such as X-Type bracing, Rigid beam, and Strut system are considered in aerodynamic stability analysis.

These proposed measures are effective to improve the torsional stiffness of deck as shown in Fig 5.49. But X-Type bracing need to adjust its length of cable for each erection phase. The Rigid beam limited usage can be adapted for short hanger part only.

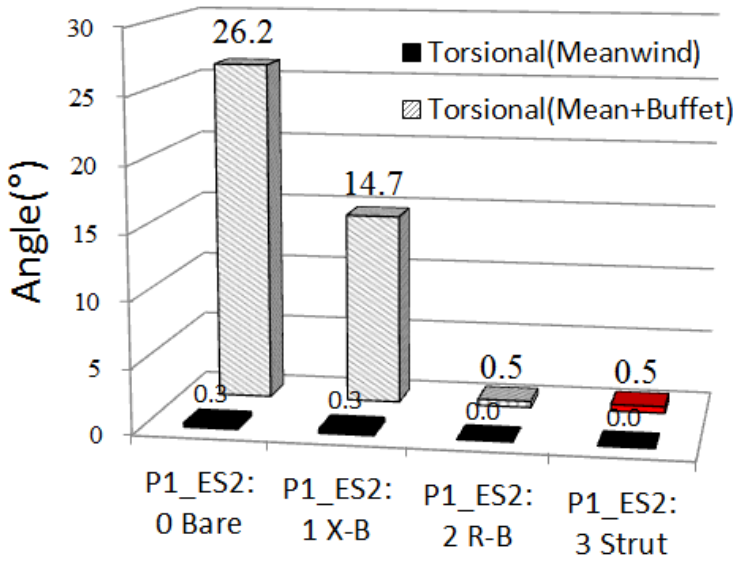

Fig. 5. 49 The torsional displacement of deck under different structural measures for P1_ES2

However, strut system has less limitation compared to other structural stabilization measures, but economic problem should be reviewed depending on the number of its uses.

In order to reduce the torsional deformation of suspended deck in construction, Strut system is the most effective structural measure. In case of applying Strut system on the main cable in Construction Plan 1, the torsional angle of suspended deck is controlled with less than 1° during the erection of suspended decks. The distribution of stay cables tensions in the each erection stage are lower than the allowable tension of each stay cable. However, the longest hanger of H21 near to junction of the cable-stayed parts and suspended part require an increase of cross-sectional area or adjust its length of cable since the installation phase in order to secure aerodynamic stability.

The lifting gantry can be applicable for an aerodynamic stabilization measure to control the rigid body torsional deformation during erection of suspended decks.

5.5 Aerodynamic feasibility study on an alternative construction plan

A feasibility study for another potential sequence of erection, which can reduce overall construction period, is performed with aerodynamic stabilizing measures combined of strut system and lifting gantry. When the suspended deck segments as well as the configuration of main cables come to the final position, the welding between suspended decks can be carried out. By delaying welding process, the deck segments can be erected in a fast-track mode. As shown in Fig. 5.50, seven erection stages were selected for construction plan based on completed erection of pylons and the side spans decks, and described as follows:

Erection stage (ES) 1: The pair of deck segments D0 to D12 with 24 stay cables in each cable plan is installed. The main cable completed and D14 to D15 with H14 to H15 are installed.

ES2: The pair of decks D16 to D17 and the stay cables S16 to S17 are installed.

ES3: The pair of decks D18 to D19 and the stay cables S18 to S19 are installed.

ES4: The pair of decks D20 to D21 and the stay cables S20 to S21 are installed.

ES5: The pair of decks D22 to D23 and the stay cables S22 to S23 are installed.

ES6: The pair of decks D24 to D25 and the stay cables S24 to S25 are installed.

ES7: The pair of decks D26 to D28 and the stay cables S26 to S28 are installed

The notation of A1 in Fig. 5.50 is indicated alternative construction plan.

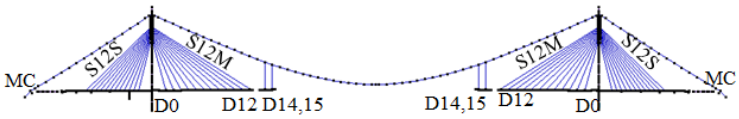

(a) A1_ES1; deck erected 52%

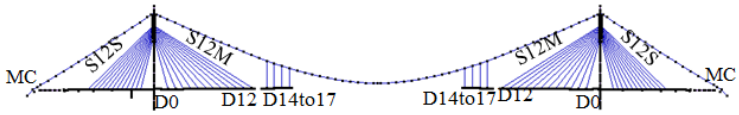

(b) A1_ES2; deck erected 58%

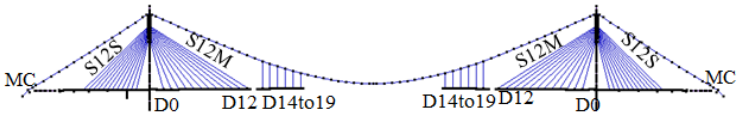

(c) A1_ES3; deck erected 65%

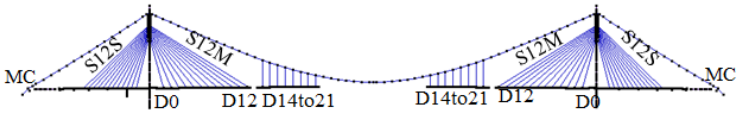

(d) A1_ES4; deck erected 72%

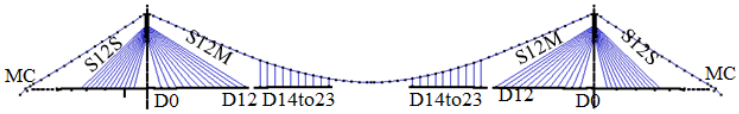

(e) A1_ES5; deck erected 79%

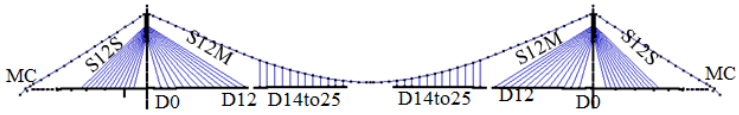

(f) A1_ES6; deck erected 86%

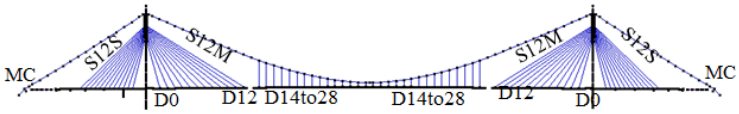

(g) A1_ES7; deck erected 96%

Fig. 5. 50 FE models of erection sequence in alternative construction plan

The construction period for the erection of main span decks is calculated, as listed in Table 5.12. The cable-stayed parts is assumed to use free cantilever method by derrick crane and 1cycle of 8days for erection of the deck (i.e., lift and erect of deck segment is 1day, install stay cable is 3days, welded deck segment is 4days). Otherwise, the suspension part is considered to use strand jack method for the lifting of deck segment and 1cycle of 1days for erection of the deck (i.e., lift and erect of deck segment, install hanger is 1day).

Table 5. 12 The estimated construction durations for alternative construction plan

Erection sequence	Activity	Duration (Days)	Cumulative (Days)
A1_ES1	D00, D01 to D12, S01 to S12 D14 to D15, H14 to H15	106 (=8day+12block×8day +2block×1day)	106
A1_ES2	D16 to D17, H16 to H17	2 (=2block×1day)	108
A1_ES3	D18 to D19, H18 to H19	2 (=2block×1day)	110
A1_ES4	D20 to D21, H20 to H21	2 (=2block×1day)	112
A1_ES5	D22 to D23, H22 to H23	2 (=2block×1day)	124
A1_ES6	D24 to D25, H24 to H25	2 (=2block×1day)	126
A1_ES7	D26 to D28, H26 to H28 Welding	75 (=3block×1day +18 block×4day)	201
Etc.	1st (D13) and 2nd (D99) key segment	12 (=1block×5day +1block×7day)	**213**

Note: D** - deck segment number, S**- stay cable number, and H**-hanger number

Alternative construction plan can be reduced by 58 days compared with construction Plan 0 based on the completed erection of pylons and the decks of side spans. However, it is required to verify the aerodynamic stability on the construction phase of suspended deck.

In this section, the feasibility of an alternative construction plan examines in terms of aerodynamic stability with aerodynamic stabilizing measures combined of strut system and lifting gantry. Fig 5.51 shows the position of Strut system and lifting gantry for each erection phase of deck in suspended part.

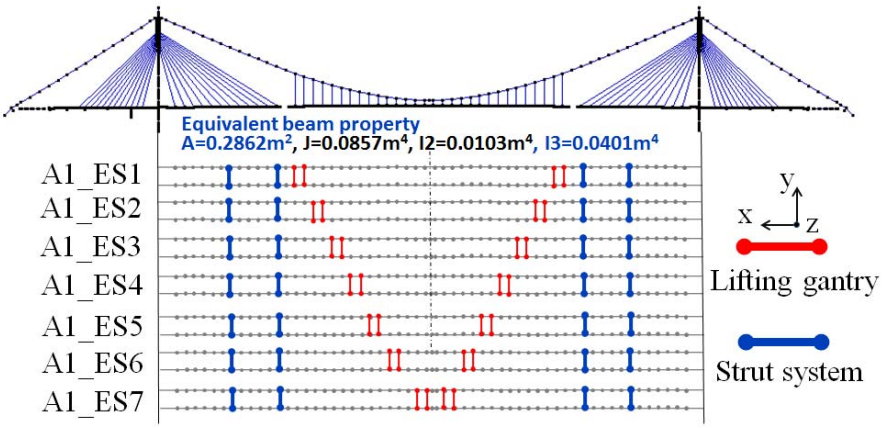

Fig. 5. 51 The position of the lifting gantry for the erection phase of deck in alternative construction plan

For the dominant frequency of deck at the suspended part, the 1st torsional frequency of deck in each erection phase is reduced. However, the 1st vertical frequency increases as erection of suspended deck is increased and the 1st lateral

frequency of deck in each erection phase is constant, as shown in Fig. 5.52.

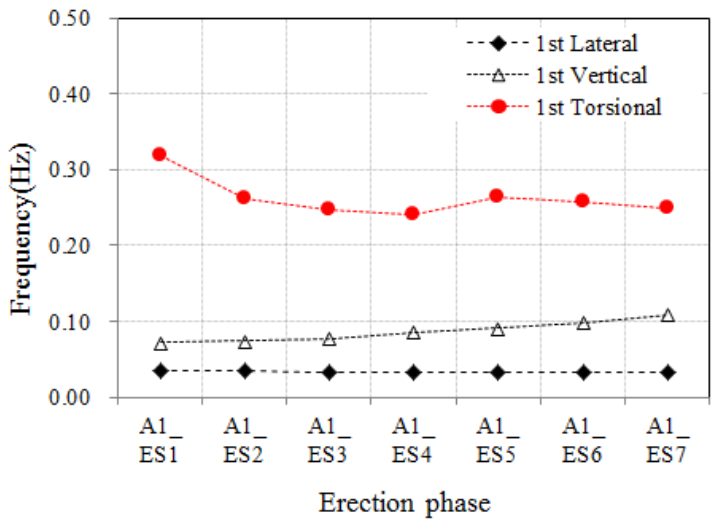

Fig. 5. 52 The dominant frequency of suspended deck for alternative construction plan

Fig 5.53~5.55 show the maximum torsional displacement, lateral displacement, and vertical displacement at the tip of cantilever deck under wind load, respectively. The maximum torsional displacement at the tip of cantilever tends to descend as the increase of deck erection, as shown in Fig. 5.53. The largest maximum torsional displacement of deck at the suspended part can be found to be equal to 3.6° under combined results of mean wind and buffeting at the erection stage of A1_ES2. The maximum lateral displacement of deck is decreased from 6.7m to 5.5m in the erection phases for alternative construction plan, as shown in Fig. 5.54. On the other hand, the maximum vertical displacement of deck can be found at the initial erection stage of A1_ES2 and its value is 3.6m, as shown in Fig. 5.55.

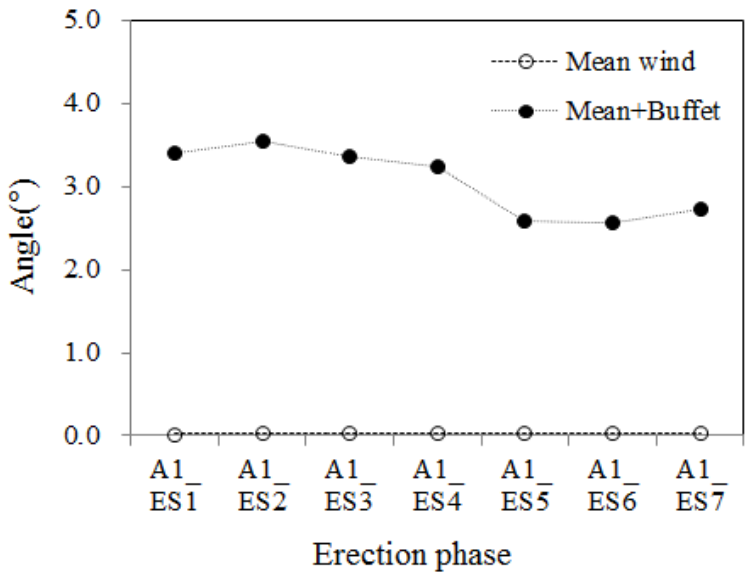

Fig. 5. 53 The maximum torsional displacement of deck in alternative construction plan

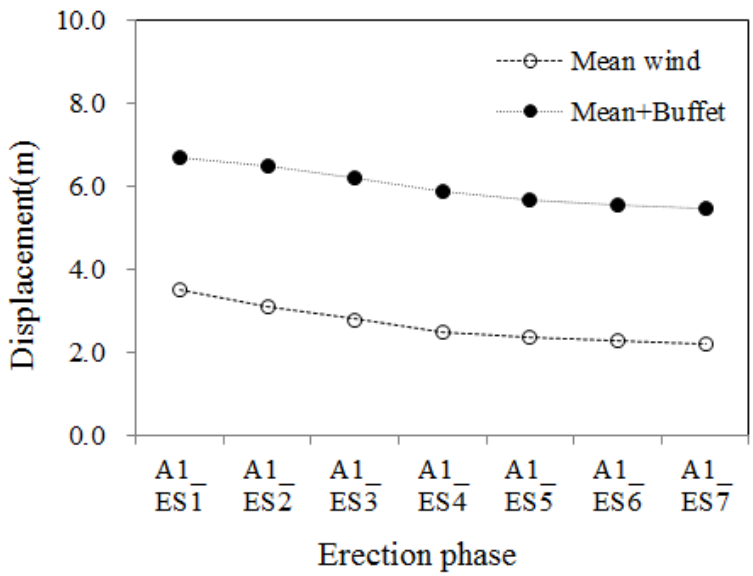

Fig. 5. 54 The maximum lateral displacement of deck in alternative construction plan

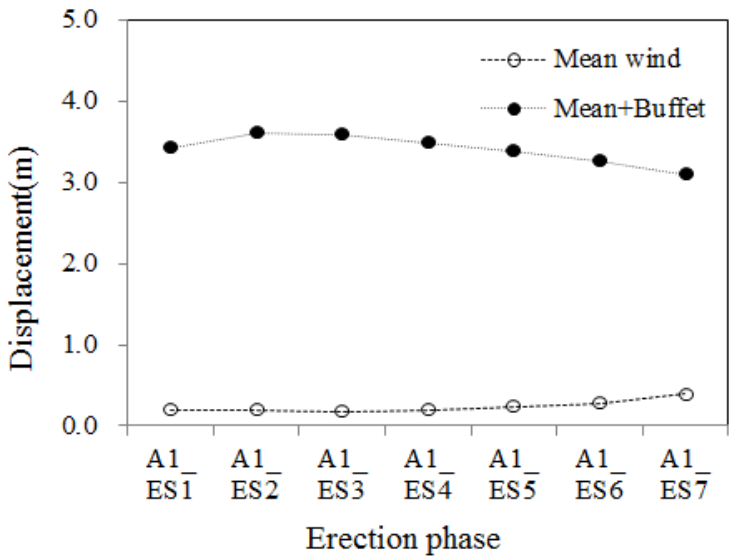

Fig. 5. 55 The maximum vertical displacement of deck in alternative construction plan

Fig 5.56 and 5.57 show the distribution of tension for stay cables and hangers under combined dead load (D) and wind load (W) for erection stages in alternative construction plan. In all cases, the tensions of stay cables are limited to allowable equivalent tension, as shown in Fig. 5.56. The hanger of H14 and H17 to H23 exceeded the allowable equivalent tension after their installation in erection stage, as shown in Fig 5.57. In order to secure the aerodynamic stability, those hangers need to increase the cross-sectional area or adjust its length of cable after their installation.

In conclusion, the alternative construction plan seems to be feasible in terms of secured aerodynamic stability by combined of strut system and lifting gantry as aerodynamic stabilizing measures.

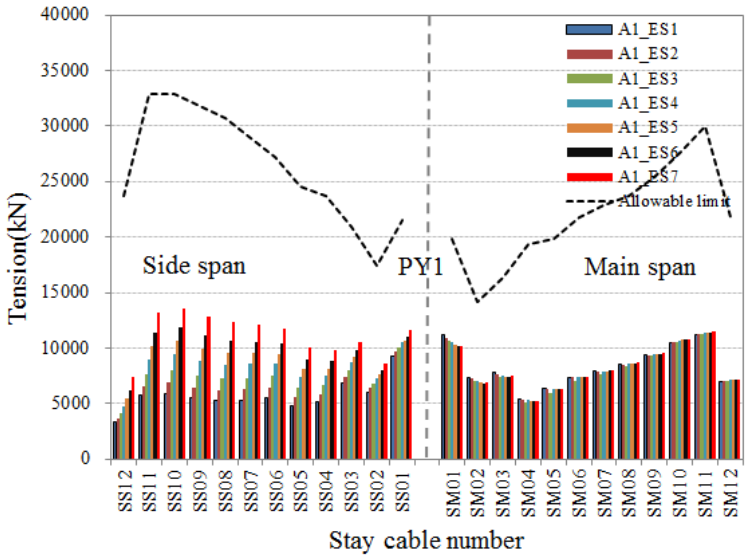

Fig. 5. 56 Distribution of stay cables tension under D+W in alternative construction plan

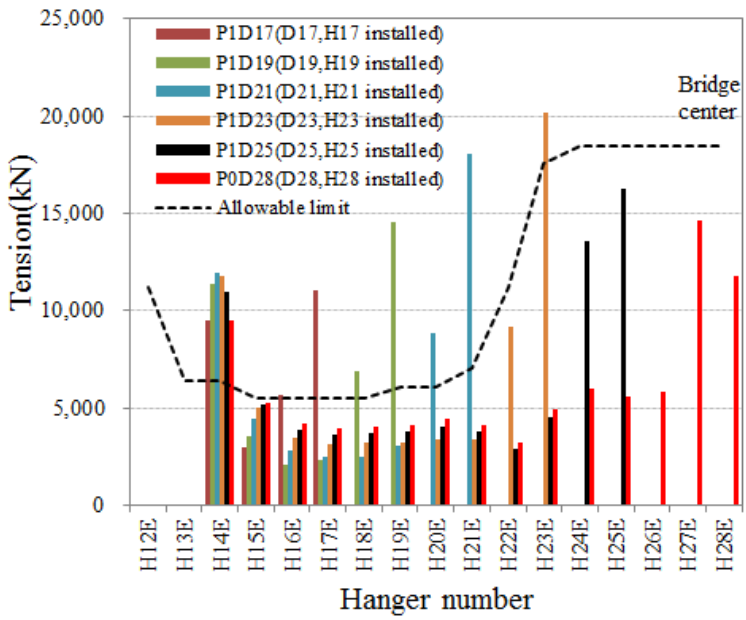

Fig. 5. 57 Distribution of hangers tension under D+W in alternative construction plan

5.6 Summary

This study examines the aerodynamic stability of a cable-stayed suspension bridge in erection sequences of suspended deck. The overall results are as follows.

1. In the case of applying Construction Plan 0 as series construction scheme, aerodynamic stability of the suspended deck in construction phase is assured, however, the longest hanger of H21 near to junction required an increase of cross-sectional area or adjust its length after installation in order to secure aerodynamic stability.
2. In the case of applying Construction Plan 1, the excessive rigid body torsional deformation of 26° in the suspended deck is found in the initial construction stage due to the rigid body motion of the suspended deck by the vertical mode of main cable. In order to control the rigid body torsional deformation of the suspended deck, the most effective structural stabilization measure is the strut system by installing on the main cables.
3. In the case of applying Strut system on the main cable in Construction Plan 1, the rigid body torsional angle of suspended deck is controlled less than 1° during the erection of suspended decks. The distribution of stay cables tensions in the each erection stage are lower than the allowable tension of cable. However, the longest hanger of H21 near to junction of

the cable-stayed parts and suspended parts required an increase of cross-sectional area or adjust its length since the installation phase in order to secure aerodynamic stability.

4. When Construction Plan 1 as simultaneous construction scheme using Strut system, construction assuring aerodynamic stability is possible and construction period can be reduced by 48 days compared to Construction Plan 0 as series construction scheme. However, it is required to have proper construction management of two type of bridge structure according to simultaneous construction in both deck of cable-stayed parts and suspended part.
5. The lifting gantry can be applicable for an aerodynamic stabilization measure to control the rigid body torsional deformation during erection of suspended decks.
6. When alternative construction scheme in which suspended decks are erected from tower side to center of mid-span with combined of strut system and lifting gantry, construction assuring aerodynamic stability is possible and construction period can be reduced by 58 days compared to Construction Plan 0 as series construction scheme.

Chapter 6

Conclusions

In order to comprehensively understand and a realistically predict the structural behavior of a cable-stayed suspension bridge, both parametric study and aerodynamic stability in construction stage are investigated. The following conclusions can be made based on the obtained results:

Firstly, parametric study is carried out. Two design parameters, the suspension-to-span ratio and length of transition part are considered and studied for their effects on the structural behavior under live loads consisting of trains and road vehicles. A suspension-to-span ratio of 0.22 to 0.56 is effective to increase the overall rigidity of structure compared responses of cable-stayed bridge and suspension bridge. As the suspended portion in main span increases, the vertical displacement of the deck gradually increases and the negative vertical bending moment of deck at the junction between cable-stayed parts and suspended part in main span sharply increases. Also, the cable tension in the longest hanger rapidly increases due to difference stiffness in two structure system such as cable-stayed and suspension part. This can lead to fatigue problems which can be solved by installing the transition part. The transition part to cable-stayed part ratio ranging from 0.1 to 0.45 is favorable for this case study bridge. An equally distributed dead load in transition parts is efficient to reduce the secondary stress of main cable.

Secondly, applicable construction sequences considered fast-track erection for the cable-stayed suspension bridge were defined based on the established construction method, and studied on the aerodynamic stability of its construction sequences which focuses on the erection of suspended deck. Based on the deck erection, two different construction schemes are considered to investigate aerodynamic stability of construction scheme by buffeting analysis for the cable-stayed suspension bridge. The first construction scheme is the construction Plan 0 (series sequence) and the second scheme is the construction Plan 1 (simultaneously construction sequence). As a result, applying construction Plan 0 scheme, aerodynamic stability of the suspended deck is assured. However, one of hangers is required to increase of cross-sectional area or adjusts its length of cable after installation in order to secure aerodynamic stability. In the case of applying construction Plan 1, the excessive torsional deformation in the suspended deck is found in the initial construction stage due to the rigid body motion of the suspended deck by the vertical mode of main cable. In order to control the torsional displacement of deck, X-Type bracing, Rigid beam and Strut system are considered as structural stabilization measures. The most effective structural stabilization measure is the strut system by installing on the main cables. When Construction Plan 1 as simultaneous construction scheme installing six strut systems, construction assuring aerodynamic stability is possible and construction period can be reduced by 48 days compared than Construction Plan 0 as series construction scheme. However, it is required to have proper construction management of two

type of bridge structure according to simultaneous construction in both deck of cable-stayed parts and suspended part. The lifting gantry can be applicable for an aerodynamic stabilization measure to control the rigid body torsional deformation during erection of suspended decks. When alternative construction scheme in which suspended decks are erected from tower side to center of mid-span with combined of strut system and lifting gantry, construction assuring aerodynamic stability is possible and construction period can be reduced by 58 days compared to Construction Plan 0 as series construction scheme.

In conclusion, cable-stayed suspension bridges provide better structural performance under train load compared conventional system of cable-stayed bridges and suspension bridge. Consequently, cable-stayed suspension bridges are expected to be more widely used for long-span cable supported bridge including railway bridges. Also, proposed aerodynamic stabilizing measures of strut system and lifting gantry can be applicable to mitigate the rigid body torsional deformation of suspended decks during construction stages for cable-stayed suspension bridges and long span suspension bridge.

In reviewing the study, the following points are suggested for further research. The reasonable finished dead load state is a lack of convenient method in case of complex boundary conditions at side spans as can be found in the example bridge of this paper. Therefore, analysis method for determination of reasonable completed dead load state is required based on the optimization concepts in order to economic design of structure. Also, effect of some design parameters should be

investigated such as the rise-span ratio and the number of subsidiary piers in side spans on structural static and dynamic behaviors under loading of live and wind.

The proposed aerodynamic stabilizing measures of strut system and lifting gantry can be successfully applied to control the rigid body torsional deformation of suspended decks during construction stages for a cable-stayed suspension bridge. However, the extension to application of aerodynamic stabilizing measures for the long span and multi span suspension bridges should be studied. Also, flutter analysis should perform with proposed aerodynamic stabilizing measures considering aerodynamic derivatives by wind tunnel test to ensure the validity of the stability limits.

REFERENCES

Ahn, S.S., 1991. Static and dynamic nonlinear analysis of spatial cable networks using elastic catenary cable element, M. S. thesis, Seoul National University, Seoul, Korea.

Andreu, A., Gil, L., Roca, P., 2006. A new deformable catenary element for the analysis of cable net structures, Comput. Struct. 84, 1882-1890.

Bathe K., 1996. Finite element procedures. Prentice-Hall, Englewood Cliffs, N.J.

Brancaleoni, F., 1992. The construction phase and its aerodynamic issues, Aerodynamics of large bridges, A. Larsen, ed., Balkema, Rotterdam, The Netherlands, 147-158.

Bruno, D., Greco, F., Lonetti, P., 2009. A Parametric Study on the Dynamic Behavior of Combined Cable-Stayed and Suspension Bridges under Moving Loads. International Journal for Computational Methods in Engineering Science and Mechanics 10(4), 243-258.

Choi, J.H., 2013. Initial shape analysis for cable-stayed and suspension bridges by

nonlinear FEM considering unstrained length, M. S. thesis, SungKyunKwan University, Seoul, Korea.(in Korean)

Chopra, A. 2007. Dynamics of structures. Pearson Prentice Hall.

Cobo del Arco, D., Aparicio, A.C., 2000. Improving the wind stability of suspension bridges during construction. J. of Struct Engrg, ASCE 127(8), 869-875.

European Committee for Standardization, EN 1991-2, 2003. Traffic loads on bridges, Brussels, CEN

Gavin, H. P., 2012. Geometric stiffness effects in 2d and 3d frames, Lecture notes, Duke University, Fall.

Ge, Y.J., Tanaka, H., 2000. Aerodynamic stability of long-span suspension bridges under erection. J. of Struct Engrg, ASCE 126(12), 1404-1412.

Greisch, 2013. 3rd Bosphorus bridge - Actions – wind, Design report, Greisch, Belgium.

Greisch, 2014. 3rd Bosphorus bridge – Model description – General beam model, Design report, Greisch, Belgium.

Gimsing, N.J., Georgakis, C.T., 2012. Cable supported bridges: concept and design, 3rd Edition, Wiley, New York.

Honda, A., Miyata, H., Shibata, H., 1998. Aerodynamic stability of narrow decked suspension bridge (Aki-nada Ohashi Bridge), J. of wind Engineering and Industrial Aerodynamics 77&78, 409-420.

Irvine, H. M., 1981. Cable structures. MIT Press, Cambridge.

Jayaraman, H., Knudson, W., 1981. A curved element for the analysis of cable structures, Comput Struct. 14(3-4), 325-333.

Jung, M.R., Min, D.J., Kim, M.Y., 2013 Nonlinear analysis methods based on the unstrained element length for determining initial shaping of suspension bridges under dead loads, Computers and Structures, 128, 272-285.

KBDC, 2015. Korean Highway Bridge Design Code (Limit State Design) – Cable supported Bridges.

Kim, K.H., 2011. Initial equilibrium configuration analysis for bridges supported with stayed and suspended cables. M. S. thesis, Seoul national university, Seoul, Korea. (in Korean)

Kim, H.K. 1993. Three dimensional analyses of suspension bridges considering construction stages. Ph. D. thesis, Seoul National University, Seoul, Korea.

Kim, H.K., Kim, K.T., Lee, H., Kim, S.J., 2013. Performance of unpretensioned wind stabilizing cables in the construction of a cable-stayed bridge. J. Bridge Eng. 10(1061), 722-734

Kim, K.S., Lee, H.S., 2001. Analysis of target configurations under dead loads for cable-supported bridges. Comput Struct 79, 2681-2692.

Kim, H.K., Kim, M.Y., 2012. Efficient combination of a TCUD method and an initial force method for determining initial shapes of cable-supported bridges. Int J of Steel Struct, 12, 157-74.

Kim, H.K., Lee, M.J., Chang, S.P., 2002 Nonlinear shape-finding analysis of a self-anchored suspension bridge, Engineering Structures, 24(12). 1547-1559.

Kim, H.K., Shinozuka, M., Chang, S.P., 2004. Geometrically nonlinear buffeting responses of a cable-stayed bridge. J. Eng. Mech. 130(7), 848-857.

Kubo, K., 2007. Basic research on the feasibility and aerodynamic stability of hybrid suspension bridge for super long suspension bridges, Ph.D. thesis, Kyushu

Institute of Technology, Kyushu, Japan.

Kyung, Y.S., 2002. An improved method for initial shape analysis of cable supported bridges, M. S. thesis, SungKyunKwan University, Seoul, Korea. (in Korean)

Larsen, A., 1995. Prediction of aeroelastic stability of suspension bridges during erection. PROC., 9th Int. Conf. on Wind Engrg., New Delhi, India.

Lee, M.J., Kim, H.K., 2015 Angular change and secondary stress in main cables of suspension bridges, International Journal of Steel Structure 16(2), 573-585

Lee, H., Kim, H.K., Kim, M.S., Cho, E.K., 2015 Enhancement of wind stability of a cable-stayed suspension bridge in construction, Proceedings of Annual Academic Conferences, Jeju, KSSC.(in Korean)

Lonetti, P., Pascuzzo, A., 2014. Optimum design analysis of hybrid cable-stayed suspension bridges. Advances in Engineering Software 73, 53-66.

MathWorks. 2013. MATLAB R2013b. MathWorks, Simulink.

McGuire, W., Gallagher, R.H., Ziemian, R.D., 2000. Matrix structural analysis 2nd

edition, John Wiley & Sons, New York.

Michel Virlogeux, 2013. Presentation du pont, The conceptual design of the Third Bosphorus Bridge

Nakamura, K., 2006. Ultimate instability problem of long-span cable-stayed bridges and applicability to ultra-long span, Ph. D. thesis. Tokyo Metropolitan University, Tokyo, Japan. (in Japanese)

O'Brien, W.T., Francis, A.J., 1964. Cable movements under tow-dimensional loads, J. Struct. Div. ASCE 90, 89-124.

Simiu, E., Scanlan, R.H., 1996. Wind effects on structures, Wiley, New York.

Strømmen, E. N., 2010 Theory of bridge aerodynamics, Springer, Berlin.

Sun, B., Cai, C., Xiao, R., 2013. Analysis strategy and parametric study of cable-stayed-suspension bridges. Advances in Structural Engineering 16,1081-1102.

Von Karman, T., 1948. Progress in the statistical theory of turbulence, J. of Maritime Research 7.

Wang, P.H., Yang, C.G., 1996. Parametric studies on cable-stayed bridges. Comput Struct. 60(2), 243-260.

Xiang, H., Ge, Y.J., 2007. Aerodynamic challenges in span length of suspension bridges, Frontiers of Architecture and Civil Engineering in China 1(2), 153-162

Yang, Y.B., Kuo, S.R., 1994. Theroy and analysis of nonlinear framed structures. Prentice Hall, Singapore.

Zhang, X., Stern, D., 2008. Wind-resistant design of cable-stayed-suspension hybrid bridges. Transportation and Development Innovative Best Practices, 444-449.

Zhang, X.J., Sun, B.N., 2005. Aerodynamic stability of cable-stayed-suspension hybrid bridges. Journal of Zhejiang University SCIENCE 6A, 869-874.

Zhang, X.J., 2006. Study of design parameters on flutter stability of cable-stayed-suspension Hybrid bridges. Wind Struct. 9(4), 331-344.

Zhang, X.J., 2007. Investigation on mechanics performance of cable-stayed-suspension hybrid bridges. Wind and Structures 10, 533-542.

http://www.3kopru.com/eng/photogallery

http://highestbridges.com/wiki/index.php?title=Wujiang_Bridge_Lanhai

국 문 초 록

도로-철도 병용교에 적용이 가능한 사장-현수교의 구조특성 분석을 위한 변수연구와 내풍안정성을 확보한 가설 순서에 대한 연구를 수행하였다. 8차선 도로와 2차선 열차하중을 수용하는 주경간 1408m 사장-현수교를 예제 교량으로 선정하였다.

디자인 변수연구는 전체 강성에 영향이 큰 suspension-to-span ratio를 고려하여 7개의 해석모델을 작성하였다. 열차하중과 차량하중을 포함하는 활하중 모델을 고려하여 정적 비선형 해석을 수행하였다. 연직 강성 측면에서 응답을 분석하였다. 검토결과 사장교와 현수교의 응답 대비 연직 강성 확보 측면에서 가장 효과적인 suspension-to-span ratio 비율은 0.22~0.56 이다. 현수구간이 증가할 수록 연직 변위가 증가하고, 사장교부와 현수교부의 경계 위치에서 거더의 급격한 부모멘트 증가 현상이 발생한다. 특히, 사장교부와 현수교부의 경계 위치의 선단 행어에 큰 장력이 발생하며, 이는 피로 문제를 발생시킬 수 있다. 이러한 문제는 사장교와 현수교의 결합에서 발생하는 강성 차이로 인해 발생하며, transition구간을 설정하여 해결이 가능하다. 효과적인 transition part-to-cable-stayed part 비율은 0.1~0.32 이다.

케이블 교량의 가설단계 구조계는 완성계에 비해 상대적으로 강성이

작고, 바람에 의한 진동에 취약하다. 따라서 가설 중 내풍안정성 확보는 중요한 디자인 이슈이다. 가설 중인 장경간 사장-현수교를 대상으로 거더의 가설 관점에서 적용 가능한 가설 순서인 순차가설 방법과 주케이블 시공이 완료된 상태에서 사장교구간과 현수구간을 동시에 시공하여 가설 공기를 줄일 수 있는 동시시공 방법을 고려해 내풍 안정성을 평가하였다. 내풍 안정성은 버페팅 해석으로 평가하였다. 검토 결과 순차가설 방법으로 deck를 시공할 경우 특별한 안정화 방안 없이 시공이 가능하다. 하지만 가설기간 동안 일부 행어의 길이조정 작업이 요구된다. 반면, 동시시공 방법은 현수구간 가설 초기 현수구간 deck에 과도한 비틀림 변형이 발생한다. 이를 개선하기 이한 구조 안정화 방안으로 X-type bracing, Rigid beam 과 Strut system을 검토하였다. 검토 결과 가장 효과적인 안정화 방안은 Strut system 이다. 동시시공 방법으로 deck를 시공할 경우 주케이블에 Strut system을 설치하여 내풍 안정성을 확보한 시공이 가능하다. 이는 순차 시공 대비 시공공기를 단축 시키는 효과를 얻을 수 있다. 하지만 동시 시공에 따른 두 가지 시스템의 가설 관리가 필요 하다는 점을 고려해야 한다. 가설 중 내풍 안정화 방안인 Strut system은 가설 구조물인 리프팅 겐트리로 대체 가능하다. 사장-현수교의 현수구간 deck 가설 중 발생하는 불안정성은 Strut system과 리프팅 겐트리를 적절히 조합하여 적용하면 효과적인 제진이 가능하며

내풍 안정성을 확보한 급속 시공이 가능하여 가설 공기를 줄일 수 있다. 제안된 구조적 내풍 안정화 방안은 장경간 현수교 및 사장-현수교의 현수구간 가설 중 발생하는 deck의 불안정성을 제어하는 하나의 방안으로 활용이 가능 할 것으로 기대 된다.

주요어: Cable-stayed suspension bridge, Suspension-to-span ratio, Transition part, aerodynamic stability, Construction phase, Deck erection sequence, Parameter study

Student Number: 2012-30248